NTNU – Trondheim
Norwegian University of
Science and Technology

Fatigue of Steel Catenary Risers

Anne Cecilie Grindstad

June 2016

MASTER THESIS

Department of Marine Technology

Norwegian University of Science and Technology

Supervisor: Prof. Svæn Sævik

NTNU Trondheim
Norges teknisk-naturvitenskapelige universitet
Institutt for marin teknikk

MASTER THESIS FALL 2015

for

Stud. tech. Anne Cecilie Grindstad

Soil modelling and fatigue of Steel Catenary Risers

Jordmodeller og utmatning av fritthengende stigerør

Steel catenary or steel long wave risers may be an attractive alternative to flexible risers in deep water oil&gas projects. The critical sections with regard to fatigue is known to be the top connection and seabed touch down sections where large relative motions occur due to vessel motions. At the top connection point, the resulting cyclic curvature can be controlled by application of bending stiffeners and/or flex-joints. At the touch down area, however, the response is governed by pipe-soil interaction effects. In many deep water projects the soil is cohesive (clay) where the reaction forces will be load history dependent with significant inherent uncertainties. The choice of soil model is an important issue when dealing with dynamic analysis of Steel Catenary Risers. The cyclic motions of the floater in a 3D sea environment induces stochastic vertical and lateral motions of the riser at the touch down point. The resulting stress histories and associated fatigue life of the riser depend on the state of the surrounding soil in terms of e.g. non-linear time dependent effects like suction and riser self-burial. Significant research efforts have been made into this in terms of model testing and formulation of models that can be implemented into a time-domain finite element framework to obtain reliable response predictions. The master thesis work is to be carried out as a continuation of the project work as follows:

1. Literature study with focus on resent research efforts done to establish relevant pipe/soil interaction soil models (Pipestab, Carisima, Safebuck, Texas, etc.), the latest developments with regard to qualification of free hanging steel risers for deep water apllications, relevant standards and also the numerical methods used as basis for the computer codes Sima/Riflex and Simla.

2. Define a free-hanging riser scenario including geometry, sea state, vessel motion transfer functions, cross-section parameters, soil mechanical parameters.

3. Establish steel catenary riser models in Sima/Riflex (eventually Simla) for a free hanging steel riser that includes both a standard Coulomb friction model and the Carisima model.

4. Validate that the model works for selected load cases.

5. Formulate the Aubeny degradation soil model and test it out in MATLAB

6. Formulate the degradation Aubeny model in FORTRAN90 using the given soil routine developed by Arifian Agusta as basis

7. Based on a simplified load case, validate the behavior using SIMLA

8. Establish a global model in SIMLA that includes the lower part of the catenary riser modelled item 3-4.

9. Based on the motions identified for specific load cases in the SIMA model prescribe same motions in the truncated SIMLA model and investigate the effect of soil degradation on the bending fatigue of the SCR at the TDP.

10. Conclusions and recommendations for further work

The work scope may prove to be larger than initially anticipated. Subject to approval from the supervisors, topics may be deleted from the list above or reduced in extent.

In the thesis the candidate shall present his personal contribution to the resolution of problems within the scope of the thesis work

Theories and conclusions should be based on mathematical derivations and/or logic reasoning identifying the various steps in the deduction.

The candidate should utilise the existing possibilities for obtaining relevant literature.

Thesis format
The thesis should be organised in a rational manner to give a clear exposition of results, assessments, and conclusions. The text should be brief and to the point, with a clear language. Telegraphic language should be avoided.

The thesis shall contain the following elements: A text defining the scope, preface, list of contents, summary, main body of thesis, conclusions with recommendations for further work, list of symbols and acronyms, references and (optional) appendices. All figures, tables and equations shall be numerated.

The supervisors may require that the candidate, in an early stage of the work, presents a written plan for the completion of the work.

The original contribution of the candidate and material taken from other sources shall be clearly defined. Work from other sources shall be properly referenced using an acknowledged referencing system.

The report shall be submitted electronically in DAIM:
- Signed by the candidate
- The text defining the scope included
- In bound volume(s)

- Drawings and/or computer prints which cannot be bound should be organised in a separate folder.

Ownership
NTNU has according to the present rules the ownership of the thesis. Any use of the thesis has to be approved by NTNU (or external partner when this applies). The department has the right to use the thesis as if the work was carried out by a NTNU employee, if nothing else has been agreed in advance.

Thesis supervisors:

Prof. Svein Sævik, NTNU

Deadline: June 10, 2016

Trondheim, January, 2016

Svein Sævik

Candidate – date and signature:

Abstract

This thesis considers development and application of soil models of for the riser-soil interaction. The interaction is generally complex and difficult to model. At deep water, the soil is made of clay which introduces sensitive parameters. The stiffness contribution that the soil exerts on the riser has an impact on the level of stress in the pipe. Bending stresses in the riser at the touchdown point may become excessive.

A nonlinear pipe-soil interaction models are frequently employed when assessing the fatigue life of a riser with soil interaction. A vertical soil model is adopted for describing the soil interaction of a steel catenary riser during vertical cycle motion. Aubeny proposed a force-deflection curve for non-degradation of the soil which considers the suction and the pipe-soil separation. Another vertical model is the Bridge's model which proposed three soil stiffnesses for modeling the pipe-soil interaction; static stiffness, small and large dynamic soil stiffness.

A lateral pipe-soil interaction model for a pipeline during lateral buckling may be obtained as a model for a riser with lateral motions. For small lateral displacement, the DNV's model is appropriate. The model takes into account the hydrodynamic stability problem where the pipe digs itself into a cavity. For large lateral displacement, SAFEBUCK's model may be applied. In this model berm accretion, soil suction and consolidation effects are taken into account.

A vertical degradation soil model was developed in this thesis. The formulation was based on Aubeny's nonlinear soil model and a degradation rule. The code was written in the programming languages FORTRAN and MATLAB. The FORTRAN subroutine was integrated within the software tool SIMLA.

SCR analyses were conducted in SIMLA to assess the significance of the soil degradation. A truncated riser model was applied to study the soil interaction. An analysis of a flat seabed and another with a trench profile were conducted using a linear soil model. Cohesive stress histograms of riser elements in the vicinity of and at TDP were plotted using rain flow counting. The histograms were presented and discussed with reference to the effect of soil degradation.

Sammendrag

Denne masteravhandlingen omhandler utvikling og anvendelse av jordmodeller for beskrivelse av jord-stigerør interaksjon. På dypt vann, er jorda bestående av leire noe som introduserer sensitive parameterer. Det gjør modelleringen av jorda mer kompleks enn om den var bestående av sand. Jordstivheten påvirker stressnivået i et stigerør. Nær og i kontaktpunktet der riseren møter jorda kan bøyespenningene bli store, noe som medfører reduksjon av utmattelseslivet.

Ulinære rør-jordinteraksjonsmodeller blir ofte brukt under vurdering av utmattelseslivet til et kjedelinje-stigerør i stål. En vertikal jordmodell kan brukes til å beskrive jord-stigerør interaksjon under vertikal bevegelse. Aubeny etablerte en kraft-nedbøyingskurve for ikke-degradering av jorda. Elementer som sug og jord-stigerør seperajon var inkludert. En annen vertikal jordmodell, utviklet av Bridge, konkluderte i at jord interaksjonen kunne modeleres med tre typer jordstivheter; statisk stivhet og, liten-og stor dynamisk stivhet.

En rød linje fra et knekkingsscenario av en rørledning på havbunne kan bli trukket til lateral bevegelse av et stigerør. Jordmodeller for en rørledning på havbunnen kan derfor bli brukt når den vertikale stigerørsbevegelsen skal modelleres. Ved liten nedbøying, er DNV sin modell adekvat. Modellen tar hensyn til det hydrodynamiske stabilitetsproblemet, der bølger og strøm graver røret ned i en grop. Ved større laterale forskyvninger, kan SAFEBUCK sin modell anvendes. I denne modellen inkluderes akkumulering av grøfter, sugkrefter og kosolideringseffekter.

I avhandlingen utvklies en vertikal jorddegradaderingsmodell. Kurveformuleringene er basert på Aubeny sin ulinære jordmodell og en regel for degradering. Koden er skrevet i programmeringsspråkene FORTRAN og MATLAB. FORTRAN subrutinen integreres i programverktøyet SIMLA.

Analyser av et kjedelinje-stigerør i stål er utført i SIMLA for å vurdere viktigheten av jorddegradering. I analysen brukes en trukert modell for å studere jord interaksjonen. En analyse med en flat sjøbunn og en analyse med et grøfteprofil er utført ved bruk av en linært elastisk jordmodell. Sammenhengende spenningshistogrammer av stigerørselementer i nærheten av TDP er plottet ved hjelp av regnfall telling. Histogrammene er diskutert i lys av effekten av jorddegradering.

Preface

This master thesis was written as a part of my education in Marine Technology at the Norwegian University of Science and Technology. During the process I have explored models of pipe-soil interactions, and enhanced my understanding of the physical mechanisms involved.

The master thesis is a continuation of my project thesis last fall. A basic knowledge about stress and fatigue are recommended in order to appreciate the thesis.

Trondheim, 2016-06-10

(Your signature)

Anne Cecilie Grindstad

Acknowledgment

I would like to thank my supervisor Prof. Svein Sævik (NTNU,Marintek) for being a great mentor throughout the entire process. His guidance and advice have been helpful and educational, and have given me inspiration for further work. I also want to acknowledge my gratitude to the PhD student in marine technology Xiaopeng Wu for assisting me in SIMA at the weekly sessions.

I would also like to thank Statoil for providing riser and environmental data for the SCR analysis, and SeoYeon Park for installing SIMLA on my computer.

Contents

List of Figures

List of Tables

List of Symbols

Latin symbols

a,b = backbone curve parameters

a = lateral oscillation amplitude

$\mathbf{a}^i$ = connectivity matrix for element i

$\bar{a}$ = material constant defining the intercept of the design S-N curve

A_e = pipe external cross sectional area

A_i = pipe internal cross sectional area

A_s = pipe steel cross section area

B = Bearing width

C = damping matrix

C_d = drag coefficient

C_m = mass coefficient

D = External riser diameter

D_o = Outer diameter, no coating included

D_{fat} = Accumulated fatigue damage

D_i = internal diameter!!is this used

D_j = Accumulated fatigue damage in the j-th block in scatter diagram of H_s and T_p

DFF = design fatigue factor

E = Young's modulus of riser

$\dot{\mathbf{E}}^{(p)}$ = plastic part of Green's rate tensor

E_w = work done

E_{xx} = green's strain tensor

f = volume forces

f = wave frequency

F_c = vertical contact force between pipe and soil

F_L = the lift force

f_p = spectral peak frequency

F_r = passive resistance

f_s = stress function

F_y = lateral reaction force

F_z = vertical force per unit length of the soil resistance

g = acceleration of gravity

G = shear modulus

G_c = soil strength parameter

h = trench depth

$h_{breakout}$ = horizontal dimensionless breakout resistance

h_{cr} = stability limit for numerical integration

H = Effective residual lay tension

$H_{breakout}$ = Breakout resistance from as laid position

$H_{residual}$ = soil resistance when pipe is moving

H_s = spectral peak period

I = area moment of inertia

J = torsional constant

K_s = Secant soil stiffness

K_x = axial stiffness

K_y = lateral stiffness

K_z = vertical soil stiffness

$\mathbf{K}_i$ = Incremental stiffness matrix

$\hat{\mathbf{K}}_t$ = effective stiffness vector

k_C = cyclic loading factor

k_{DT} = consolidation time factor

k_{DV} = empirical breakout factor

$k_D, k_{DTF}, k_F, K_{TF}, n_d, n_F, C_{TF}$ = empirical constants based on STRIDE and CARISIMA tests

k_{stiff} = parameter based on the assumption of a hyperbolic soil model

k_V =empirical pull-out velocity factor

k_0 = hyperbolic parameter defining the initial stiffness of elastic rebound

$\mathbf{K}$ = global stiffness matrix

$\hat{\mathbf{K}}_t$ = effective stiffness

L = riser length

m = negative inverse slope of the S-N curve

M = mass matrix

n_i = number of cycles in stress block i

N_A = true axial force

N_c = dimensionless shape and depth factor

N = number of cycles to failure at corresponding stress range ΔS

N_{DOF} = number of degrees of freedom

N_p = bearing factor

N_{pmax} = maximum bearing factor

N_s =number of blocks in scatter diagram of H_s and T_p

p_e = external pressure

p_i = internal pressure difference compared to as laid

P_{bl} = vertical soil resistance at arbitrary reversal points on bounding loop

P_j = weighted sea state probability of sea state block j

P_{pr} = vertical soil resistance of previous calculation step

P_r = vertical soil resistance at arbitrary reversal points within bounding loop

P_1, P_2, P_3 = soil resistance at reversal point on P-y bounding loop

P_1^* = maximum soil resistance when soil degradation is considered

q_U = ultimate bearing pressure

Q_c = maximum bearing capasity per unit length in undrained soil

Q_S, max = maximum soil suction force

Q_U = maximum soil resistance per unit length in undrained clay

$\mathbf{r}$, $\dot{\mathbf{r}}$, $\ddot{\mathbf{r}}$: = structural displacement, velocity and acceleration vectors respectively

R = unbalance force vector

$\mathbf{R}^I$ = inertia force vector

$\mathbf{R}^D$ = damping force vector

$\mathbf{R}^S$ = internal structural reaction force vector

$\mathbf{R}^E$ = external force vector

$\Delta\hat{\mathbf{R}}_t$ =effective incremental load vector

S = stress vector

S_{init} = Critical buckling force

s_u = soil undrained shear strength

s_{ug} = undrained shear strength gradient

$s_{u,h}$ = soil undrained shear strength at base of the trench

s_{u0} = undrained shear strength at mudline

S = effective axial compressive force

$\mathbf{S}^i$ = nodal force for element i

S_1 = deformed surface

S_t = Soil sensitivity parameter

S_{nom} = nominal stress range

S_{post} = Axial force in the post-buckling stage

S_0 = effective axial compressive force for a restrained pipe

S(f) = Sea spectrum as a function of frequency

SCF = stress concentration factor

ΔS = stress range

$(\frac{t_{fat}}{t_{ref}})^k$ = material constant

t = surface traction

t_p = pipe thickness

T = axial tension

T_0 = horizontal top tension

T_p = spectral peak period

ΔT = Temperature difference compared to as laid

u = displacement vector

ü = acceleration field

$u_{0,x}$ = axial strain

V = vertical load of the pipe

V_{residual} = vertical residual resistance

V_1 = deformed volume

v = dimensionless vertical load V/s_uD

$v_{0,x}$, $v_{0,xx}$ = 1st and 2nd order derivative of lateral displacement

w = Trench width

$w_{0,x}$ = 1st order derivative of the vertical displacement

X = soil parameter

y = lateral soil displacement

y_b = lateral displacement

Y = dimensionless lateral pipe penetration

z = vertical soil penetration

z_{bl} = soil deformation at arbitrary reversal points on bounding loop

z_b = vertical deflection

z_D = dynamic displacement

z_{init} = initial penetration depth calculated by SAFEBUCK

z_p = total penetration depth calculated by DNV

z_{pr} = soil deformation of previous calculation step

z_{pi} = initial penetration

z_{pm} = penetration due to riser motion

z_r = soil deformation at arbitrary reversal points within bounding loop

z_{startup} = embedment depth at startup

z_1, z_2, z_3 = vertical coordinated at reversal point on P-y bounding loop

z_1^* = maximum penetration when degradation is considered

Δz_i = vertical incremental soil riser deflection

Z_U = mobilization distance of breakaway

Greek symbols

α_d, β_d = degradation backbone curve parameters

α_T = thermal expansion coefficient

$\alpha, \beta, \gamma, \theta$ = parameters for numerical integration

γ = submerged unit weight of the soil

γ_j = defining the steepness of the JONSWAP spectrum

γ_s = dry unit soil weight

γ' = defines artificial damping

${}^{i}\Delta r$ = displacement correction vector

Δ_B = breakout displacement

ϵ = Natural strain tensor

ε = tolerance requirement for an iteration procedure

η = non-dimensional strength gradient parameter

λ_c = load factor for volume forces

$\dot{\lambda}$ = parameter for determining the plastic part of the rate of Green's strain

λ_n = accumulated deflection

λ_v = load factor for current forces

Λ = factor for obtaining maximum soil force

κ = strain-hardening parameter

ν = Poisson's ratio

μ = friction coefficient

μ_e = equivalent friction coefficient

ρ_{coating} = coating density

ρ_i = internal fluid density

ρ_m = material density

ρ_s = steel density

σ = parameter that describe the relative width of the single peak in JONSWAP spectrum

σ_Y = yield stress

$\boldsymbol{\sigma}$ = Cauchy stress tensor

ϕ = tension suction limit, controls the maximum suction on P-y bounding loop

χ = load direction parameter in hyperbolic path formulations

ψ = parameter controlling soil-riser separation on P-y bounding loop

ω = parameter controlling the curvature in hyperbolic path formulations

ω_s = pipe submergence weight

List of Acronyms

SCR Steel Catenary Riser

TDP Touchdown Point

TDZ Touchdown Zone

HHT -α method Hileber-Hughes-Taylor method

JIP Joint Industry Product

NGI Norwegian Geotechnical Institute

PVD Principles of Virtual Displacement

FEM Finite Element Modeling

GUI Graphical User Interface

JONSWAP JOint North Sea WAve Project

HT/HP High Temperature/High Pressure

TSJ Tapered Stress Joint

RAO Response Amplitude Operator

Chapter 1

Introduction

To satisfy the global demand for fossil fuel, the oil companies have been entering deeper water than before. In these water areas, the development of new fields requires more advanced methods and higher technical skills than in shallow water due to more complex field development in deep water. Steel Catenary Risers (SCR) are the preferred riser solution in deep water in the Mexico Gulf and along the coast of West Africa. In Norway, there are presently only two deep-water projects, Ormen Lange where all equipment is located at sea bottom and the gas field and Aasta Hansteen. Both located outside Nordland.

Critical to SCR behavior is the development of fatigue stresses at the touchdown point and the connection point between vessel and riser due to the motions of the floating production unit (see Fig. 1.1). Large bending moments arise as the riser oscillates from its hang-off point, leading to reduction of fatigue life. The most critical to the riser fatigue life, are the pipe-soil interaction effects at the point where the pipe touches the soil. In deep water, the soil consists mainly of clay. The soft clay at the sea bottom contains significant inherent uncertainties due to the cohesive effects and stiffness degradation. As a consequence, a reliable soil model for pipe-soil interaction effects in vertical and lateral directions may be difficult to obtain.

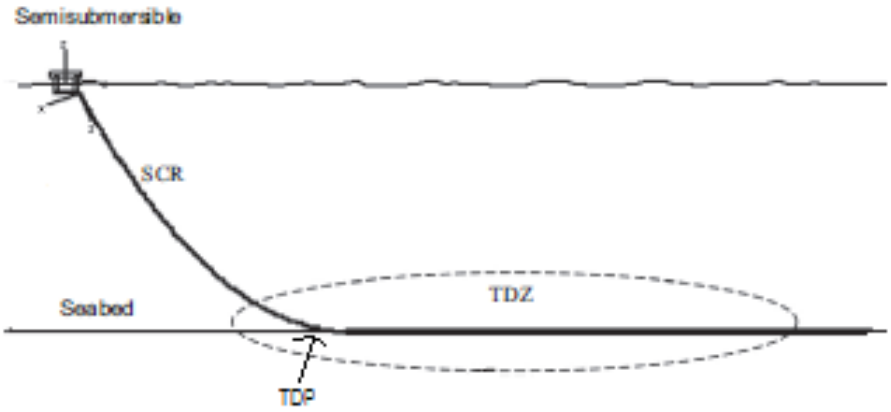

Figure 1.1: Touchdown Point and Touchdown Zone (Elosta et al., 2013)

1.1 Objective

The aim of the study is to examine the effect of soil degradation on the bending fatigue of a steel catenary riser at the TDP in soft clay. Analyses were conducted of a riser hanging from a pontoon of a semi-submersible on the Aasta Hansteen field with soil parameters and metocean-data from the same field. Two software, RIFLEX and Simla, were used to conduct simulations of the established model. In Riflex, a standard Coulomb friction model was applied to compute translative motions for a storm scenario. In Simla, the dependency of degradation on fatigue was investigated by applying the computed motion histories. This was achieved by comparison of stresses in the riser using a trenched and a flat seabed profile. In order to gain a better understanding of how different factors such as degradation and external load contribute to fatigue, the following question is being investigated.

- To what extent does the degradation of the soil affect the fatigue life of a steel catenary riser?

After conversation with my supervisor, the analysis of a free hanging riser using the CARISIMA model is cancelled.

1.2 Scope of Work

A literature study is provided to obtain a general understanding of the processes behind the pipe-soil interaction and the development of soil models. It also includes guidance on the numerical methods that may be used to analyze the riser-soil interaction problem in the applied software.

A vertical degradation soil model is developed for soil-riser interaction in clay. The model is based on the nonlinear Aubeny degradation formulation and a degradation rule, and is written in the programming languages FORTRAN90 and MATLAB. The model is validated upon existing literature before it is implemented in the engineering program SIMLA. The effect of soil degradation on the bending fatigue of a steel catenary riser at the touchdown area is then evaluated.

1.3 Organization of the Thesis

The thesis starts with an introductory including introduction, objective, scope, organization of the thesis and a literature review. The introduction addresses the need to study the riser-soil interaction effect as it has a major effect on fatigue of an SCR. The literature study offers insights in the published literature and substantive findings that are concerning the thesis. Extensive prior knowledge about this theme is not required. Processes and expressions will be explained when reading this study.

In Ch. 2 a theoretical background introduces important themes that are not covered in the scope of work: a definition of an SCR, calculation of fatigue and the effect it has of an SCR, the pipe-soil interaction effects, the software tools, SIMLA and RIFLEX and the theory behind numerical modeling.

In Ch. 3 the features of the vertical riser-soil interactions are described and a vertical nonlinear force-deflection curve of the soil is presented. In Ch. 4 some previously established vertical soil models are described. Among these are, the Bridge's model, the Aubeny non-degradation model. The degradation rule, which accounts for the soil degradation, is also highlighted.

As Ch. 3-4 describe vertical pipe-soil interactions and soil models, Ch. 5 gives an introduction to the lateral pipe-soil interaction process while Ch. 6 introduces lateral soil models. The magnitude of the displacement of the pipe indicates what type of model that is representative. If pipe displacements are small, the DNV model may be utilized. For larger pipe displacements, the SAFEBUCK may may be applied.

Ch.7 presents the numerical methods for static and dynamic analysis applied for a riser-analysis in the software tools SIMLA and RIFLEX. A combination of Euler-Cauchy incremental procedure and Newton-Raphson iteration is the common method for solving the static equilibrium equation. For dynamic analysis, the numerical integration method, HHT-α method is used in SIMLA while RIFLEX incorporates the Newmark β-family.

In this thesis, a vertical degradation soil model was developed based on Aubeny's non-degradation model and a degradation rule. Ch. 8 describe the structure of and the formulation in the code. The model was integrated inside SIMLA and Ch. 9 contains a description of the communication system between the developed model and the software. In Ch. 10 this model was validated by comparison of existing literature.

In Ch. 11 the effect of soil degradation on fatigue is investigated. First, an SCR analysis was executed to obtain a trench profile after one-hour storm scenario. Further analyses were conducted using linear elastic soil material for the computed trenched soil profile and a flat seabed. The bending stresses in the riser were computed to give an indication of the impact of fatigue the state of the surrounding soil may have.

1.4 Literature Review

Most of the previous studies considering the riser-soil interaction process are based on what happens in the vertical plane. Fig. 1.2, of a riser connected to a spar in deep water in the Gulf of Mexico, explains the reason. The plot shows TDP movements over the service life of the riser. 97 percent of the movements of the riser along its longitudinal axis occur over a +-17m band around the TDP at static configuration while the transverse displacements are in comparison much smaller. The vertical riser motions have thus the largest contribution to the dynamic responses of the riser. Bridge et al. (2004) and Clukey et al. (2005), rendered by Jiao (2007), addressed the vertical interactions between the riser and the soil. Bridge et al. (2004) formulated empirical models based on published data from experiments of vertical pipe-soil interactions conducted by CARISIMA JIP's and STRIDE and other published data. These two projects concentrated on the process of repeated penetration and particularly the development of suction during pullout of a pipe. They proposed models of dynamic soil stiffness and suction. Aubeny et al. (2006) developed a non-degradation model based on data from laboratory model tests of a vertically loaded horizontal pipe in weak sedimentsDunlap et al. (1990); Bridge et al. (2004).

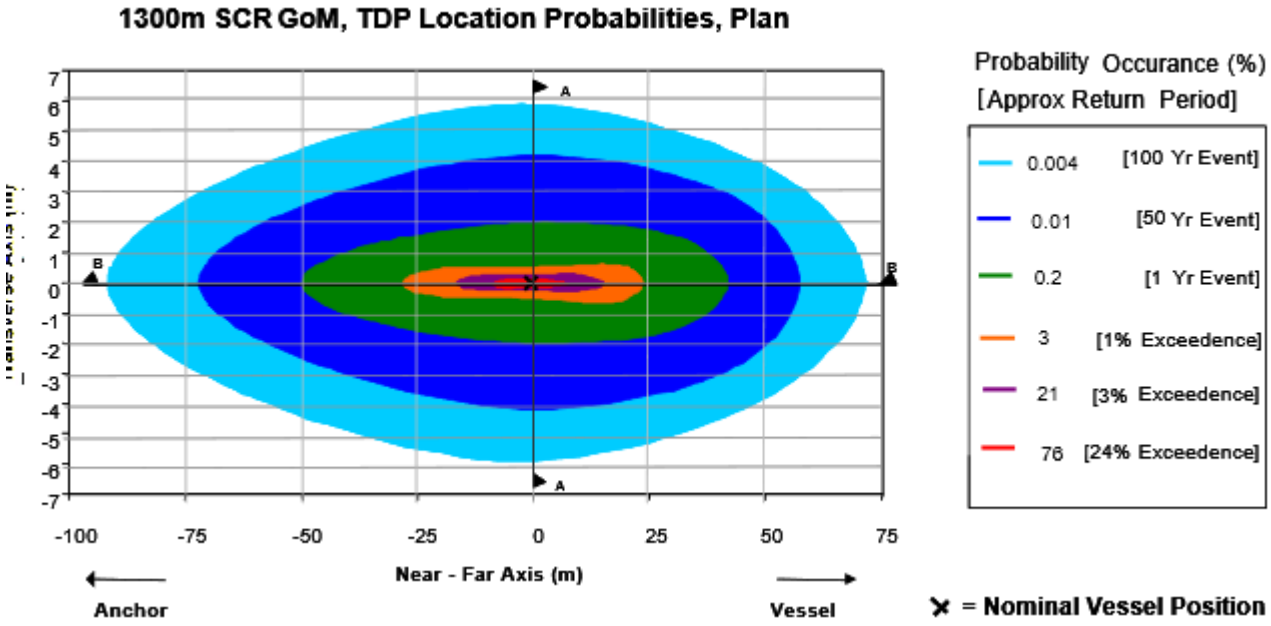

Figure 1.2: Global Dynamic Movements of a Riser at TDP (Theti and Moros, 2001a)

The soil will experience degradation due to cyclic loading, consolidation and thixotropy. Displacement controlled test made by Aubeny et al. (2008) indicated that the soil stiffness may be reduced with increasing loading cycles, even if there are no extreme loading conditions. The authors established a degradation rule for calculation of the soil degradation. Less time has been spent to examine the effect of lateral riser-soil interactions because this state is less severe. The problem can be solved by drawing parallels to a pipeline resting on the seabed. There are two different ways of determining the lateral soil resistance depending on the amplitude of the lateral displacement of a pipeline. DNV implemented a model for small displacements subjected to hydrodynamic loads (DNV, 2011). The model, for a pipe in clay soil, is developed by Verly and Lund. In the case of deep water with high temperature (near the reservoir), high pressure (HPHT) pipeline large lateral displacements occur and thus, the simple Coulomb friction model is not appropriate in the detailed design of lateral buckling. SAFEBUCK developed a methodology for this associated aspect (Bruton et al., 2006).

Chapter 2

Theoretical Background

2.1 Steel Catenary Riser

Steel Catenary Risers (SCR) is used for transfer of fluids such as oil and gas from the seabed to a floating production platform or vessel in deep water. They have the shape of a catenary as depicted in Fig 2.1. From the hang off-point at the structure, they hang close to vertically and bend until they lie onto the seabed.

SCR are widely used in deep water areas only, due to occurrences of large bending moments. The bending moments are a major concern of an SCR. In shallow water, the curvature becomes excessive when the pipeline is forced into a catenary shape. To cope with the internal forces and moments that arise, the SCR may have a large diameter to increase the resistance.

Compared to other types (e.g. flexible risers), SCR is a cheap alternative due to the simple pipe configuration, limited use of subsea equipment and installation methods. This is the reason why the SCR is the preferred choice in deep water.

There are different types of catenary risers such as free hanging, lazy wave and buoyancy supported. This project only concentrates on free hanging risers as seen in Fig. 2.1.

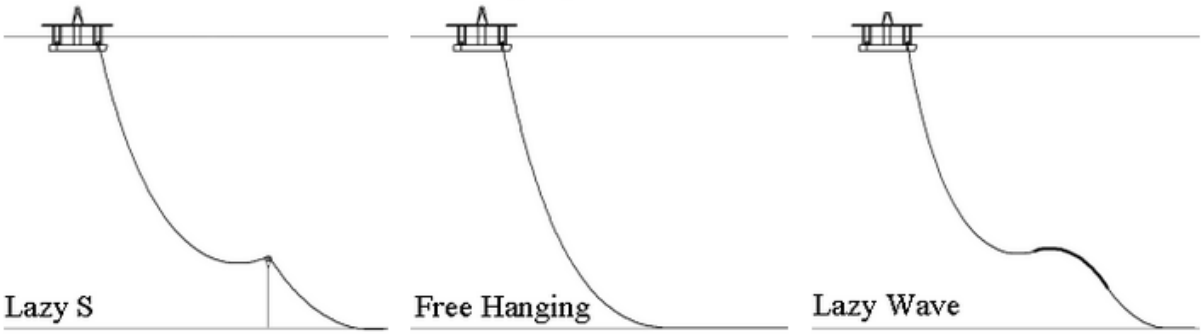

Figure 2.1: Different Types of Steel Catenary Risers

2.2 Fatigue Life

Fatigue is a phenomenon related to crack initiation and growth when an object is subjected to cyclic loading. This indicates a dynamical problem. Fatigue can be estimated by establishing a long-term stress history and an S-N curve.

2.2.1 S-N Curve

An S-N curve, stress-life diagram, is determined by testing the performance of the material/-components. The curve, depicted in Fig. 2.2, shows the relationship between the magnitudes of the stress range, ΔS, against the corresponding number of cycles to failure, N.

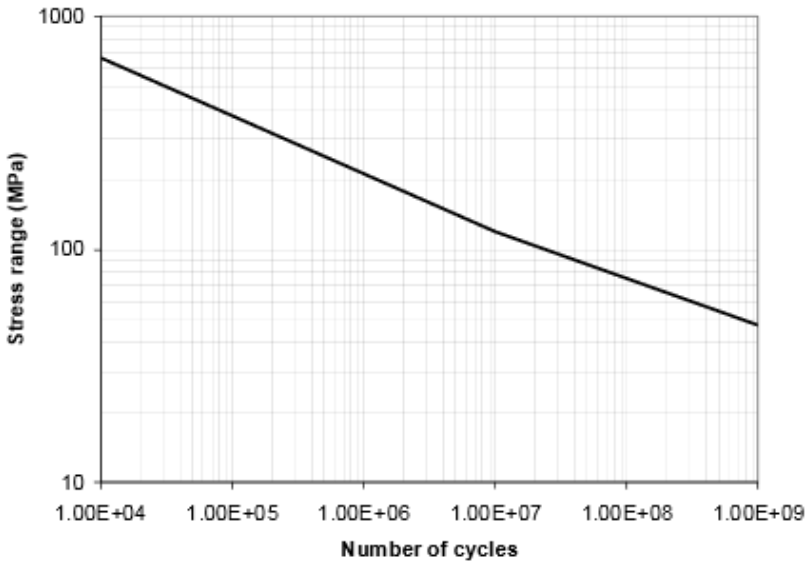

Figure 2.2: One Sloped SN-Curve

The design S-N curve is given by:

$$N = \bar{a}(\Delta S)^{-m} \tag{2.1}$$

Eq. 2.1 can be rewritten as a linear curve in a log-log scale:

$$log(N) = log(\bar{a}) - mlog(\Delta S) \tag{2.2}$$

where

$$\Delta S = S_{nom} * SCF * \left((\frac{t_{fat}}{t_{ref}})^k \right) \tag{2.3}$$

The thickness correction factor $(\frac{t_{fat}}{t_{ref}})^k$ and $\bar{a}$ are material constants, S_{nom} is the nominal stress range and SCF is the stress concentration factor. m is the negative inverse slope of the S-N curve. For a narrow-banded process S_{nom} is equal to two times the stress amplitude. This is a conservative assumption. For a real broad-band process the stress ranges are somewhat smaller.

S-N curves are generally applicable for high cycle fatigue (above 10^5 cycles), as the strain is within the elastic range. In low-cycle fatigue, the stresses tend to give plastic strains. A better approach is to estimate the fatigue based on strain ranges instead of stress ranges.

2.2.2 Palmgren-Miner's Rule

The accumulated fatigue damage, D_{fat}, may be estimated by the linear model, Palmgren-Miner's rule, as shown:

$$D_{fat} = \sum_i \frac{n_i(\Delta S_i)}{N_i(\Delta S_i)} = \frac{1}{\bar{a}} \sum_i n_i (\Delta S_i)^m \tag{2.4}$$

where n_i is the number of cycles in the i-th stress range and N_i is the total number of cycles to failure at the corresponding stress range. n_i is obtained by the stress history while N_i is calculated from the S-N curve.

This formula is widely used in fatigue design due to its simplicity and the approximately same level of uncertainty compared to more complicated approximations. One drawback is that stress interactions are neglected. In cases of low stress cycles followed by higher cycles, the rule overestimates the fatigue damage.

2.2.3 Rain Flow Counting

A short-term stress history of the riser is obtained from realizations of the sea surface and applied current and wind profiles. The sea surface is modeled as a random stochastic process containing irregular waves. As a result, the oscillations of the riser produced by the floater is complex and random. The stress history is likewise. Fig. 2.3 of an irregular stress history defines some important terminology.

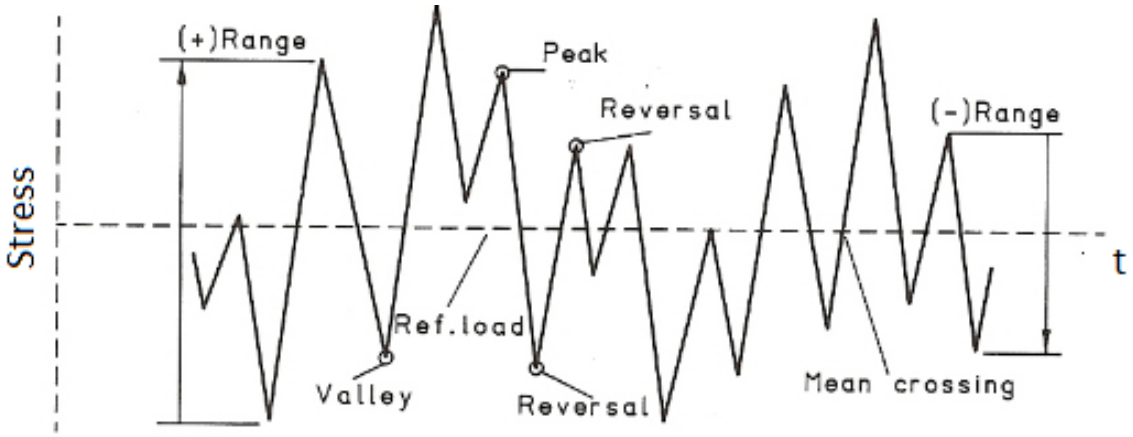

Figure 2.3: Strain History and the Corresponding Stress-Strain Curve

Peak: the derivative of the load-time history changes sign from positive to negative

Valley: the derivative of the load-time history changes sign from negative to positive

Reversal : peak or a valley

Range: the difference between the peak and valley stress

Mean crossing: or zero crossing, is the number of times the given stress history crosses the mean level.

The stress history is broadband time series, see Fig 2.4 , as there may be more than one peak and one valley between the zero-crossings. A broad band process has varying mean. For such series, there is no evident approach for reducing the time series in order to estimate the fatigue life.

One approach frequently used in high cycle fatigue is the rain flow counting method. The stress history is transformed into predefined stress ranges with a corresponding number of cycles. Thus, the algorithm allows the application of miner's rule.

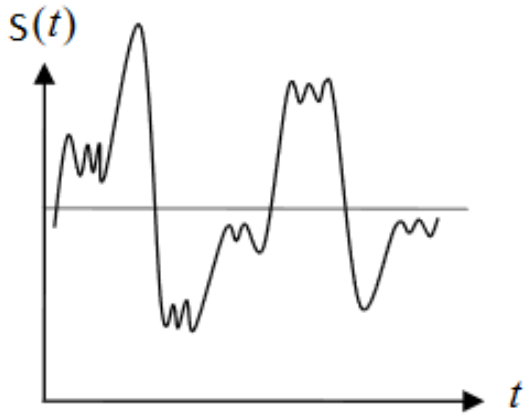

Figure 2.4: Broad Band Time Series

The name originates from an analogy where rain water flows down a pagoda. By imagining that, the following rules are derived:

- A rain flow start at each peak and valley
- When the water falls from the tip of the roof, drops down and joins an earlier path, a cycle is closed.
- If the flow starts from a valley and the opposite valley is more negative, one half cycle is closed.
- If the flow starts from a peak and the opposite peak is more positive, one half cycle is closed.

The algorithm is used to count full cycles and half-cycles with respect to the material's stress-strain relationship. The strain history and the stress-strain relationship in Fig. 2.5 illustrate the method.

By looking at the strain-history, a full cycle 1-4 and a half cycle 2-3-2' is completed. The hysteresis loop always counts for a cycle.

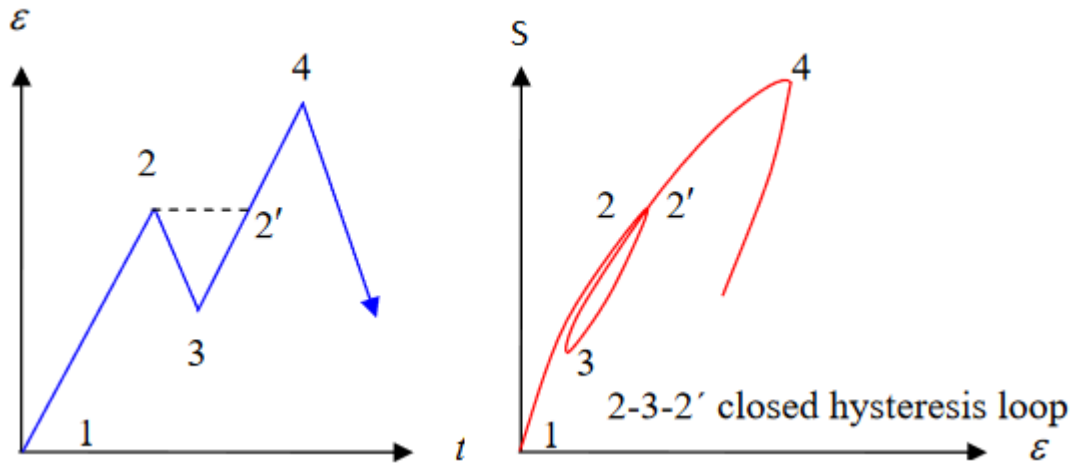

Figure 2.5: Strain History and Corresponding the Stress-Strain Curve

2.2.4 Mean Stress Correction

2.2.5 Long-Term Fatigue Damage

To compute fatigue damage (DNV, 2010), a scatter diagram showing the occurrence of short-term sea-states during many years is a starting point. The diagram is divided into appropriate blocks. One single sea state is chosen to represent all the sea states within the corresponding block. There are different ways to select the representative sea state according to how many times these sea states have occurred relatively to the other in the same block e.g. the mean or 2/3 of the sea states in the block.

The short-term fatigue damage, D_j is calculated for the selected sea states. Then an evaluated long-term fatigue damage is computed by the short-term fatigue damage and the sum of the weighted sea state probability, P_j, see Eq. 2.5. As the selected sea state is representing the corresponding block, the probability of occurrence for the sea states within the block, P_j, adds to the selected sea state (DNV, 2010). The long-term fatigue damage, D_{fat} is given by:

$$D_{fat} = \sum_{j=1}^{N_s} D_j P_j \tag{2.5}$$

where N_s is the number of blocks. The calculation of D_j may be based on a one-hour simulation

of the representative sea states. To obtain the long-term fatigue damage, the calculated short term fatigue damage must be scaled. The fatigue criterion for failure is given by:

$$D_{fat} * DFF <= 1 \tag{2.6}$$

where DFF is the Design Fatigue Factor.

2.3 Fatigue Damage of Steel Catenary Risers

The waves induce cyclic motions of a production vessel/ship. The vertical motions are due to heave and pitch on the production vessel/ship while lateral motions are caused mostly by sway and yaw motions. The motions are transmitted to the riser through an end connector. The riser will interact with the soil and may create excessive bending moments around the TDP. In the vicinity of the top connection the restrictions of the riser against rotating lead to large bending moments. The stresses that arise in the riser in these areas are excessive and a major cause of fatigue of an SCR.

2.3.1 Touchdown Point

The point where the pipe touches the soil is termed the touchdown point (TDP). At this spot the highest stresses and the largest fatigue damage occur due to slug forces, vortex-induced vibrations and pipe-soil interactions (Bridge et al., 2003; Bridge et al., 2004). These are complex phenomena, and subsequently prediction of fatigue life is calculated with a degree of uncertainty.

This thesis presents the effect of pipe-soil interactions on fatigue for an SCR since this mechanism is the most critical. Both lateral and vertical interactions with the soil contribute to fatigue damage. These interactions involve nonlinear processes such as trench formation, soil stiffness, soil suction and breakaway from the seabed (Aubeny and Biscontin, 2009)

SCRs are sensitive to both vertical and lateral pipe-soil interactions. The degree of uncertainty

is dependent on soil properties, riser configuration and dimension, vessel dimension, environmental condition etc.

2.3.2 Top Connection

SCRs are connected to a floating structure through a hang-off system (Wang et al., 2011). The system may either consist of a flexible joint, a tapered stress joints (TSJ) or a J-tube. The most common SCR flexible joint is the type FlexJoint while the titanium TSJ is the most preferred TSJ for an SCR. These joints are depicted in Fig. 2.6 and Fig. 2.7. J-tube is used in deep water on a Spar buoy when the pipe diameter is small.

The top region in an SCR is sensitive to fatigue due to the relative rotation between the riser and the floating production unit and the high tension in the riser due to its submerged weight. The fatigue damage in this region can be minimized by application of a FlexJoint.

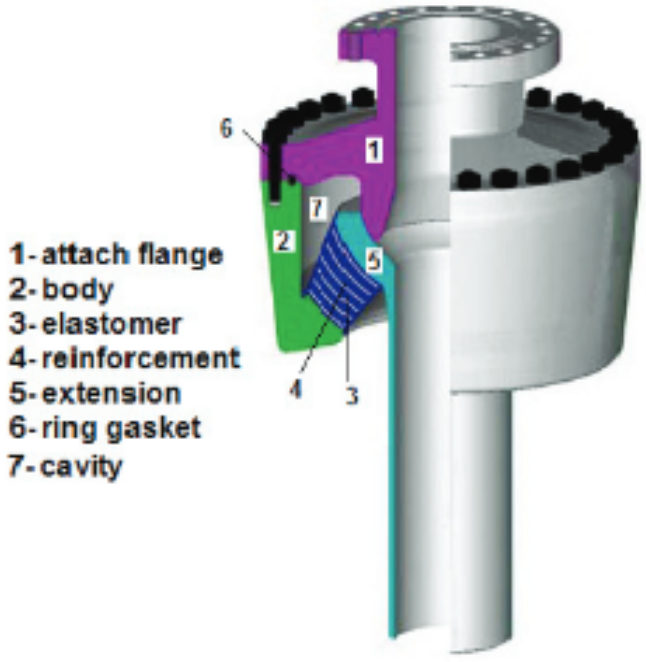

Figure 2.6: FlexJoint Configuration (Wang et al., 2011)

These joints consist of layers of elastomeric materials and spherical shaped steel (i.e.,.reinforcement) which are vulcanized together inside a cup-shaped member (Wang et al., 2011). This combina-

tion allows the riser to rotate while longitudinal and lateral movements are constrained. The joint provides flexibility and does not produce any additional bending moments in the riser as the platform or vessel moves.

Another alternative for reducing fatigue is by application of a titanium-TSJ, see Fig. 2.7. There are no moving parts of the joints. The joint is fixed to a hang-off basket through an upper tapered section while the lower taper section allows the taper joint to rotate. To allow more rotations and lower bending stresses, a steel TSJ may be connected between the SCR and the titanium-TSJ. The steel TSJ may be applied to a pipe with a small diameter that experiences large relative rotations (Wang et al., 2011).

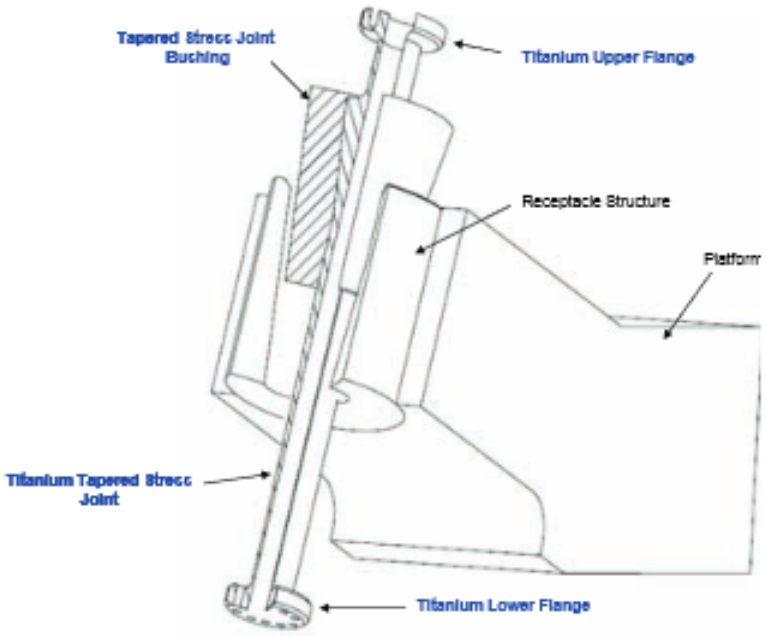

Figure 2.7: Titanium TSJ-Configuration (Wang et al., 2011)

2.4 Pipe-Soil Interaction Effects

The soil resistance is calculated differently if riser motion is in vertical, lateral or axial direction. The vertical resistance shows different characteristic for downward and upward riser movements. For downward riser motion (small deflection), the soil behaves to some extent elastically. For larger deflection, the soil will experience plasticity (Willis et al., 2001). The degradation of the soil is beneficial for the fatigue life of the riser touchdown point. For upward motion, the soil generates a suction force due to the cohesive effects of the weak sediments. The suction force prevents the riser from breaking out of the soil.

Lateral resistance consists of friction between the riser and the seabed soil and passive resistance due to shear fraction of the soil. The passive resistance of the soil is mainly acting when the riser moves out of a depression or impacting with a trench. The axial resistance is determined by axial friction.

2.4.1 Soil Degradation

What is meant by soil degradation is that the soil stiffness is reduced under the complex loading cycles. Tests conducted by Idriss et al. (1978), show reduction in stiffness of cohesive soils as the number of loading cycles is accumulated. During loading and unloading, the soil will remold and consequently the stiffness will be reduced according to Fontaine et al. (2004). Predominantly, it is the vertical motions of the riser that reduce the soil stiffness. However, some are due to coupled effects with lateral motions. The reduction of stiffness is due to plastic deformation and self-burying (Theti and Moros, 2001b). Another contribution is due to water entrainment into or out of the soil caused by the cyclic riser motion. This creates a ”pumping” mechanism that will amplify the soil degradation. The effects of water entrainment, reconsolidation, erosion of soil and thixotropy of the soil on the seabed are all contributing to stiffness reduction(Nakhaee and Zhang, 2010).

(**?**) examined the riser-soil interaction through a series of vertically loaded tests (Jiao, 2007). Load and displacement controlled tests were conducted under small, intermediate and large

displacement cycles. The result indicated that a unload/reload hyperbolic curve predicts adequately the riser soil interaction when the riser is subjected to small uplift force compared to the downward vertical forces. If riser-soil separation occurs, the hyperbolic curves are no longer a good fit. As the riser separates from the soil, the soil stiffness before hardening of the stiffness during further penetration. They concluded that the stiffness reduction was correlated to soil-water mixing and pumping action during the separation. As the pipe is re-penetrating the soil after separation, water is being pushed downward by the pipe.

2.4.2 Formation of Trench

In deep water, the clay is assumed fully saturated. The soil behaves as incompressible when subjected to the cyclic loading. This means that the volume remains unchanged during tension/compression. The Poisson ratio is 0.5, and the soil will deform plastically, i.e. the material yields. A trench formates due to plastic deformations of the soil and pumping actions of water caused by cyclic riser motions according to Theti and Moros (2001b).

The vertical cyclic motions of the riser will introduce formation of a trench. As the riser hits the soil, the soil (clay) will start deforming plastically behind the TDP. During motions, the riser will penetrate the soil and be dragged somewhat forward. A trench develops and berms at the sides and in front of the riser start to formate. The continuous motion cycles result in a change of TDP. The area of dynamical interactions between pipe and soil is denoted the touchdown zone (TDZ).

The lateral interactions between the riser and the soil cause a trench to form. The soil is dragged along the riser resulting in a "trumpet" formation with a trench at each side of the riser.

2.5 Displacement- Based Finite Element Method

Finite Element Method (FEM) is a numerical tool for solving differential equations for field problems. To accomplish this, the differential equations for the problem (strong form) are reformulated into an equivalent weak form formulation using the Principle of Virtual Displacements (PVD). The solution is thus approximate as the weak form of the differential equation is applied. The displacement-based finite element method is a generalization of the displacement method for analysis of beams and trusses.

The structural model discretizes into finite elements which are connected by nodes. For each element, three fundamental laws apply.

- Equilibrium: Relation between stresses and applied loads
- Kinematic compatibility: Strain -displacement relationship
- Constitutive equation: Stress- strain relationship

2.5.1 Equilibrium

The displacement-based finite element method is based upon the principle of virtual displacement. If the approximate displacement function does not satisfy the differential equilibrium equation, a residual force is introduced. The residual force is smoothed over the element employing the principle of virtual work. For equilibrium to be achieved according to PVD, any compatible, virtual displacements (which are zero to the corresponding prescribed displacement) imposed on the body in the equilibrium state, the internal virtual work is equal to the external virtual work. The equilibrium is satisfied in an average sense through weight functions (virtual displacements) and volume integrals. The weight function must be carefully selected to satisfy the boundary condition in the best possible way. Even if the boundary condition is satisfied, the differential equation is not necessarily fulfilled at any point within the element.

The principle of virtual work in an arbitrary equilibrium state may be written as:

$$\int_{V1}(\rho_m \ddot{\mathbf{u}} - f)\delta\mathbf{u}dV + \int_{V1}\boldsymbol{\sigma} : \delta\boldsymbol{\epsilon}dV_1 - \int_{S1}\mathbf{t}\delta\mathbf{u}dS_1 = 0 \tag{2.7}$$

where ρ_m is the material density, $\ddot{\mathbf{u}}$ is the acceleration field, $\mathbf{f}$ is the volume forces, $\boldsymbol{\sigma}$ is the Cauchy stress tensor, $\boldsymbol{\epsilon}$ is the natural strain tensor, $\mathbf{t}$ is the surface traction and $\mathbf{u}$ is the displacement vector. The integration limits are referred to the deformed volume, V_1 and surfaces, S_1.

2.5.2 Kinematic Compatibility

The kinematic compatibility requirement states that the boundaries between two neighboring elements have the same displacement such that no gapping or overlapping occur. The assumed displacement field must be compatible with the strain field (Mathisen, 2014).

In general, pipes are modeled by beam elements. In SIMLA and RIFLEX, Euler-Bernoulli hypothesis applies; plane sections remain plane and normal to the beam's axis after deformation. This statement is valid for small strains and implies no shear deformations. For large rotations, but small strains von Karman strains are introduced. In SIMLA, the second order longitudinal strain term and the coupling terms between longitudinal strain and torsion are neglected.

For an elastic beam element, the Green's strain may thus be formulated as (Sævik, 2008):

$$E_{xx} = u_{0,x} - y_b v_{0,xx} - z_b w_{0,xx} + \frac{1}{2}(v_{0,x}^2 + w_{0,x}^2) \tag{2.8}$$

2.5.3 Stress-Strain Relationship

If the stress is below the proportional limit, the stress-strain relationship is linearly described by Hooke's law. If the limit is exceeded, an elasto-plastic formulation is needed to account for the two-dimensional state of stress consisting of hoop stress and axial stress (Sævik, 2008). The plastic part of the formulation contains three essential features:

- Yield condition or yield surface: The criterion determines which state of the multi-axial stresses that leads to plastic deformations. The yield criterion is commonly written as:

$$f(\mathbf{S}, \kappa) = 0 \tag{2.9}$$

where κ is the strain-hardening parameter which is a function of the loading history during plastic deformations. f_s is a scalar function and its value defines the stress state (Moan, 2003):

  - $f_s < 0$: Elastic state of stress
  - $f_s = 0$: Plastic state of stress
  - $f_s > 0$: Inadmissible

  During plastic deformations, the stress state remains on the yield surface.

- Hardening rule: The yield criterion changes due to strain hardening during plastic deformations. The elasto-plastic property of the material is described by kinematic or/and isotropic hardening rule. According to isotropic hardening rule, the shape of the yield surface remains the same as for initial yield, however, the size increases with higher stress. This implies that the yield strength is the same in tension and compression initially and during plastic strain. The kinematic hardening considers the Bauschinger effect i.e. hardening in tension causes the material to soften in subsequent compression. Fig. 2.8 illustrates isotropic and kinematic strain hardening for a two-dimensional stress state.

- Flow rule: the plastic strain increments can be determined at each point in the loading history. There are mainly two theories for describing the plasticity; deformation theory and flow theory. Solving problems with general loading paths such as reversed and cyclic loading, flow theory is the better alternative according to experiments (Moan, 2003).

  The material is assumed to follow Drucker's postulate for a stable material. This implies normality i.e.; the plastic strain vector is equal to the outward normal to the yield surface.

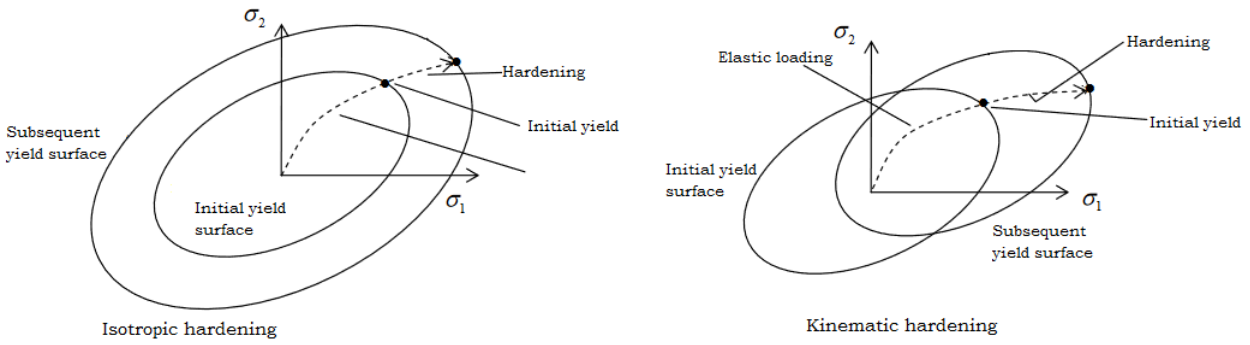

Figure 2.8: Hardening Models for Two-Dimensional Stress State (Moan, 2003)

The normality condition is given by (Sævik, 2008):

$$\dot{\mathbf{E}}^{(p)} = \dot{\lambda}\frac{\partial f}{\partial \mathbf{S}} \tag{2.10}$$

where $\dot{\boldsymbol{E}}^{(p)}$ is the plastic part of the rate of Green's strain tensor and the parameter $\dot{\lambda}$ depends on the current stress and strain, and on the stress rate. Further, the yield surface must be convex which ensures that the entire elastic region lies to one side of the tangent plane to the yield surface (Moan, 2003).

2.6 Software Tools for Modeling the Pipe-Soil Interaction

There are different computer software tools for modeling the pipe-soil interaction effect. This section focuses on the programs SIMLA and RIFLEX, which may utilize finite element modeling to analyze structural problems. Both programs may be used for offshore pipelines and provide static and dynamic analysis in the time domain and provide 3D graphical visualization.

SIMLA is a computer tool for analyzing the process of design, installation and operation of offshore pipelines (sin, b). The pipe-soil interaction can be modeled by using hyperelastic, elasto-plastic or non-degradation nonlinear material. In this thesis, a vertical degradation non-linear soil model is programmed and integrated into SIMLA.

RIFLEX is a software for hydrodynamic and structural analysis of slender marine structures (sin, a). It has a graphical user interface (GUI).

Chapter 3

Vertical Riser-Soil Interaction

Model tests and numerical simulations are used for modeling the nonlinear behavior of the soil. A non-degradation force-deflection curve is proposed to represent the behavior. In connection with a storm and large vessel movements, the curve may be divided into five paths as depicted in Fig. 3.1. The resistance force of the soil per unit length, P, is shown against the vertical penetration, z, of the riser along the horizontal axis. The figure summarizes the following description of these paths. The name convention for the different paths is taken from (Aubeny et al., 2006).

1. Path 0-1, the so-called backbone curve shows the initial plastic penetration of the riser into virgin soil. The final penetrated depth is reached when the soil force is equal the penetration force.

2. Elastic rebound occurs when the pipe follows the unloading path 1-2. When the pipe is moving upwards, the soil resistance reduces to zero. As the pipe moves further upwards, the space between the soil and pipe creates a suction force to prevent the motion of the pipe. The suction force is developed due to the cohesive effects of the clay that attracts the pipe from moving upward.

3. Model tests agree that the force-displacement curve reduces towards zero in point 3 after the suction force has reached a maximum. The tension force decays along the partial pipe-soil separation path. If the magnitude of the unloading is sufficiently large, the riser experiences full separation from the seabed in point 3 and moves further upwards follow-

ing the horizontal axis. There is no suction force after full separation. The self-weight of the riser reverses the pipe motion and in point 3 the re-connection occurs.

4. Previous studies (Dunlap et al., 1990; Bridge et al., 2004) indicate that the soil resistance does not respond directly to the re-connection with the pipe. As a result, the soil resistance forms a much steeper curve from point 3 to 1.

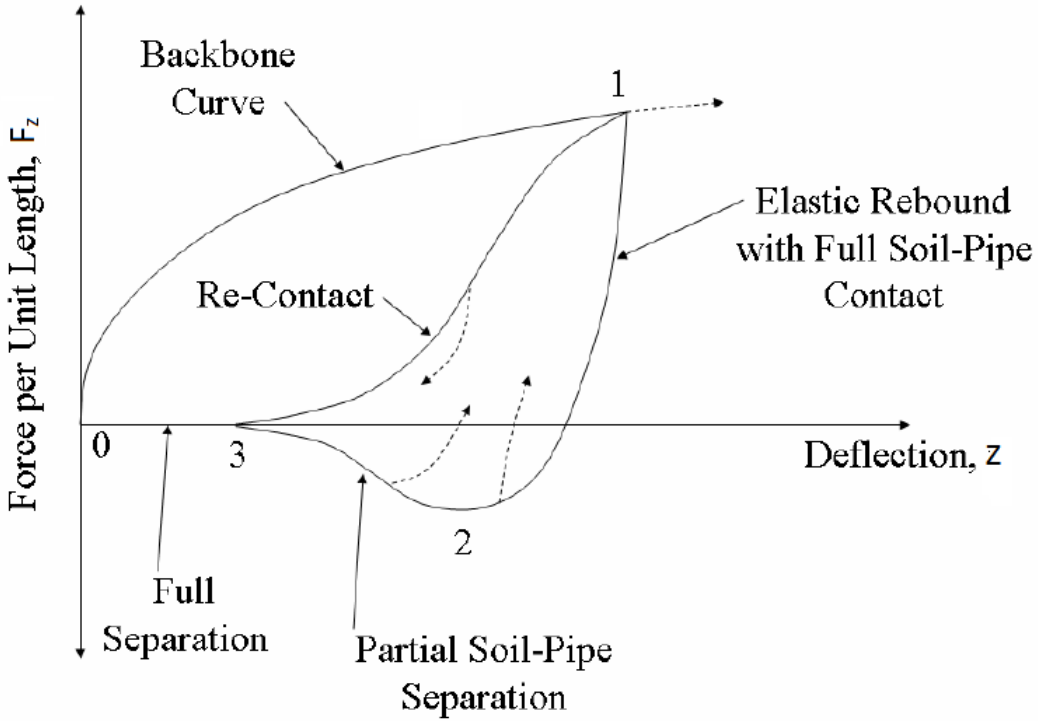

Figure 3.1: Load-Deflection Curve (Aubeny et al., 2006)

The enclosed cycle 1-2-3-1 is called the bounding loop. The bounding loop represents the case where extreme motion leads to full separation during uplifting. The motion of the pipe may be reversed, if the unloading (i.e. upwards motion)/reloading (i.e. downwards motion) is not large enough. Arbitrary reversals from the bounding loop are marked with a dashed line as shown in Fig. 3.1 and may occur at any point along the loop.

An effect that is not considered in the force-deflection curve is that the continuous load cycles will degrade the soil, see Sec. .

Chapter 4

Vertical Soil Models

A soil model may be established upon model tests and calibrated through numerical simulations (Aubeny et al., 2006; Bridge et al., 2004). It is crucial that the models adequately describe the soil stiffness. The state of the surrounding soil affects the level of bending moments and consequently the fatigue life of a riser. Soft clay is nonlinear and complex. Special care must therefore be given to the choice of models and soil parameters when studying the soil-riser interaction in the touchdown area. Traditionally, linear stiffness models was applied. For detailed modeling of the interaction in soft clay, a more proper description is needed.

In the following sections, the soil models by Aubeny et al. (2006) and Bridge et al. (2004) are presented which are denoted Aubeny's non-degradation model and Bridge's model respectively. These two proposed models involve only the vertical deflections of the riser. The effect of suction is considered, however, in the Aubeny's model the soil degradation is neglected. In Sec. 4.3 the calculation of the soil degradation is studied by Aubeny et al. (2008).

4.1 Bridge's Model

Bridge et al. (2004) developed models for description of the soil stiffness and suction for vertical movements based on the published test data from STRIDE, CARISIMA and other previous published literature. Fig. 4.1 depicts the pipe- soil interaction curve developed by Bridge et al. (2004).

STRIDE JIP was the first full-scale test program for investigating the effect of fluid and riser-soil interaction on a catenary riser at the touchdown point. The test was conducted over a period of three months in a tidal Harbour in West England by 2H Offshore Engineering (Willis et al., 2001). An 110m long SCR was suspended from an actuator on the harbor and fixed by an anchor to a soft, flat and undisturbed seabed at the other end. Wave and vessel drift forces were applied at the top end of the riser to simulate motions of a spar platform in 1000m water depth. Strain gauges along the riser measured vertical and horizontal bending strain.

The CARISIMA JIP (Giertsen et al., 2004) was developed through small-scale pipe-soil interaction test on soft clay conducted by The Norwegian Geotechnical Institute (NGI). Suction force and horizontal resistance force were measured through different tests.,

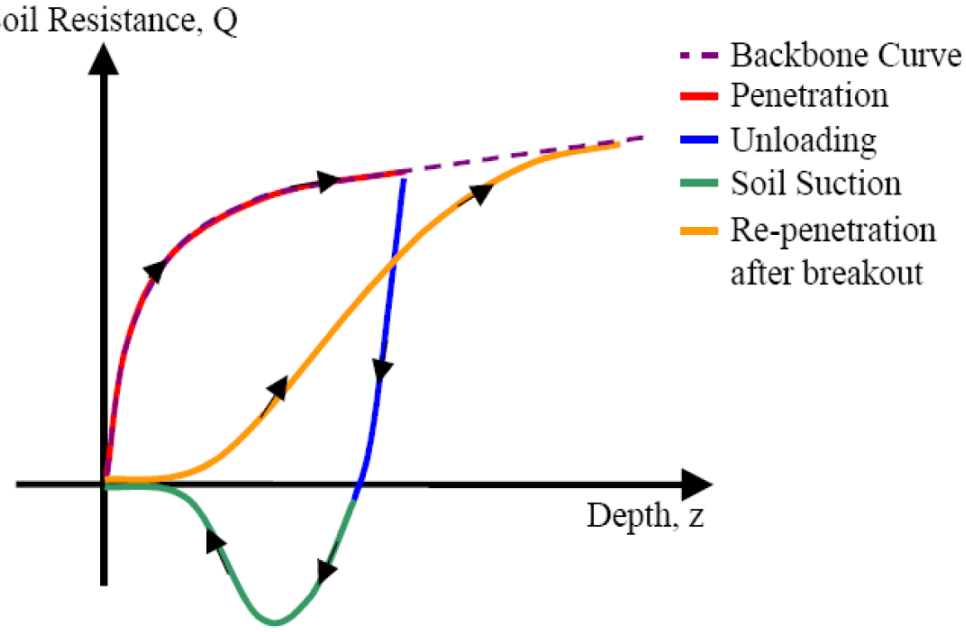

Figure 4.1: Pipe-Soil Interaction Curve (Bridge et al., 2004)

4.1.1 Backbone Curve

By use of bearing capacity theory estimation of the backbone curve per unit length in undrained clay, Q_U, is given by Bridge et al. (2004):

$$Q_U = q_U B \tag{4.1}$$

$$q_U = N_C s_u + \gamma z \tag{4.2}$$

q_U : ultimate bearing pressure
B : bearing width
N_c : dimensionless shape and depth factor
γ : submerged unit weight of the soil
z : depth at pipe invert

The undrained shear strength of the soil, s_u, is evaluated at the pipe invert and assumed linear varying as given by Eq. 4.17. Eq. 4.1 is only valid if the pipe is lying freely on the seabed due to the term γz. N_C is computed by using Skempton's method as follows (Bridge et al., 2004):

$$N_C = \text{Min}\left[5.14\left(1 + 0.23\sqrt{\frac{z_I}{B}}\right)\right] \tag{4.3}$$

If the soil penetration is larger than half the external pipe diameter, the bearing width, B, is taken as the pipe diameter. If the penetration is smaller, the bearing width is obtained by:

$$B = 2\sqrt{Dz_I - z_I^2} \tag{4.4}$$

4.1.2 Soil Stiffness

According to Bridge et al. (2004), there are three types of soil stiffnesses for determining the pipe-soil interaction; static, large displacement dynamic, and small displacements dynamic. Static soil stiffness is the secant stiffness of initial pipe penetration into the virgin soil. Small displacement dynamic stiffness is used for modeling of unloading/re-loading as the pipe re-

mains in-contact with the soil while large displacement dynamic soil stiffness is a modified secant stiffness which includes plastic deformation when the pipe gets partially separated from the soil. Fig. 4.2 illustrate static and small displacement dynamic soil stiffness.

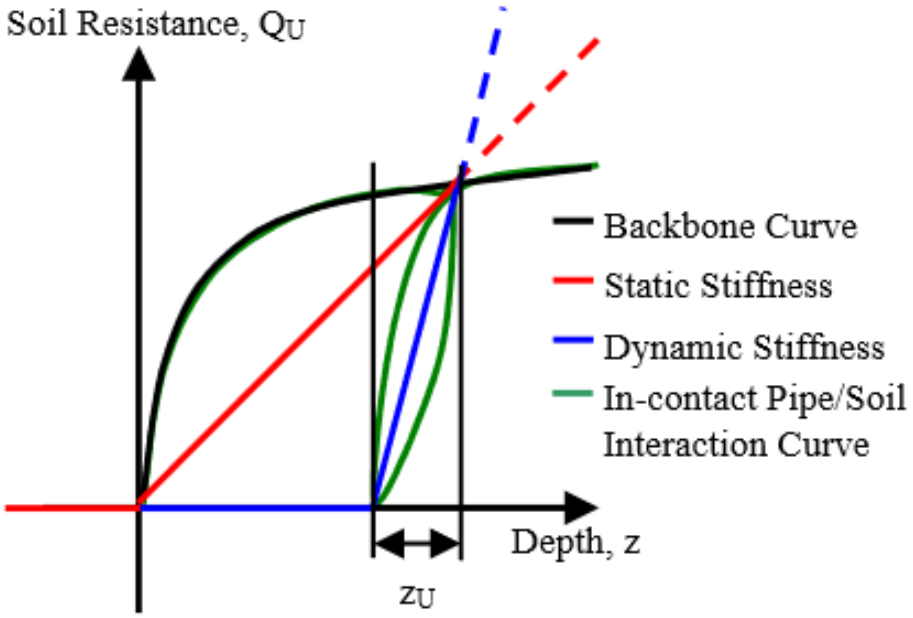

Figure 4.2: Static and Small Deflection Dynamic Stiffness (Bridge et al., 2004)

4.1.3 Small Displacement Dynamic Soil Stiffness

If the pipe remains in contact with the soil throughout the cycle motion, the small displacement dynamic soil stiffness may be used as shown in Fig. 4.2. This soil stiffness may be taken as the tangent stiffness for very small displacements or by using the secant stiffness for larger displacements. The small displacement dynamic soil stiffness,K_z may be expressed by the bearing pressure q_U given by (Bridge et al., 2004):

$$K_z = k_{\text{stiff}} q_U \tag{4.5}$$

$$k_{\text{stiff}} = \frac{1}{\Lambda(1-X) + \frac{X z_D}{D}} \tag{4.6}$$

where k_{stiff} is based on the assumption of a hyperbolic soil model by Audibert which is proposed by STRIDE JIP (Bridge et al., 2004). z_D is the dynamic displacement and X is the soil parameter

equal 0.85 for soft clays. When the soil stiffness is taken as the value at the origin i.e. z_D=0, the most conservative result is obtained.

4.1.4 Large Displacement Dynamic Soil Stiffness

If the riser experiences breakaway or partial separation from the soil, the large displacement dynamic soil stiffness, K_z, is determined, see Fig. 4.3.

The stiffness must be modified compared to the small deflection stiffness due to soil suction. The plastic degradation during partial soil separation must be considered. By assuming the soil surface to be linear elastic, the nonlinear pipe-soil interaction curve can be linearized such that (Bridge et al., 2004):

$$K_z = \frac{Q_U}{Z_U} = \frac{Q_U}{\Lambda D} \tag{4.7}$$

where Z_U is the mobilization distance of the breakaway defined by ΛD. Λ is a non-dimensional parameter that corresponds to the distance the pipe must reach to obtain full soil force. The mobilization distance is the displacements of the unloading curve between the backbone curve and 0 soil resistance, see Fig. 4.2 above. The STRIDE and CARISIMA test data indicated that the normalized mobilization distance to be approximately Λ = 0.025 (Bridge et al., 2004).

In general, the penetration depth is larger than 1/2D. In this case the bearing width of the dynamic stiffness can be taken to 1D. By assuming that the trench depth is smaller than the term γz and by using Λ = 0.025, the large dynamic soil stiffness may be written as:

$$K_z = \frac{1}{\Lambda} N_C s_u = 40 N_C s_u \tag{4.8}$$

The Eq. 4.8 is conservative due to the elastic unloading curve is only taken into account. A less conservative approach is to compute K_z by the force between the backbone curve and the soil suction curve for an appropriate normalization distance, see Fig. 4.3.

By assuming the soil suction to be equal to the penetration force from the backbone curve and using Λ = 0.1 according to STRIDE and CARISIMA data, the large dynamic displacement dy-

namic soil stiffness is estimated by:

$$K_z = \frac{1}{\Lambda} 2 N_C s_u = 20 N_C s_u \tag{4.9}$$

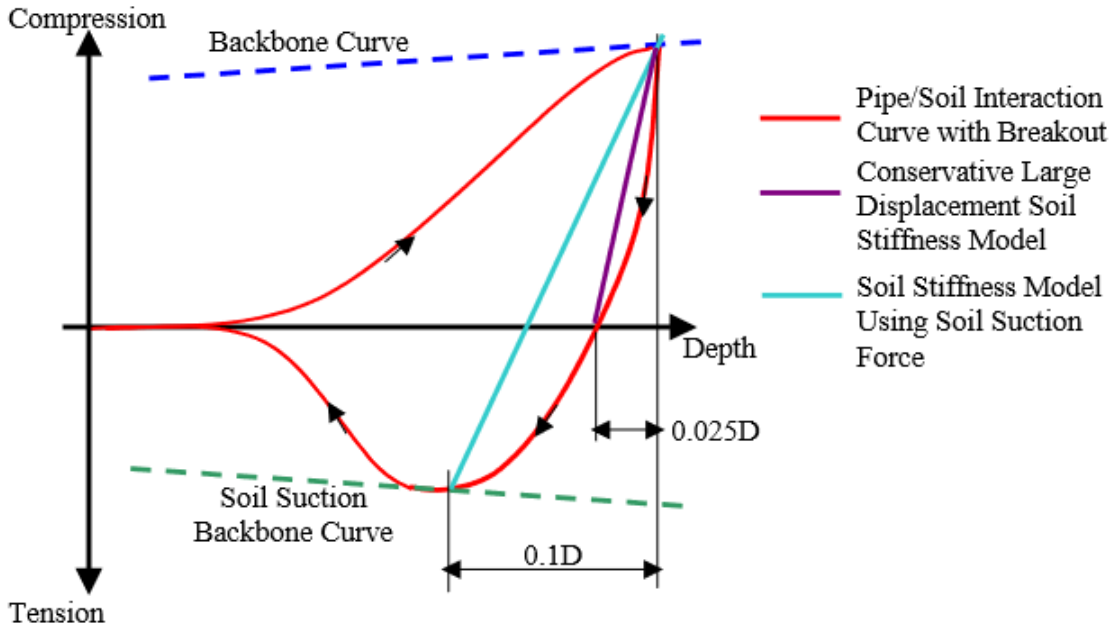

Figure 4.3: Large Deflection Dynamic Stiffness (Bridge et al., 2004)

4.1.5 Soil Suction

Bridge and Willis (2002) developed an upper bound curve considering the soil suction based on small scale tests performed in the STRIDE project (Willis et al., 2001). Fig. 4.4 illustrates the model. The horizontal axis shows the pipe displacement while the vertical axis gives the uplift resistance force. The curve consists of three linear phases:

- Suction mobilization - The suction force increases to a maximum value as the pipe moves upwards.
- Suction plateau - The riser moves further upwards while suction force remains constant.
- Suction release - The suction forces reduce to zero as the pipe moves further upwards.

Two parameters define the soil suction model: the maximum soil suction per unit length $Q_{S,MAX}$

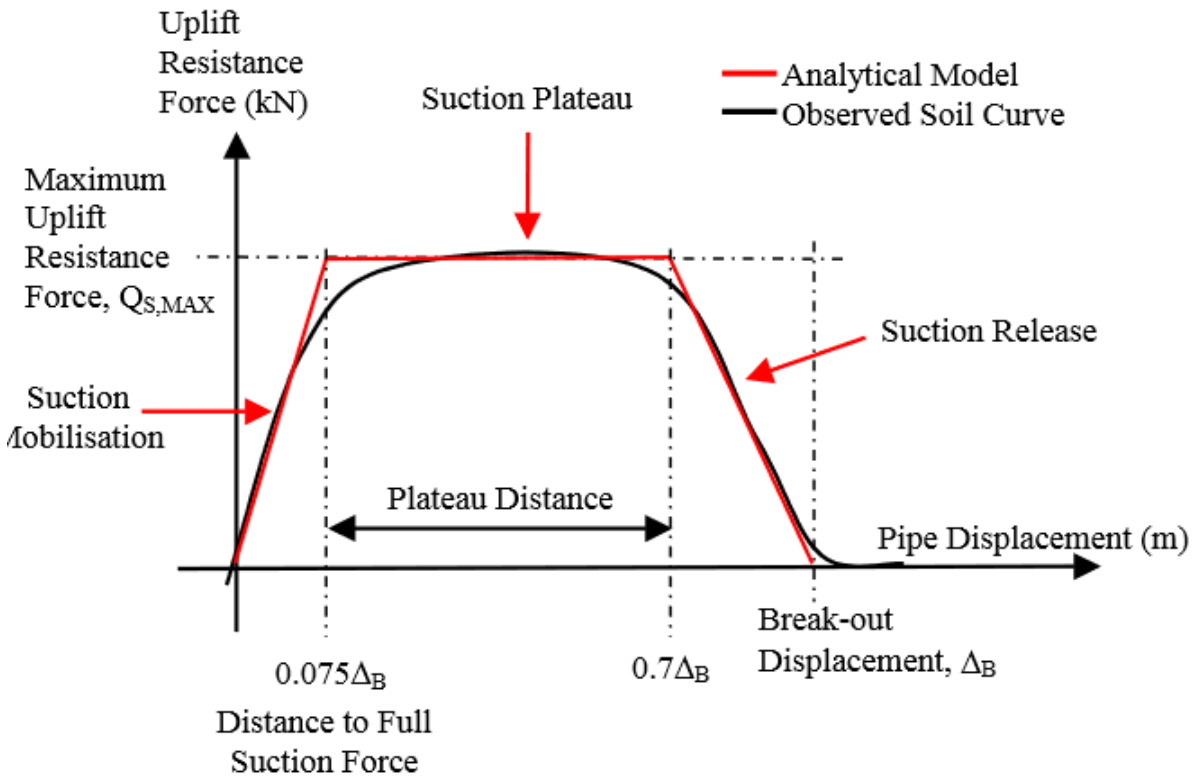

Figure 4.4: Soil Suction Model (Bridge et al., 2004)

and breakout displacement Δ_B. Maximum soil suction force may be calculated based on the following equation (Bridge et al., 2004):

$$Q_{S,MAX} = k_C * k_V * k_T * N * D * s_u \tag{4.10}$$

$$k_V = k_F \left(\frac{V}{D}\right)^{n_F} \tag{4.11}$$

$$k_T = k_{TF} \frac{F_C \sqrt{c_V t}}{LD^2} + C_{TF} \tag{4.12}$$

k_C: Dimensionless cyclic loading factor

k_V: Dimensionless empirical pull-out velocity factor

V: Pull-out velocity

C_V: Coefficient of consolidation [m^2/year]

F_C: Consolidation force [N]

t: Consolidation time

k_F, k_{TF}, n_F, C_{TF}: Empirical constants based on CARISIMA and STRIDE tests

The breakout displacement is given by the expression (Bridge et al., 2004):

$$\Delta_B = k_{DV} * k_{DT} * D \tag{4.13}$$

$$k_{DV} = k_D * V^{n_D} \tag{4.14}$$

$$k_{DT} = k_{TF}\frac{F_C\sqrt{c_v t}}{LD^2} + C_{TF} \tag{4.15}$$

k_{DV}: Non-dimensional empirical breakout displacement factor

k_{DT}: Non-dimensional consolidation time factor

k_D, n_D, k_{DTF}, C_{DTF}: Empirical constant based on STRIDE and CARISIMA test data

The equations above assume the following (Bridge et al., 2004):

- Breakout displacement does not depend on trench depth.
- The suction mobilization distance is proportional to the breakout displacement.
- The plateau distance is proportional to the breakout displacements.
- There is no pipe peeling.

4.1.6 Evaluation of STRIDE

Full-scale response measurements from the harbor test were used to determine the validity of the soil suction model. Maximum and minimum bending moments were computed at strain gauge position during pull-up and lay down tests respectively. The computed bending moments and an analytical suction model were plotted. The analytical model was obtained by numerical modeling of the upper bound curve and calibrated to the full-scale harbor test data. The result showed good correspondence as indicated in Fig. 4.5.

The difference in bending moment response between a pull-up and lay down test is a result of soil suction. This was investigated and following conclusions were drawn (Bridge and Willis,

2002):

- After a period of rest, a sudden vertical displacement of a catenary riser at TDP may initiate a peak in bending stress.
- Soil suction forces are subject to hysteresis effects
- The consolidation time influences the soil suction. Short consolidation time may reduce the soil suction.
- Pull up velocity have little impact on bending moment response on a remolded seabed
- Rapid release of suction as the riser moves fast upwards can cause bending responses to oscillate.

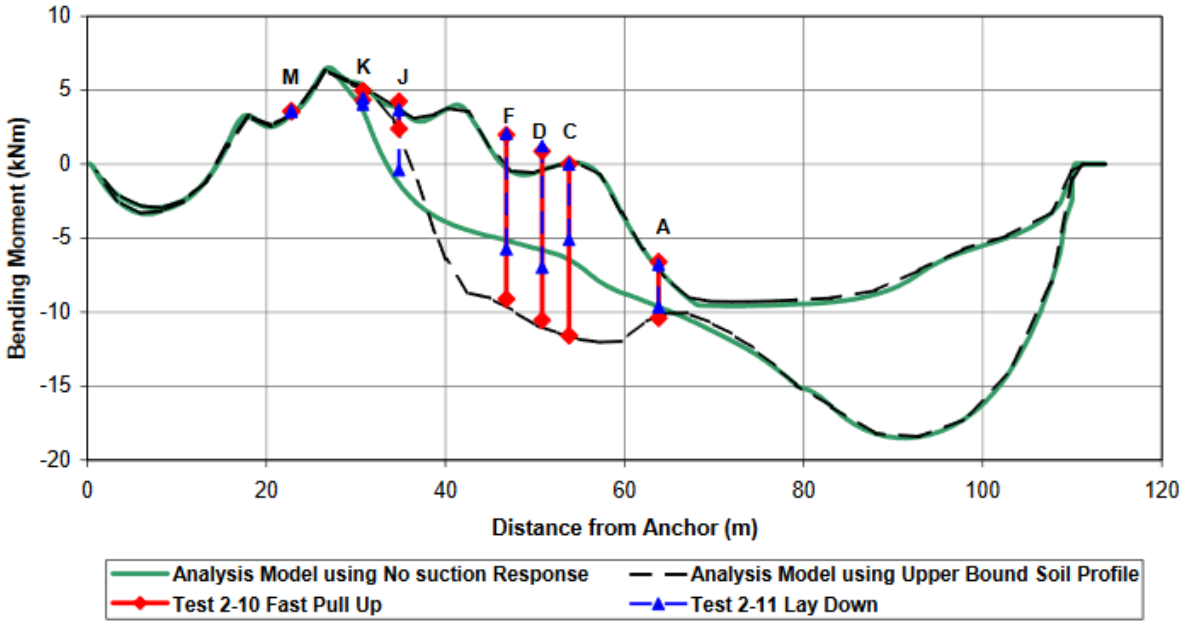

Figure 4.5: Comparison of Test Data and Analytical Bending Moment Envelope (Bridge and Willis, 2002)

4.2 Aubeny's Non-Degradation Model

The non-degradation model developed by Aubeny et al. (2006) neglects the degradation of the soil due to cyclic loading of the SCR. Therefore, trench formation is neglected. The model is based on laboratory model test of a horizontal pipe moving vertically into weak sediments, (Dunlap et al., 1990; Bridge et al., 2004).

Bridge's model defines three types of soil stiffnesses, static stiffness, small- and large displacement dynamic stiffness as described in sec. 4.1.2. The Aubeny's model presents formulations of the soil resistance. Differentiation of the force-deflection curve may be used to determine the soil stiffness.

4.2.1 Backbone Curve

A backbone curve represents the relationship between the maximum compressive soil resistance per unit length as the pipe penetrates the virgin soil. This means that the curve represents the initial penetration due to self weight and further penetration into the soil. The general approach to estimate the penetration into virgin soil is based on bearing capacity theory.An expression for the collapse load, F_z, for a horizontal cylinder embedded in a trench is given by:

$$F_z = N_p s_u D \tag{4.16}$$

where N_p is the non-dimensional bearing factor, s_u is the shear strength of undrained soil and D is the external cylinder diameter.

Murff et al. (1989) presented an estimate for the collapse load for a horizontal embedded cylinder up to a trench of D/2. An upper and lower bound plasticity solution for full or no adhesion was investigated, where effects of soil heave and strength were considered. Aubeny et al. (2005) studied the collapse at an embedded pipe invert in cohesive soil. They extended this plasticity solution for a trench depth up to 5D for a linearly increasing static undrained soil shear strength, s_u given by Willis et al. (2001):

$$s_u = s_{u0} + s_{ug} z \tag{4.17}$$

where s_{u0} is the shear strength of the soil at seabed surface and s_{ug} is the shear strength gradient. (See Fig. 4.6 for explanation).

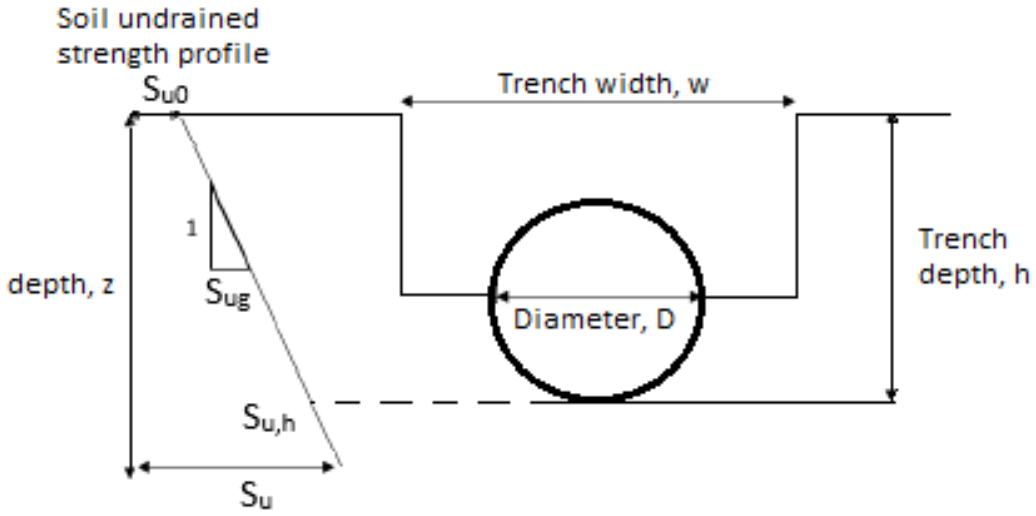

Figure 4.6: Seabed Characteristics (Aubeny et al., 2006)

A power law function was formulated for the bearing factor N_p for trench width $w/D = 1$ at the pipe invert in terms of the static undrained shear strength given by Aubeny et al. (2005):

$$N_p = \frac{F_z}{s_{u,h}D} = a(h/D)^b \tag{4.18}$$

where a and b are fitting constants depending on pipe roughness and the trench depth, h for initial penetration and soil profile. Values can be found in Tab. 4.1.

Table 4.1: Fitting Coefficients for Power Law Function, N_p, at trench depth (Aubeny et al., 2005)

Pipe roughness	$\frac{h}{D} < 0.5$	$\frac{h}{D} > 0.5$
Smooth	$a = 4.97$ $b = 0.23$	$a = 4.88$ $b = 0.21$
Rough	$a = 6.73$ $b = 0.29$	$a = 6.15$ $b = 0.15$

Aubeny et al. (2005) studies showed that the the bearing factor in Eq. 4.18 is not affected by the change of soil strength as indicated by the non-dimensional parameter $\eta = s_{ug}D/s_{u0}$. This may be assumed as long as the shear strength at the bottom of the trench, $c_{u,h}$ in Fig. 4.6, is used as the strength in Eq. 4.17. The estimation of the quasi-static collapse load may hence be written

as:

$$F_z = a(h/D)^b(s_{u0} + s_{ug}h)D \tag{4.19}$$

The pipe, however, may generate a larger trench width than 1D. The width of the trench affects the bearing factor N_p. (Aubeny et al., 2006) studies showed that a widened trench, experiences a reduction in the maximum bearing resistance N_{pmax} at large h/D. When a sufficiently large w/D is reached, the side wall effects become negligible. This is shown in Fig. 4.7.

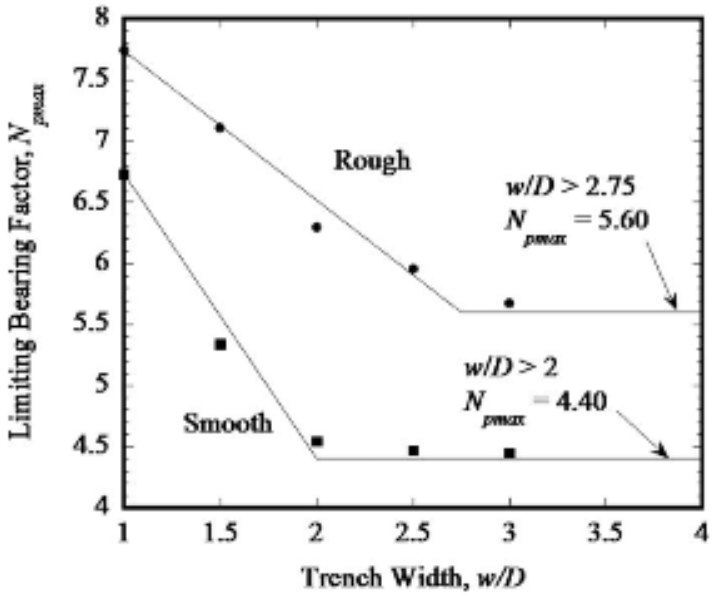

Figure 4.7: Effect of Trench Width on Maximum Soil Resistance, N_{pmax} (Aubeny et al., 2006)

The limit for which trench effects are taken into account is approximate $w/D = 2.75$ and $w/D = 2$ for a rough and a smooth pipe respectively. For different ratio w/D and boundary roughness, the maximum bearing capacity is estimated by following equations (Aubeny et al., 2006):

$$\text{Rough pipe:} \quad N_{Pmax} = 7.74 - 1.22(w/D - 1) \qquad w/D < 2.75 \tag{4.20}$$

$$N_{Pmax} = 5.60 \qquad w/D > 2.75 \tag{4.21}$$

$$\text{Smooth pipe:} \quad N_{Pmax} = 6.73 - 2.33(w/D - 1) \qquad w/D < 2 \tag{4.22}$$

$$N_{Pmax} = 4.40 \qquad w/D < 2 \tag{4.23}$$

4.2.2 Bounding Loop

As touch upon earlier, the bounding loop is defined by the enclosed loop 1-2-3-1 shown in Fig. 3.1. Only sufficiently large unloading and re-loading after the initial penetration will end the bounding loop i.e. condition of extreme displacement. In this subsection, the different paths of this loop will be given a thorough description.

Elastic rebound stretches from point 1 to point 2 and describes the soil resistance when riser is uplifted. Point 1, which is positioned at the end of the backbone curve, is the starting point of the unload- reload process. Point 2 points out the maximum soil suction force and can be calculated by the relation to the maximum compressive soil force at point 1:

$$F_{z2} = -\phi F_{z1} \tag{4.24}$$

where ϕ is the dimensionless tension limit. The penetration depth at point 2, z_2 is found by application of Eq. 4.26:

$$z_2 = z_1 - \frac{(1+\omega)F_{z1}}{k_0}\frac{1+\phi}{\omega-\phi} \tag{4.25}$$

where the parameters k_0 and ω determine the asymptotic value of the hyperbola as seen in Fig. 4.8.The estimation of the soil resistance along the elastic rebound curve, F_z, is based on a hyperbolic relationship:

$$F_z = F_{z1} + \frac{z - z_1}{\frac{1}{k_0} + \chi\frac{z-z_1}{(1+\omega)F_{z1}}} \tag{4.26}$$

where the parameter χ is 1 for loading and -1 for unloading.

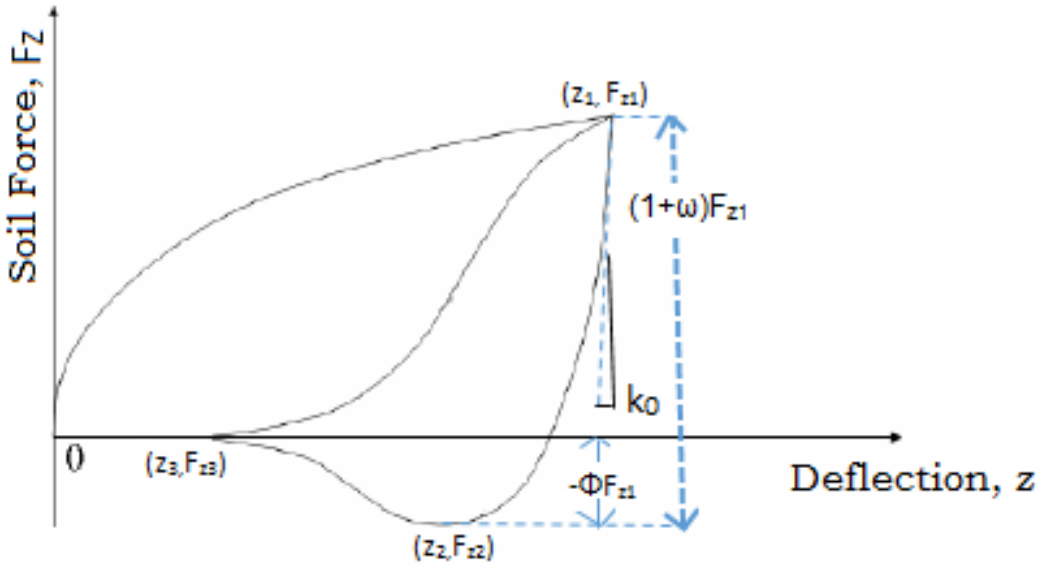

Figure 4.8: Model Parameters of Elastic Rebound Curve (Jiao, 2007)

Partial soil separation denotes the curve that stretches from point 2 to point 3. The suction force reduces after point 2 until the pipe is fully separated from the soil at point 3. Vertical deflection at point 3, z_3, is calculated by using a model parameter ψ and the following relation:

$$z_3 = z_2 - \psi(z_1 - z_2) \tag{4.27}$$

The soil resistance along path 2-3 on the curve is determined from the cubic relationship given by:

$$F_z = \frac{F_{z2}}{2} + \frac{F_{z2}}{4}\left[3\left(\frac{z - z_0}{z_m}\right) - \left(\frac{z - z_0}{z_m}\right)^3\right] \tag{4.28}$$

$$z_0 = \frac{z_2 + z_3}{2} \tag{4.29}$$

$$z_m = \frac{z_2 - z_3}{2} \tag{4.30}$$

Re-contact, that defines the path from point 3 to point 1, shows an increase in the soil resistance as the riser moves downwards. A cubic relationship describes the re-contact with soil resistance

defined by:

$$F_z = \frac{F_{z1}}{2} + \frac{F_{z1}}{4}\left[3\left(\frac{z-z_0}{z_m}\right) - \left(\frac{z-z_0}{z_m}\right)^3\right] \tag{4.31}$$

$$z_0 = \frac{z_1 + z_3}{2} \tag{4.32}$$

$$z_m = \frac{z_1 - z_3}{2} \tag{4.33}$$

4.2.3 Arbitrary Loop Reversals

In general, the cyclic motions of the riser are not large enough for the soil resistance to follow the bounding loop. Instead deflection reversal may occur at any arbitrary point on the bounding loop. If an arbitrary deflection occurs on path 1-2 or 3-1, the soil resistance may be found from a hyperbolic function:

$$F_z = F_{zrb} + \frac{z - z_{rb}}{\frac{1}{k_0} + \chi\frac{z-z_{rb}}{(1+\omega)F_{z1}}} \tag{4.34}$$

where (P_{rb}, z_{rb}) is an arbitrary reversal point on the curve and the parameter χ is 1 for loading and -1 for unloading. If a deflection reversal occurs on path 2-3 on the bounding loop, the soil resistance will follow a cubic relation:

$$F_z = \frac{F_{z1} + F_{zrb}}{2} + \frac{F_{z1} - F_{zrb}}{4}\left[3\left(\frac{z-z_0}{z_m}\right) - \left(\frac{z-z_0}{z_m}\right)^3\right] \tag{4.35}$$

$$z_m = \frac{z_1 - z_{rb}}{2} \tag{4.36}$$

$$z_0 = \frac{z_1 + z_{rb}}{2} \tag{4.37}$$

An arbitrary reversal may occur within the bounding loop from path Eq. 4.34 or Eq. 4.35. This is shown in Fig. 4.9 which also includes a reversal on the bounding loop at point (P_{rB}, z_{rB}) . The calculation of soil resistance from a reversal at point (P_r, z_r) is formulated by:

$$F_z = F_{zr} + \frac{z - z_r}{\frac{1}{k_0} + \chi\frac{z-z_r}{(1+\omega)F_{z1}}} \tag{4.38}$$

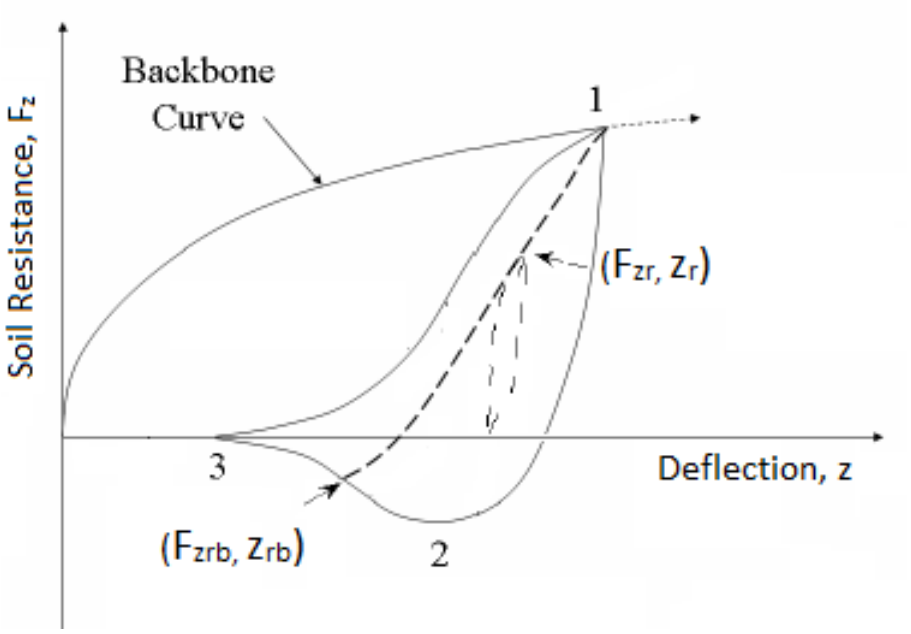

Figure 4.9: Arbitrary Reversals within and from Bounding Loop

The time history of the riser motions predicts further development of the load-deflection curve. The following parameters determine the description of the path:

- Load direction parameter χ
- (F_{z1},z_1), Point of maximum resistance
- (F_{zrb},z_{rb}), Point of last deflection reversal on bounding curve
- (F_{zr},z_r), Point of last deflection within bounding loop

The riser-soil interactions are a complex process. Especially the soil stiffness is hard to determine. A minor error in the measurements of the stiffness will provoke even larger deviation in the result of the analysis. Tab. 4.2 tabulates different soil parameters interpreted from tests. k_0 may be measured from the tangent of the load-deflection curve.

At small vertical deflection, a small error in the k_0 will be amplified in load or deflection measurements. The soil parameters of the mudline strength, s_{u0}, and the soil strength gradient, s_{ug}, have a large impact on soil stiffness. The soil provides stiffness which is added to the stiffness contributions of the riser elements. Stiffness affects the responses and the bending stresses in

Table 4.2: Soil Model Parameters Based on Dunlap et al.(1990) Test Data

Parameter	Description	Value
a	Backbone Curve Coefficient	6.70
b	Backbone Curve Exponent	0.254
k_0/s_{u0}	Unload Initial Stiffness	660
ω	Unload Large Deflections	0.433
ϕ	Unload Tension Limit	0.203
ψ	Soil-Riser Separation	0.661

the riser. The fatigue life may be significantly altered by a change in the stiffness parameters.

4.3 Aubeny's Degradation Model

The soil stiffness reduces due to cyclic loading and consequently there is a formation of a trench. A trench has a positive effect on the fatigue life of an SCR. It reduces the curvature of the riser at TDP and consequently leads to a reduction of bending moments.

To account for the soil stiffness reduction under cyclic loading an empirical formulation is proposed. The accumulated deflection, λ_n , is computed by (Jiao, 2007):

$$\lambda_n = \sum_{i=1}^{n} |\Delta z_i| \tag{4.39}$$

This expression is a measure of energy dissipation. Δz_i is the penetration per incremental step, i, as one moves along the curve. The apparent maximum penetration, z_1* is calculated by Aubeny et al. (2008):

$$z_1^* = z_1 + \alpha_d (\lambda_n)_d^{\beta} \tag{4.40}$$

where z_1 is the deflection due to self-weight of the riser. Aubeny et al. (2008) studied the rate of soil deformation through the degradation parameters α_d and β_d. They found that α_d is dominant in the initial face of the degradation while β_d has a large influence on the maximum penetration when the number of cycle is large. The maximum apparent load, P_1^* is always located on the backbone curve.

$$F_{z1}^* = a(z_1^*/d)^b (s_{u0} + s_{ug} z_1^*) D \tag{4.41}$$

where the parameters a and b represent the shape of the backbone curve and depend on trench conditions and pipe roughness. s_{u0} is the shear strength at the mudline while s_{ug} defines the strength gradient. D is the external diameter of the riser. As the vertical deflection accumulates, point (z_1^*, F_{z1}^*) moves along the backbone curve controlling the degree of soil degradation as illustrated in Fig. 4.10.

By inserting this degradation rule into the non-degradation soil model established by Aubeny et al. (2006), the soil behavior during riser motions in a more realistic way. In this thesis, such a complete model is developed. More information of how the model is formed is written in

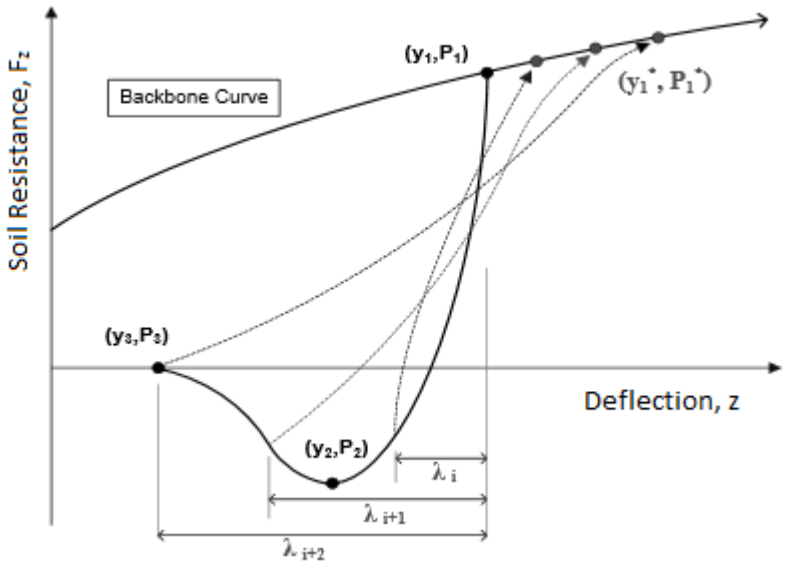

Figure 4.10: Degradation Rule (Aubeny et al., 2008)

subsections 8.1.2 to 8.1.6.

Due to cyclic loading, the soil will deform plastically and consequently start forming a trench. Fig. 4.11 depicts a load-deflection curve accounting for degradation of the soil for some loading cycles. The magnitude of the applied loading is the same for each cycle. The soil degradation parameter is equal to $\beta = 0.5$ (Jiao, 2007). The effects of water entrainment, reconsolidation, erosion of soil and thixotropy of the soil on the seabed are neglected (Nakhaee and Zhang, 2010; Nakhaee et al., 2008). On the other hand, the plastic deformation of the seabed soil and thus trench formation is considered. Every single cycle as seen in the figure is identical to the non-degradation loop in Fig 5.1 except the soil deformation. The vertical deflection increases after every cycle and the loops are moving towards the right as the soil degrades. Fig. 4.11 is exaggerated to demonstrate the effect os stiffness reduction. In reality, many loading cycles must occur for the soil degradation to be a concern.

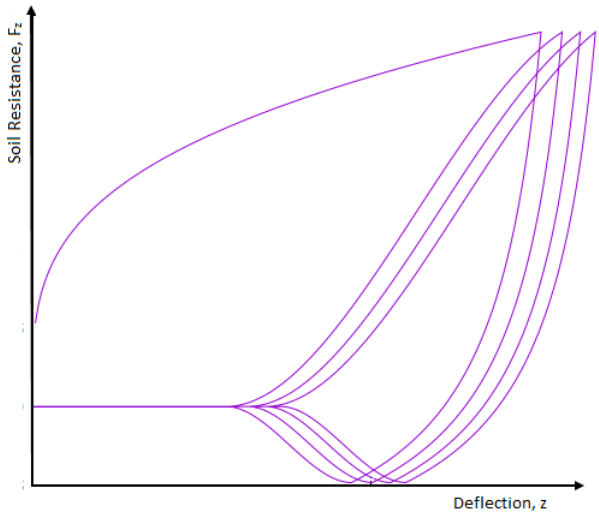

Figure 4.11: Degrading Soil Model under Repeatedly Loading Cycles

Chapter 5

Lateral Pipe-Soil Interaction

Lateral displacements of an SCR are due to a combination of high temperature, high pressure and horizontal vessel motions. These components create compressive forces in the riser. Global buckles will start to initiate when the axial compressive forces become significant. Also, the vessel motion induces buckles.

For the lateral riser interaction problem, a lateral soil model for a pipeline resting on the seabed is adopted. This link is not valid to the vertical riser interaction problem. Vertical riser interaction models are based on cyclic motions of the riser while its catenary shape is maintained. The vertical soil model for a riser problem includes stages of initial plastic penetration, elastic unloading and elastic/plastic reloading. Vertical soil models for a pipeline, however, reflect upon a buried pipe that exhibits global buckling, the so-called upheaval buckling. The pipe will tend to move upwards due to the interaction between axial compressive force and overbend imperfections in the pipeline (DNV, 2007c). There exist models and standards for pipelines, and thus, the lateral soil behavior is approximated by these.

Soil models for small or large lateral displacements of a pipeline involve different physical mechanisms. In Sec. 5.2 and in Sec. 5.3 these mechanisms are described. First, the physical process of global buckling is described by considering the effective axial force.

5.1 Formation of Lateral Buckling of Pipeline

A pipeline resting on the seabed experiences lateral displacements due to high internal pressure and temperatures when operating (Bruton et al., 2008). The pipe tends to expand. The expansion, however, is restricted by axial friction between the soil and the pipe. Large axial compression stresses are developed in the pipe wall due to restrictions to expand axially. Thus, the internal axial pressure must be relieved through buckling. If the pipeline is allowed to buckle uncontrolled, the pipeline can be severely damaged. A deep water solution is to control the formation of lateral buckling of the pipe at specified location by buckle spacing.

At each end of the pipeline, there are usually no constraints. Thus, the forces there are zero. By introducing the effective axial force, global buckling can be calculated without studying the details of the internal and/or global pressure. The effective axial force is obtained by considering the external and internal pressure to act over a closed surface (Fyrileiv and Collberg, 2005). Fig. 5.1 illustrate a section of pipeline subjected to external pressure and an axial force, denoted the true wall force, N_A, which is the only sectional force acting.

The true problem can be decomposed into two parts, as shown to the left in Fig. 5.1. The middle pipe section is exposed to external hydrostatic pressure over a closed surface. The resultant gives the buoyancy force of the section. In the right section external force, $p_e A_e$, and the axial force are acting.

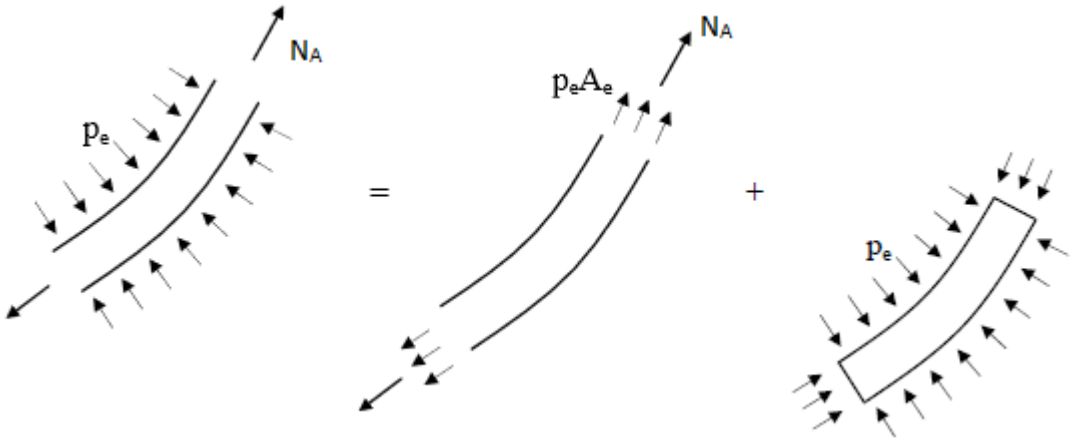

Figure 5.1: The "true" Problem Split into an Equivalent Physical Problem- External Pressure (Fyrileiv and Collberg, 2005).

The same way of thinking is applied to the internal force consideration as seen in Fig. 5.2. The internal pressure of the liquid, p_i, is acting over a closed surface. The force is balanced by the axial force, N_A, and the end cap force $p_i A_i$. According to the report DNV (2007a), temperature

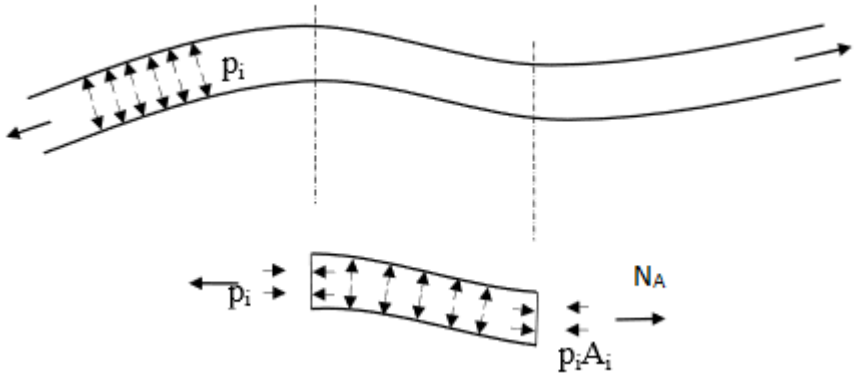

Figure 5.2: The"true" Problem Split into an Equivalent Problem- Internal Pressure (Fyrileiv and Collberg, 2005)

and internal pressure create effective axial compressive forces, S_0, in the pipeline:

$$S_0 = N_A - p_i A_e + p_e A_e \tag{5.1}$$

Sectional forces such as shear force and bending moments are here omitted for simplicity. Integrated effects of the pressure must also be taken into account, which gives the buoyancy and the weight of internal liquid. Here the "true" system is replaced by an equivalent physical system. When the effective axial force is large enough, global buckling of the pipeline may be initiated. Local buckling, however, is dominated by the local stress, the so-called true stress, and the hoop stress in the pipe wall (Bruton et al., 2008).

The largest uncertainties in the lateral interaction models are due to the formation of buckles (Bruton et al., 2008) in combination with the sensitivity in axial and lateral soil resistance. In the design of lateral buckling, an upper and lower bound of the axial soil friction may be obtained to capture the uncertainty in the soil behavior. Somewhere between the friction ranges, an appropriate friction factor is obtained (Bruton et al., 2008).

A low bound friction means that the pipe is not fully constrained and may experience significant end expansion. Pipeline walking can be initiated due to continuous shutdowns and restarts of

an operation. A heated pipeline will expand, but the axial soil resistance restricts the motion. By cooling the pipe, the pipe will not return to its original position due to the axial soil resistance.

A fully constrained condition can occur for an upper bound friction. Pipeline walking will not be present, as part of the pipe length is axially restrained from moving. An increase in effective axial force may, however, induce lateral buckling. The effective axial force for a restrained straight pipe is used.

The true force for a fully restrained straight pipe in the pipeline during operating conditions is given by (DNV, 2012):

$$N = H - p_e A_e + \nu A_s \frac{p_i D_i}{2 t_p} - A_s \alpha_T \Delta T E \tag{5.2}$$

where H is the effective residual lay tension, A_s is the pipe steel cross-section area, t_p is the steel thickness, D_i is the internal diameter and α_T is the thermal expansion coefficient. p_i and ΔT is the internal pressure difference and temperature difference respectively compared to as laid condition. E is the elastic modulus and ν is the Poisson's ratio

When the pipeline is operating, the true axial force gets a contribution from thermal expansion ($-A_s \Delta T E$) that leads to compression. The other part is due to the hoop stress ($\nu \sigma_h A_s$) resulting in tensile force as it is restrained to move axially. The radial stress, hoop stress, is assumed constant across the pipe thickness.

Assuming that buckling occurs more than one anchor length from the end of the pipeline and the pipeline is straight. The effective axial force for a restrained straight pipe is obtained by inserting Eq. 5.2 into Eq. 5.1.

$$S_0 = H - p_i A_i + \nu A_s \frac{p_i D_i}{2 t_p} - A_s \alpha_T \Delta T E \tag{5.3}$$

$$\approx H - \Delta p_i A_i (1 - 2\nu) - A_s E \alpha_T \Delta T \tag{5.4}$$

Fig. 5.3 depicts how global buckling proceeds. Before start-up, the pipe contains effective residual lay tension. At the free ends, the effective axial force is zero as there are no restrictions to move. Gradually the compression force increases away from the ends. The increase is proportional to the soil resistance until it reaches the residual lay tension. When operating the effective

axial force may increase from 0 at the free ends to a fully constrained condition over some of the pipeline's length. The effective axial compression forces build up as the pipe is restricted from moving axially due to the seabed soil. An effective axial force larger than the mean critical buckling force, shown by the dotted line, indicates a pipe susceptible to lateral buckling. The dotted line is calculated for a member in air, the so-called Euler buckling. In reality, the buckling force limit is higher. The fully constrained force will decay due to heat loss away from the reservoir (geothermic heat) (Bruton et al., 2008).

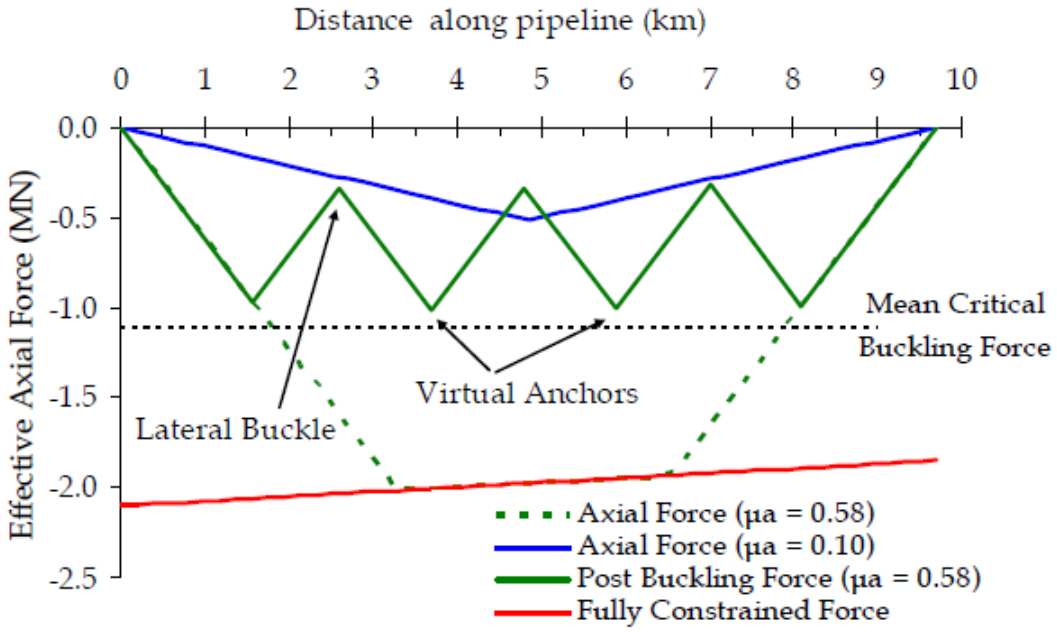

Figure 5.3: Effective Axial Force in a Short Pipeline for Pre-and Post Buckling (Bruton et al., 2008)

Lateral buckles can be formed when the effective axial force is equal to the horizontal breakout resistance (DNV, 2007c). Fig. 5.4 describes the formation of buckling due to imperfection. When the effective axial force, S_0 reaches S_{init}, the pipeline will form a buckle. In the post-buckling stage, S_0 drop to S_{post} at point B as illustrated. The shaded area, surrounded by the lines of effective axial force and the potential effective force, indicates the amount of feed-in to the buckle. The amount of feed-in describes how much potential energy that is converted to an axial strain of the pipe.

As temperature and pressure continue to increase, high axial forces build up. Imperfection in the vicinity of the initial buckle may trigger a new one as illustrated in Fig. 5.5. The axial force

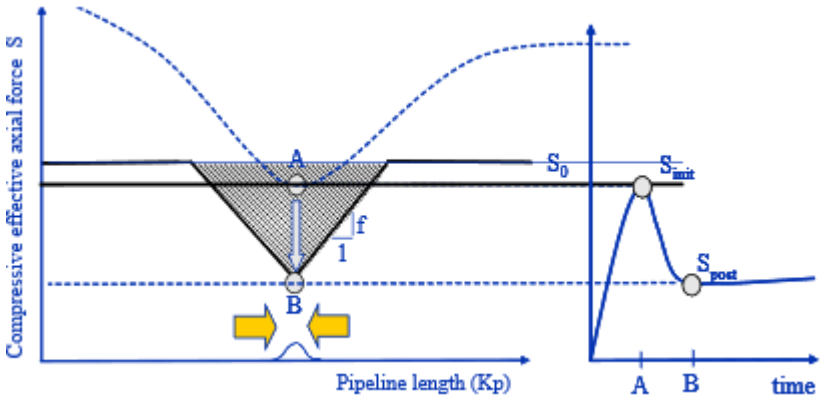

Figure 5.4: First Buckle (DNV, 2007c)

remains constant when the maximum is reached, and feed-in to the buckle will increase.

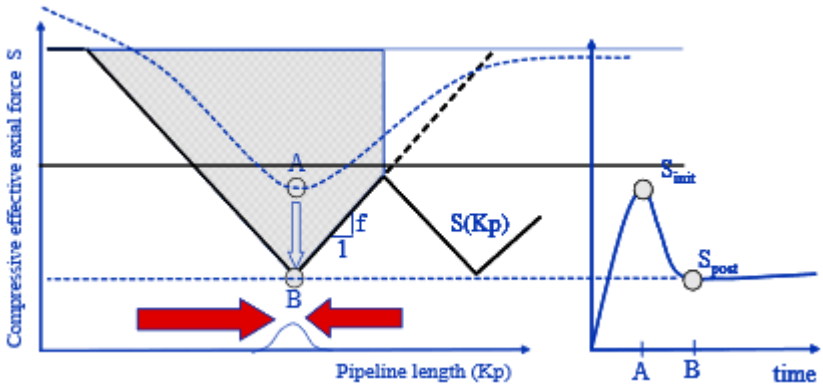

Figure 5.5: Second Buckle (DNV, 2007c)

The effective axial force is influenced by internal pressure and temperatures when operating and the axial friction. In SCR, this force is present due to considerable axial tension at the end of the flowline, high internal pressure and thermal heating from the reservoirs. These factors may cause an SCR to buckle laterally.

5.2 Small Lateral Displacements

The hydrodynamic stability problem considers only small displacements. It neglects elevated temperatures, high pressure, and fixed ends, thus, the only driving force is the hydrodynamic forces through Morison equation (DNV, 2011). Upon small displacements, the pipeline digs

itself into a cavity. The pipeline is stable in the cavity. However, a light pipe may break out several times during a design sea state and accumulate damage. The small-displacement model from the DNV rules considers this phenomenon in Sec. 6.1.1

5.3 Large Lateral Displacements

High temperature and excessive internal pressure may cause large lateral displacements. If the pipeline is subjected to large lateral displacements, the soil is heavily remolded; a berm may develop in front of the pipe and the strength of the soil increases due to consolidation effects. The SAFEBUCK model considers this phenomenon in Sec. 6.2

Chapter 6

Lateral Soil Models

To determine the pipe-soil interaction, a structural analysis of a pipeline is carried out using finite element. The pipe-soil elements may consist of spring and sliders. The simplest model provides an elastic response (spring) and plastic (slider) response in the axial and lateral directions. The nonlinear effects, such as large displacements behavior of brittle breakout behavior and cyclic berm growth, are not captured by these elements. Slider elements include the property of simple friction law (Coulomb friction). The seabed stiffness is modeled by linear or nonlinear springs. A model with linear springs is effective and may give an overview of the interaction. Due to the interaction between the soil and the riser being highly nonlinear, a nonlinear description of the soil is needed.

The Coulomb friction model is associated with a sliding friction as the friction force is acting tangentially between the surface of contacting structures (Gaul and Nitsche, 2001). Fig. 6.1 illustrates the friction model where y is the lateral pipe displacement and F_y is the lateral force. Sliding is activated when the horizontal friction force is larger than the critical limit.

More advanced models are required to examine the effect of large displacement. Several projects have been initiated to model lateral pipe-soil interaction. SAFEBUCK Joint Industry Program (SAFEBUCK JIP) models the lateral soil resistance during large lateral displacements without introducing the Coulomb friction (Bruton et al., 2006). This factor is not appropriate when modeling buckle formation and accretion of soil berms. The model calculates the breakout resistance

and the residual soil resistance. However, the calculation of residual resistance for heavy pipe is limited.

Some lateral soil models are based on small displacements while others concentrate on larger displacements. In the following sections, the different models are presented.

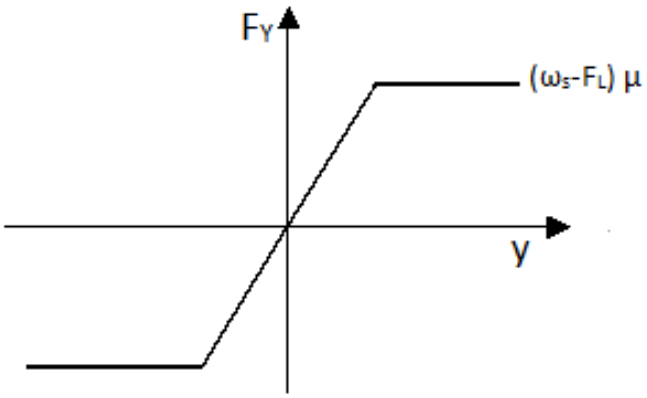

Figure 6.1: Coulomb Friction Model

6.1 Small Displacement Models

In the historical perspective, the lateral soil models developed are based on the behavior of soil resistance of partially buried pipes for small displacements. The investigated interaction problem consists of "on bottom stability" criteria. For this purpose, two frictional components must be included: Coloumb friction and passive soil resistance due to soil penetration when the pipe moves laterally. Verley and Lund developed a model for passive resistance in clay based on a number of large and small scale laboratory tests and numerical analysis. DNV recommends this model.

6.1.1 DNV-RP-F109: On-Bottom Stability Design of Submarine Pipelines

Pipelines may be subjected to ”on bottom stability” problem due to the hydrodynamic loads from current and wave loads. These loads force lateral motions of the pipeline on the seabed. The movements are somehow prevented by the Coulomb friction, a pure soil resistance term based on the nominal pipe weight. The Coulomb friction force can be estimated by:

$$F_y = (w_s - F_L)\mu \tag{6.1}$$

where μ is the Coulomb frictional component and w_s and F_L is the pipe submergence weight and lift force per unit length, respectively.

The other part of the soil resistance is the passive resistance. There is a buildup of passive resistance as the pipe penetrates into the soil. As the pipeline is exerting pressure forces on the soil, shear fracture occurs due to shear cohesive effects. Shear fracture is generated in front of the pipe due to the pipe’s nominal weight as it starts to move. As a result, berms will accrete as the pipe is moving.

A very heavy pipe will resist the hydrodynamic forces from the most extreme sea states and will have an excessive passive resistance. A lighter pipe will experience some lateral buckling from the largest waves and penetrate into the soil while building up passive resistance. The lateral displacement will be approximately less than half a diameter and will be independent of

time. A light pipe will not generate substantial shear fracture and will frequently be experiencing breakouts from its cavity. As the hydrodynamic loads create a lifting force, it may cause the pipe to break out.

Fig. 6.2 depicts the passive resistance model, where F_R is the passive resistance and Y is dimensionless lateral pipe displacement Y = y/D. The passive resistance is divided into four regions (DNV, 2011):

1. Elastic region: The lateral pipe displacement, y, is less than approximately 2 % of the pipe diameter, and the total vertical soil penetration is equal to the initial penetration, z_I.
2. For lateral displacement up to half a diameter there is an increase in penetration and subsequently increase in the passive resistance until breakout. F_{R2} is the breakout resistance.
3. After breakout region: Breakout occurs when the displacement exceeds half a diameter. Both passive soil resistance and penetration decrease. The lateral displacement y_2 is taken as 1D.
4. A larger displacement of approximately one diameter will give a constant passive resistance.

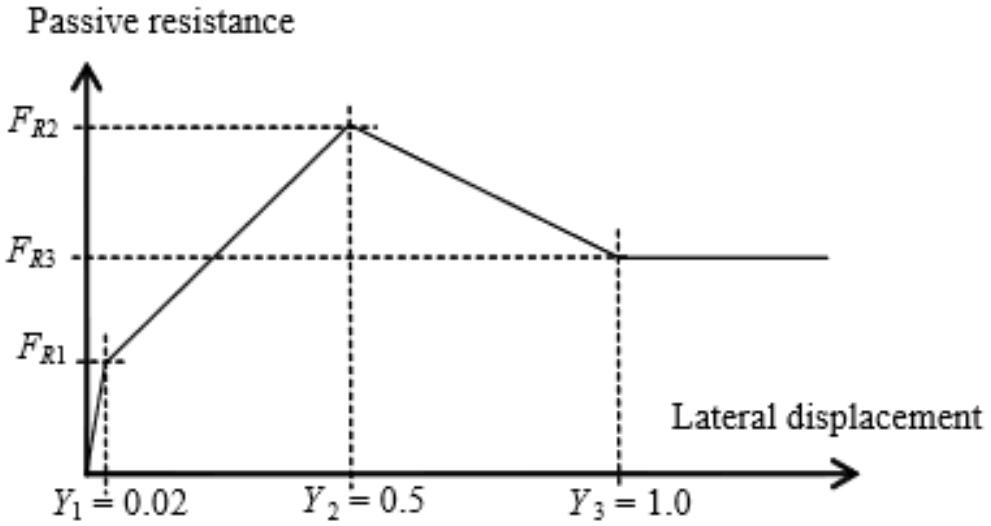

Figure 6.2: Passive Resistance Curve (DNV, 2011)

The passive resistance on clay is determined by (Sævik, 2008):

$$F_R = \frac{4.13\kappa_c(w_s - F_L)}{G_c^{0.392}}\left(\frac{z_p}{D}\right)^{1.31} \tag{6.2}$$

where G_c is the soil strength parameter and D is the external pipe diameter. The total vertical penetration depth, z_{tot} is equal to the initial penetration, z_I and the penetration due to the motion of the pipe, z_m:

$$z_{tot} = z_I + z_m \tag{6.3}$$

where the initial penetration on clay is calculated by:

$$\frac{z_I}{D} = 0.0071\left(\frac{G_c^{0.3}}{\kappa_c}\right)^{3.2} + 0.062\left(\frac{G_c^{0.3}}{\kappa_c}\right)^{0.7} \tag{6.4}$$

$$G_c = \frac{s_u}{D\gamma_s} \tag{6.5}$$

$$\kappa_c = \frac{s_u D}{w_s - F_l} \tag{6.6}$$

where s_u is the undrained shear strength, y_s is the dry unit soil weight and taken as 18 000N/m^3 for clay.

The soil stiffness in the elastic region, K_s, is approximately 20-40N/m for clay. The expression for the passive resistance in this region is given by $F_{R1} = K_s y_1$.

The maximum breakout force, F_{R2} is determined by Eq. 6.2 with the corresponding penetration z_{R2} given by:

$$\frac{z_{R2}}{D} = 0.012\xi^{0.32}\left(\frac{\omega_s}{Ds_u}\right)^{0.637}\left(\frac{a}{D}\right)^{1.31}, \tag{6.7}$$

where a is the lateral oscillation amplitude. For values of $\frac{a}{D}$ less than 0.05, the factor will be equal to 0.05. ξ is equal to $\frac{E_w}{s_u D^2}$ where E_w is the work done by the pipe on the soil.

The limit of maximum soil penetration is taken as:

$$\left(\frac{z_{R2}}{D}\right)_{max} = \frac{\omega_s}{D s_u} G^{0.4} \left(\frac{a}{D}\right)^{0.2}, \qquad \frac{z_{R2}}{D} <= 0.5 \quad \text{and} \quad \frac{a}{D} >= 0.5 \tag{6.8}$$

$$\left(\frac{z_{R2}}{D}\right)_{max} = 0.5, \qquad \frac{z_{R2}}{D} > 0.5 \tag{6.9}$$

The residual resistance, F_3 is determined by Eq. 6.2 with the corresponding penetration z_{R3} given as $z_{R3} = 0.5 z_{R2}$.

6.2 Large Displacement Models

More advanced models are required to examine the effect of large displacement. SAFEBUCK Joint Industry Program (SAFEBUCK JIP) models the lateral soil resistance during large lateral displacements. When the pipe buckles, the pipe may experience large displacements of 5 to 20 diameters (Bruton et al., 2006).

Earlier the oil and gas industry used to restrain the horizontal motion of pipelines by trenching, burying and rock-dumping or by using in-line expansion spools. Some of the pipelines, however, were lying freely on the seabed. As long as the internal pressure and the temperature in the pipeline are within limits, the displacements experienced by the pipe remain small. In deeper water, the temperature and pressure in the pipe increase and the pipeline exhibit large horizontal displacements. The hydrodynamic stability problem is no longer appropriate.

6.2.1 SAFEBUCK JIP

In SAFEBUCK JIP test programme, large scale tests were performed together with small-scale centrifuge tests for soft clay in deep water. The tests were centered on four phases of the pipe-soil interaction:(Bruton et al., 2006):

1. Initial embedment
2. Breakout and suction release
3. Large amplitude monotonic displacement
4. Cyclic response from residual friction and berm interaction

Initial Embedment

The initial pipe embedment illustrated in Fig.6.3 is hard to determine. The largest uncertainty is caused by the additional penetration that comes with the consolidation settlement due to lay-induced cyclic vertical or horizontal loads (Bruton et al., 2006). Another source of uncertainty is due to an over-estimation of the soil strength. If the embedment is small, there will be a softening of the upper part of the soil which is not encountered. The normalized initial pipe

penetration, z_I/D, can be calculated by following equation given by SAFEBUCK (Bruton et al., 2006):

$$\frac{z_I}{D} = \frac{S_t}{45} v^2 = \frac{S_t}{45}\left(\frac{V}{DS_u}\right)^2 \tag{6.10}$$

where S_t is the soil sensitivity and V is the vertical load exerted by the pipe. The design equation is based on a limited data and tends to calculate a higher embedment than the theoretical solution by (Murff et al., 1989).

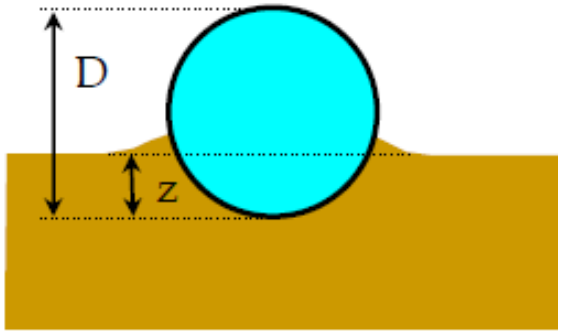

Figure 6.3: Embedded Pipeline (Bruton et al., 2006)

Breakout Resistance

The breakout resistance, $H_{breakout}$, consists of a pure friction term, and a passive resistance as the soil is remoulded and lifted in front of the pipe. The dimensionless term $h_{\text{breakout}} = H_{\text{breakout}}/s_u D$ is calculated by the empirical formula (Bruton et al., 2006):

$$h_{breakout} = 0.2\text{v} + \frac{3}{\sqrt{s_u/\gamma_s D}}\frac{z_{startup}}{D} \tag{6.11}$$

where v is the dimensionless vertical load, V/s_uD and z_{startup} is the embedment depth at startup which does not take the consolidation settlement into account. The term $s_u/\gamma_s D$ is soil strength to weight ratio where s_u is the soil strength at the pipe invert. The breakout resistance is illustrated in Fig. 6.4 for a normally and over-penetrated pipe.

Large Amplitude Monotonic Displacement

Fig. 6.4 depicts four steps of the force-displacement response for the first monotonic displace-

ment. These are described below (Bruton et al., 2006):

- Point 1 defines the first breakout resistance which is dependent on initial penetration.
- Along 1-2 there is a suction release for a normally penetrated pipe and elevation correction for an over-embedded pipe.
- In step 2-3, an active berm is increasing in front of a normally penetrated pipe while for an over-embedded pipe some of the berms are crushed and thus a reduction in resistance.
- Step 3-4 shows a steady state residual friction as no soil is added to the berm in front of the pipe.

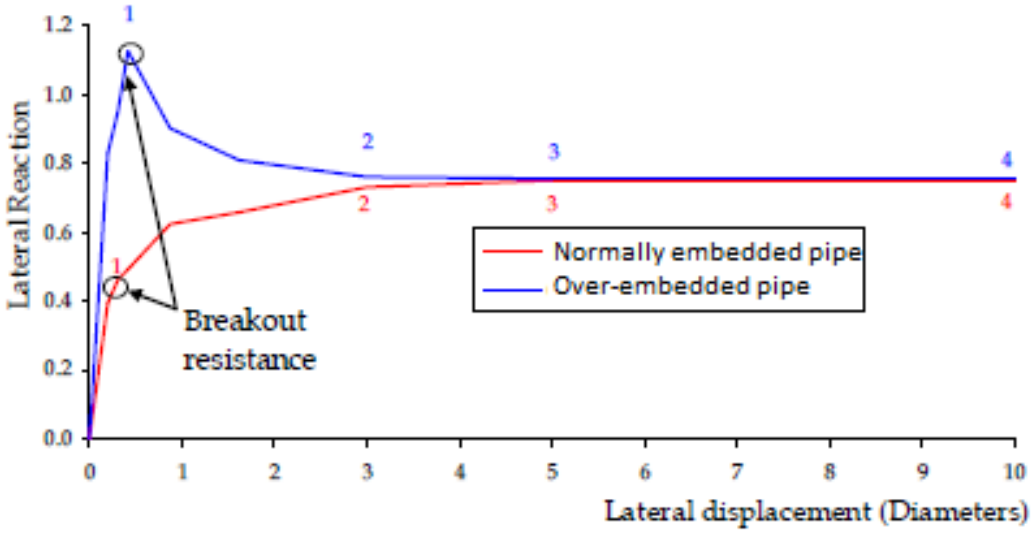

Figure 6.4: Monotonic Lateral Response (Bruton et al., 2006)

Cyclic Lateral Response

Fig. 6.5 illustrates the cyclic response from step 5 to 12 (Bruton et al., 2006). The monotonic lateral response is included as well.

- Step 5-6 Breakout
- Step 6-7 Developing of a berm in front of the pipe
- Step 7-8 Berm interaction
- Step 9-10 Breakout

- Step 10-11 Developing of a berm in front of the pipe
- Step 11-12 Berm interaction

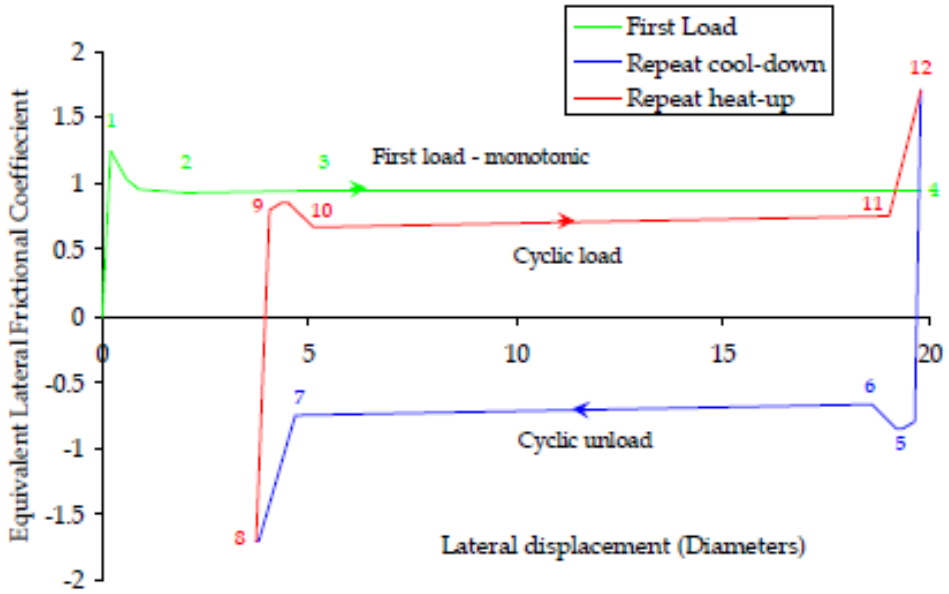

Figure 6.5: Cyclic Lateral Response (Bruton et al., 2006)

Residual Resistance

The breakout resistance for lateral pipe displacement is less than half a diameter. For displacement within 3-5 diameters, the residual resistance is dominant. This is why small displacement models focus on the breakout resistance and models for large lateral buckling concentrate mostly on the residual resistance (Bruton et al., 2006).

The horizontal residual, H_{residual} is reaching for a stabilizing resistance after a breakout. One part of this resistance is a steady state residual equal to the Coulomb friction. The other contribution is due to an additional horizontal resistance. It may be considered as a frictional term, even though it is not. This term is due to the passive resistance F_R i.e. the weight of the soil that entered the berm in front of the pipe. Thus, the horizontal residual force is written as:

$$H_{residual} = \mu(w_s - F_L) + F_R = \mu_e V_{residual} \tag{6.12}$$

The equivalent friction coefficient, μ_e, is obtained by assuming the additional residual term as

frictional.

The residual resistance is made dimensionless $h_{\text{residual}} = H_{\text{residual}} / s_{u1D} D$ and may be calculated by a trend line when plotting the equivalent friction coefficient against the dimensionless term $S_{u1D}\gamma_s D$ as seen in Fig. 6.6. The trend line gives the formula:

$$\frac{h_{residual}}{v_{residual}} = 1 - 0.65\left[1 - exp\left(-\frac{1}{2}\frac{S_{u_{1D}}}{\gamma_s D}\right)\right] \tag{6.13}$$

where the undrained soil strength at a depth of 1D is taken as a reference. The influence of the submerged weight soil is depicted in the figure. For a soft seabed, $\mu_e = \frac{h_{residual}}{v_{residual}}$ goes to 0.39 according to classical plasticity solution. Generally, this value is higher.

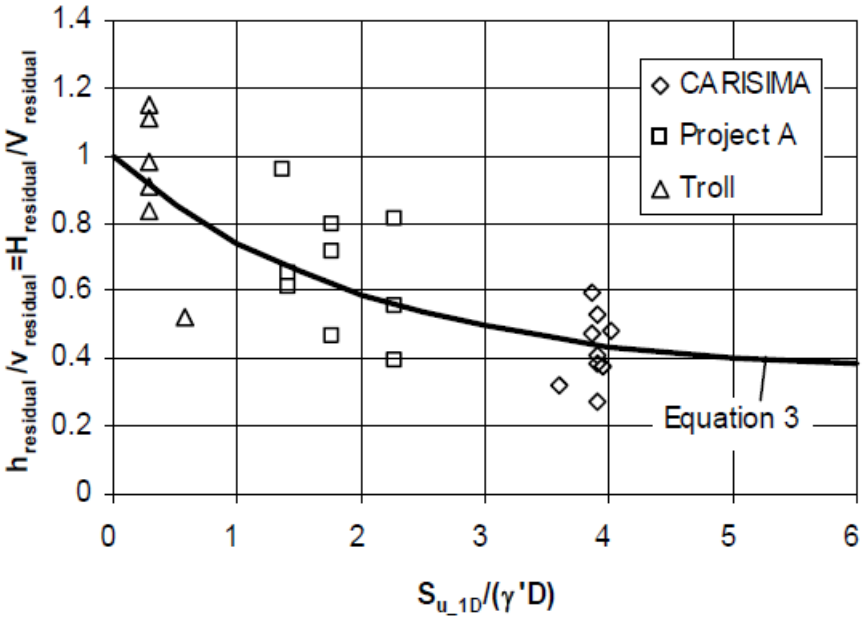

Figure 6.6: Equivalent Friction Coefficient (Bruton et al., 2006)

The ratio of flowline weight to seabed strength ratio $\frac{V}{S_u D}$ governs the large-amplitude lateral response after breakouts. The characteristic response is different for "light" and "heavy" pipes which are illustrated in Fig. 6.7 a and b respectively. The former counts for ratios of $\frac{V}{S_u D}$ approximately below 1.5. In this case, the pipe reaches for a steady residual force after breakout. During the first lateral sweeps, the residual resistance determines the initial shape of the first buckle. For $\frac{V}{S_u D}$ greater than approximately 2.5, the case of "heavy" pipes, the pipeline is forced into the soil again after breakout. The combination of the downward motion and the growing

soil berm in front of the pipe results in a monotonically increasing lateral resistance.

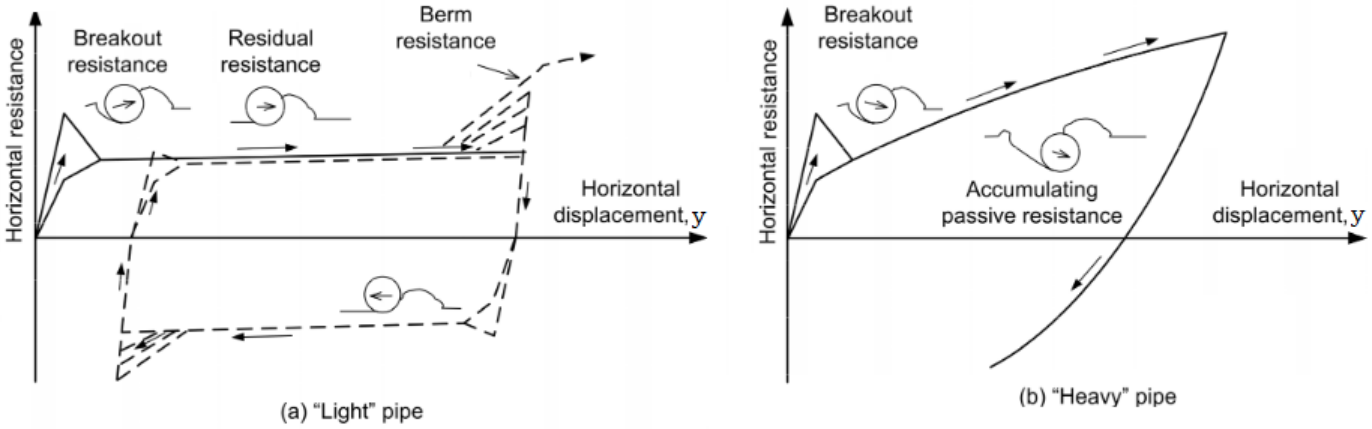

Figure 6.7: Lateral Response Pattern of ”Light” and ”Heavy” Pipe (Bruton et al., 2008)

Cyclic Response with Berm Interaction

When the pipeline is experiencing large lateral displacements, the soil will be swept in front of the pipe. On the first cycle from as laid position static soil berms develop at the ends of the turns as depicted in Fig. 6.8. After a few more sweeps, fresh soils are added to the berm and further growth of lateral displacement will be restrained by the berm. The displacement remains approximately constant.

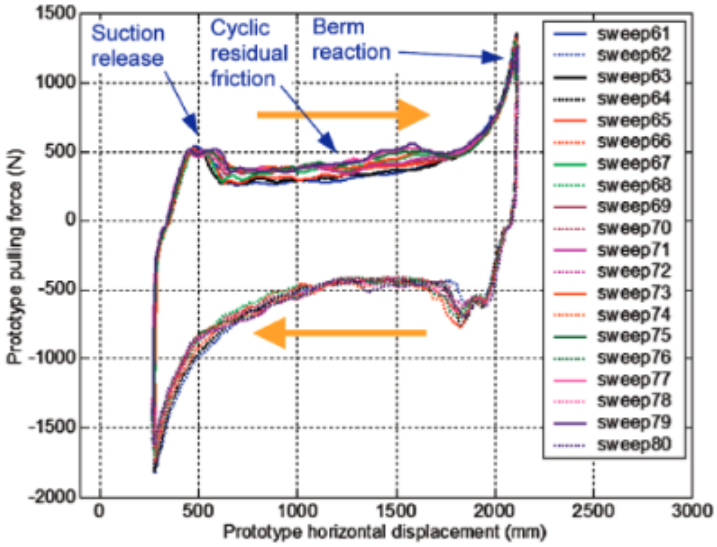

Figure 6.8: Cyclic Lateral Force-Displacement Behavior (Bruton et al., 2006)

The berm accretion in front of the pipe during the cycles helps to build up the soil berms. This is the reason why Coulomb friction, pure friction term, can not be used. This parameter assumes no development of berms and indicates that the buckles will increase for each cycle. However, static soil berms are developed during lateral buckling. Its presence restricts the growth of buckles, so higher stress ranges are obtained (Bruton et al., 2006).

The result from SAFEBUCK test shows the soil behavior over some sweeps and indicates that soil berm resistance may be significant. When the pipe comes in contact with the berm, the horizontal resistance increases from H_{residual} to a total berm resistance H_{berm} with an increase of ΔH_{berm}.

Chapter 7

Numerical Modeling of Pipe-Soil Interaction in SIMLA and RIFLEX

This chapter focuses on the theory behind the modeling of the pipe-soil-interaction with the basis in the software tools SIMLA and RIFLEX, see subsection 2.6. A static analysis followed by a dynamic analysis need to be executed in order to study the interaction. A riser problem may be solved using finite elements, see subsection 2.5. The computer programs, SIMLA and RIFLEX utilize finite elements modeling.

There are different approaches for treating the nonlinearities when computing the dynamic responses of a discretized structure; Nonlinear or linearized time domain or frequency domain analysis. The procedure of a nonlinear time domain analysis for a dynamical problem is a combination of numerical integration of the dynamic equilibrium equations and a type of Newton-Raphson iteration at each step to correct the equilibrium. In this method, the nonlinearities are being accurately described however the approach is time-consuming. The system matrices (i.e. mass, damping and stiffness) must be calculated and triangularized during the iteration. A riser-soil interaction problem requires a nonlinear time domain analysis, due to the nonlinear effect like geometric and boundary effects.

Other methods are by use of a linearized time domain analysis. The computational time is reduced; however, it can only be conducted if the hydrodynamic loading is the significantly largest

nonlinear effect. Numerical integration of the dynamic equilibrium equation is performed by linearization of mass, damping and stiffness on the static equilibrium position. This leads to a linear mechanical system, with nonlinear hydrodynamic loading.

If the solution of the dynamic equilibrium equations can be significantly simplified, frequency domain analysis may be conducted. In this approach, the system matrices are linearized and the hydrodynamic loading is computed at static equilibrium. The transfer functions, which describe the linear relation between the waves and the response, are calculated. This gives a Gaussian response completely described by the wave spectrum and the mean value.

Numerical integration is suited to find the solution of a partial differential equation like the dynamical equilibrium equation. SIMLA uses the HHT -α method while RIFLEX incorporates the numerical integration method Newmark -β family. Both are implicit methods as they address the information from the current and the next time step(s). The static solution procedure is, however, similar for both programs. In nonlinear static analyses, the stiffness matrix is usually updated at each load step. The scheme involves a user defined load control with Newton-Raphson equilibrium iteration at each load step.

The stresses may either be computed with reference to the deformed structure or the initial configuration. True stress refers to the deformed configuration while 2nd Piola- Kirchoff stress relates to the initial configuration. The latter stress is consistent with the Green's strain. By referring to the initial configuration, the physical stress is described for arbitrary rigid body motions. When performing an analysis of slender structures, the rigid body motion may be large compared to strains. In SIMLA and RIFLEX, the reference system is thus taken to be a co-rotational total Lagrange as seen in Fig 7.1, so 2nd Piola-Kirchoff stress and Green's strain is used.

7.1 Nonlinear Static Analysis

In SIMLA and Riflex, static equilibrium configuration may be obtained analytically by 2D catenary equation (rif, 2011; Sævik, 2008). Another alternative is by use of FEM. The current model is then discretized into finite elements with unknown nodal displacements and internal forces.

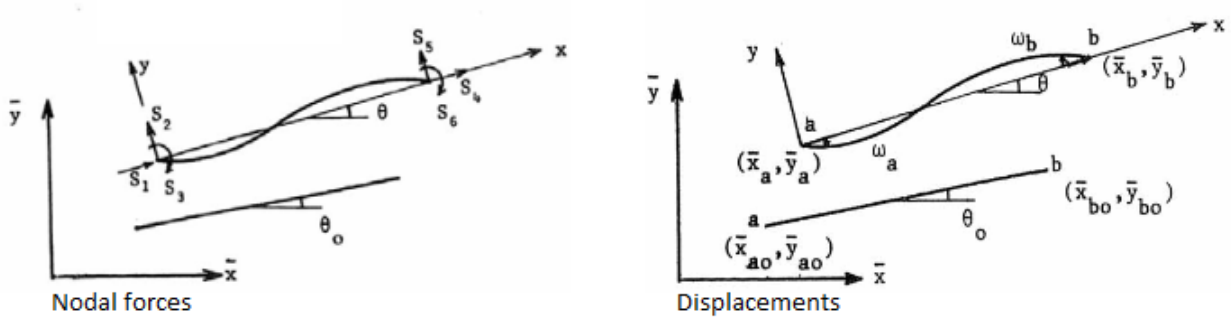

Figure 7.1: Co-Rotational Total Lagrange Formulation (Moan, 2003)

The starting position is a stress-free configuration, and by introducing numerical methods the final static nonlinear equilibrium is obtained between the external force vector $\mathbf{R}^E(\mathbf{r})$ and the internal force vector$\mathbf{R}^S$:

$$\mathbf{R}^S(\mathbf{r}) = \mathbf{R}^E(\mathbf{r}) \tag{7.1}$$

where $\mathbf{r}$ is the system nodal displacement vector that needs to be determined. The structural forces are given by:

$$\mathbf{R}^S = \sum_i (\mathbf{a}^i)^T \mathbf{S}^i = \sum_i (\mathbf{a}^i)^T \mathbf{k}^i \mathbf{a}^i \mathbf{r} = \mathbf{K}\mathbf{r} \tag{7.2}$$

where $\mathbf{a}$ is the connectivity matrix, $\mathbf{S}$ is the element nodal forces, $\mathbf{k}$ and $\mathbf{K}$ are the local and global stiffness matrix respectively, and i is the number of elements.

External loads are increased monotonically with displacements over an extended period of time to obtain the equilibrium configuration. SIMLA and RIFLEX differ between load types. The basic ones are according to (rif, 2011):

1. Volume forces i.e. weight and buoyancy.
2. Specified displacements i.e. the coordinates in stress-free configuration and the final position.
3. Specified forces i.e. nodal point loads
4. Position dependent force i.e. current forces

A load condition constitutes of one or several basic load types. Starting from the stress-free riser

configuration, the load conditions are applied one by one in a stepwise manner. When all loads are applied, static configuration is obtained.

The procedure to achieve static equilibrium is a combination of two numerical methods: Euler-Cauchy that imposes incremental loading and Newton-Raphson that reaches equilibrium by iteration.

7.1.1 Euler-Cauchy Incrementation

This method is based on a stepwise accumulation of external loading (rif, 2011). For each load step, k, a load increment containing external nodal forces, $\Delta\mathbf{R}$, is applied to the discretized model. The displacement increment, $\Delta\mathbf{r}$ is obtained from the load increment and the incremental stiffness matrix $\mathbf{K}_I$. The total displacement is determined when the desired level of external load is reached. The procedure is given by:

$$\Delta\mathbf{R}^E_{k+1} = \mathbf{R}^E_{k+1} - \mathbf{R}^E_k \tag{7.3}$$

$$\Delta\mathbf{r}_{k+1} = \mathbf{K}_I(\mathbf{r}_k)^{-1}\Delta\mathbf{R}^E_{k+1} \tag{7.4}$$

$$\mathbf{r}_{k+1} = \mathbf{r}_k + \Delta\mathbf{r}_{k+1} \tag{7.5}$$

This method does not fulfill equilibrium of Eq. 7.1. There is a deviation between external forces and the internal element forces, yielding an imbalance force vector at load step k given by:

$$\mathbf{R}_k(\mathbf{r}) = \mathbf{R}^S_k(\mathbf{r}) - \mathbf{R}^E_k(\mathbf{r}) \tag{7.6}$$

Fig. 7.2 shows the deviation between the Euler Cauchy approximation and true equilibrium.

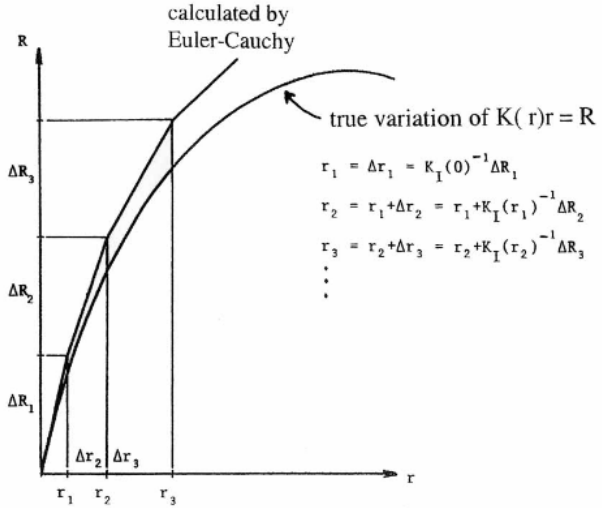

Figure 7.2: Euler-Cauchy Incrementation (Moan, 2003)

7.1.2 Newton-Raphson Iteration

In Newton-Raphson method (see Fig. 7.3), the value for x at $f(x) = 0$ after k steps is determined by:

$$x_{k+1} = x_n - \frac{f(x_k)}{f'(x_k)} \tag{7.7}$$

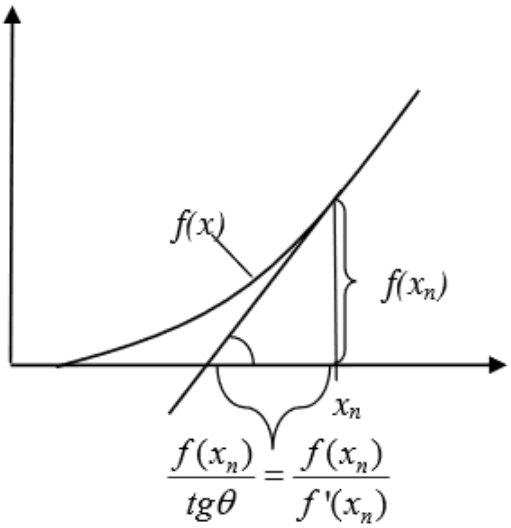

Figure 7.3: Newton-Raphson Method (Moan, 2003)

By generalization, f(x) may represent the deviation of internal and external forces and $\frac{\partial f(x)}{\partial x}$ may be equivalent to K_I(r) at literation step j. The iteration formula for the nodal displacements may hence be written as:

$$\Delta \mathbf{r}^{j+1} = -\left[\mathbf{K}_I^{-1}(\mathbf{r})\right]^j (\mathbf{R}^{S,j} - \mathbf{R}^E) \tag{7.8}$$

$$\mathbf{r}^{j+1} = \Delta \mathbf{r}^{j+1} + \mathbf{r}^j \tag{7.9}$$

The iteration procedure is shown in Fig. 7.4.

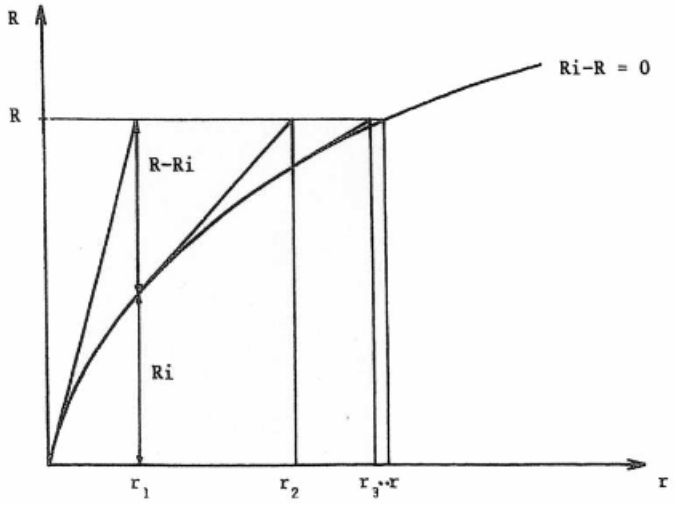

Figure 7.4: Newton-Raphson Iteration (Moan, 2003)

The incremental stiffness matrix, K_I, is computed in each iterative step to determine Δr_{k+1}. This is a time-consuming process, however by using the modified Newton-Raphson, K_I, may stay constant in some steps or for all steps before updating. The computational time reduces, and so does the convergence rate. A convergence criterion is applied to stop the iteration when the acceptable accuracy is reached.

7.1.3 Static Analysis in SIMLA and RIFLEX

In SIMLA and RIFLEX, Euler-Cauchy implementation is frequently applied together with an ordinary Newton-Raphson iteration (rif, 2011; Sævik, 2008).

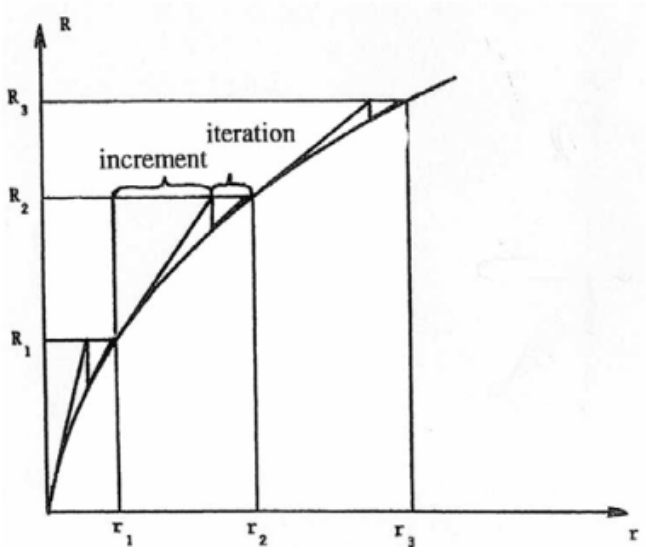

Figure 7.5: Load Step Incrementation with Newton-Raphson Iteration (Moan, 2003)

The external load is applied incrementally. The displacement increments at the next step are based on static equilibrium for the previous step and the external forces at the next step:

$$\Delta \mathbf{r}_k^0 = -\left[\mathbf{K}_I(\mathbf{r}_{k-1})^{-1}\right](\mathbf{R}_{k-1}^S - \mathbf{R}_k^E) \tag{7.10}$$

$$\mathbf{r}_k^0 = \mathbf{r}_{k-1} - \Delta \mathbf{r}_k^0 \tag{7.11}$$

Based on the computed displacements, the assumed static equilibrium at step k may be determined. The force imbalance vector becomes $\mathbf{R}^S(\mathbf{r}_k^0) - \mathbf{R}_k^{\mathbf{E}}$.

In order to achieve equilibrium for each load increment, iteration is used. The force imbalance vector and the displacement vector determined above are applied as start values. The iteration cycle number is defines as j, where $j = 0$ is the corresponding start value. The displacement vector from the incremental procedure is corrected by iteration:

$$\Delta \mathbf{r}_k^j = -\left[\mathbf{K}_I(\mathbf{r}_{k-1})\right]^{-1} \mathbf{R}_k^{j-1} \tag{7.12}$$

$$\mathbf{r}_k^j = \mathbf{r}_k^{j-1} - \Delta \mathbf{r}_k^j \tag{7.13}$$

A convergence criterion is applied to stop the iteration when the accuracy is within limits. The iteration is terminated when the difference between the displacements between two steps are

smaller than:

$$\frac{||\mathbf{r}_k^j|| - ||\mathbf{r}_k^{j-1}||}{||r_k^j||} < \varepsilon \tag{7.14}$$

where ε is the tolerance requirement. $||.||$ is a vectornorm which measures the size of a vector. The vectornorm used in SIMLA and Riflex is the so-called modified Euclidean displacement norm defined as:

$$||\mathbf{r}|| = \sqrt{\frac{1}{N_{DOF}} \sum_{k=1}^{N} \mathbf{r}_{ki}^2} \tag{7.15}$$

where N is the number of active translational degrees of freedom. Thus, the summation includes only the translational degree of freedom.

The incremental stiffness matrix, K_I, is based on previous static equilibrium. The incremental stiffness matrix may be expressed as:

$$\mathbf{K}_I = \frac{\partial \mathbf{R}}{\partial \mathbf{r}} = \frac{\partial \mathbf{R}^S}{\partial \mathbf{r}} - \frac{\partial \mathbf{R}^\mathbf{E}}{\partial \mathbf{r}} \tag{7.16}$$

where $\frac{\partial \mathbf{R}^S}{\partial \mathbf{r}}$ is the incremental structural stiffness matrix consisting of the nonlinear material and geometric stiffness matrices. $-\frac{\partial \mathbf{R}^\mathbf{E}}{\partial \mathbf{r}}$ is the load correction stiffness matrix due to change in external loading caused by a change in nodal displacements.

The contact area between the riser and the soil does provide stiffness as well. Due to the boundary condition, the soil, the applied load will not correspond linearly to the deflection. The stiffness contribution from seabed contact may be modeled by vertical bi-linear springs which represent the vertical bottom stiffness. Another part of the stiffness contribution comes from friction forces which are caused by sliding due to current loading.

The incremental displacements vector is obtained by assuming linearity of an increment along the load-displacement curve. The incremental rotations are thus represented as some sort of a vector. This assumption is valid when the incremental rotations are small. Bending problems may cause large rotations, thus, it is important to select sufficient small load step.

7.2 Numerical Methods for Nonlinear Dynamic Analysis

The dynamic equilibrium for a nonlinear mechanical system is given by:

$$\mathbf{R}^I(\mathbf{r},\ddot{\mathbf{r}},\mathbf{t}) + \mathbf{R}^D(\mathbf{r},\dot{\mathbf{r}},\mathbf{t}) + \mathbf{R}^S(\mathbf{r},\mathbf{t}) = \mathbf{R}^E(\mathbf{r},\dot{\mathbf{r}},\mathbf{t}) \tag{7.17}$$

$\mathbf{R}^I$**:** inertia force vector

$\mathbf{R}^D$**:** damping force vector

$\mathbf{R}^S$**:** internal structural reaction force vector

$\mathbf{R}^E$**:** external force vector

$\mathbf{r}, \dot{\mathbf{r}}, \ddot{\mathbf{r}}$**:** structural displacement, velocity and acceleration vectors.

Important contributions to nonlinearities in dynamic analysis of slender marine structures are the following (rif, 2011):

- Geometric stiffness due to geometry changes
- Nonlinear material properties
- Hydrodynamic loading in generalized Morison equation with relative velocities (i.e. the structure is not fixed)
- Integration of kinematics to the free surface
- Contact problems (i.e. bottom contact, riser collision, vessel/riser, pipe/stinger, contact, etc.).

The numerical integration method HHT-α and Newmark β-Family used in SIMLA and RIFLEX respectively is studied in the following sections.

7.2.1 Newmark β-Family

Newmark' s integral equations define the relation between displacements, velocity and acceleration vectors at time t and the next time step $t+\Delta\tau$ as (rif, 2011):

$$\dot{\mathbf{r}}_{t+\Delta\tau} = \dot{\mathbf{r}}_t + (\mathbf{1}-\gamma)\ddot{\mathbf{r}}_t\Delta\tau + \gamma\ddot{\mathbf{r}}_{t+\Delta\tau}\Delta\tau \tag{7.18}$$

$$\mathbf{r}_{t+\Delta\tau} = \mathbf{r}_t + \dot{\mathbf{r}}_t\Delta\tau + (\frac{\mathbf{1}}{\mathbf{2}}-\beta)\ddot{\mathbf{r}}t(\Delta\tau)^2 + \beta\ddot{\mathbf{r}}_{t+\Delta\tau}(\Delta\tau)^2 \tag{7.19}$$

where $\Delta\tau = \Delta\theta$, θ lager than 1.0. The parameters γ, β and θ describe how the displacement, velocity and acceleration vectors are changed between the time step ,$\Delta\tau$.

The method is unconditional stable if:

$$\gamma >= \frac{1}{2} \tag{7.20}$$

$$\beta >= \frac{1}{4}(\gamma+\frac{1}{2})^2 \tag{7.21}$$

For small values of β the method is conditionally stable (i.e. time step must be small enough to obtain convergence). The stability limit is defined as:

$$h_{cr} = \frac{T}{2\pi}(\frac{1}{4}(\gamma+\frac{1}{2})^2-\beta)^{-\frac{1}{2}} \tag{7.22}$$

Newmark β-family consists of an assembly of different integration techniques with the standard value of $\theta = 1$. Special cases of this method with corresponding parameters are shown in Tab. 7.1

Table 7.1: Numerical integration methods

Numerical method	β	γ	θ	Stability
Central difference method	0	1/2	1	$h_{cr} = 0.318T$
Fox-Goodwins method	1/12	1/2	1	$h_{cr} = 0.389T$
Linear acceleration method	1/6	1/2	1	$h_{cr} = 0.551T$
Constant average acceleration method	1/4	1/2	1	Unconditionally stable

The value of γ determines the level of artificial damping of the method (decreasing amplitude for free undamped vibrations/ eigenvalue problem):

$\gamma > 1/2$, positive artificial damping i.e. the amplitude decreasing as t increases

$\gamma < 1/2$, negative artificial damping

$\gamma = 1/2$, no artificial damping

In most cases $\gamma = 1/2$ is chosen.

The integration methods are implicit due to the dependency of values at the next step. For $\beta > 0$ these methods may be rewritten into explicit form:

$$\Delta\dot{\mathbf{r}}_{t+\Delta t} = \dot{\mathbf{r}}_{t+\Delta\tau} - \dot{\mathbf{r}}_t = \frac{\gamma}{\beta\Delta\tau}\Delta\mathbf{r}_t - \frac{\gamma}{\beta}\dot{\mathbf{r}}_t - (\frac{\gamma}{2\beta} - 1)\Delta\tau\ddot{\mathbf{r}}_t \tag{7.23}$$

$$\Delta\ddot{\mathbf{r}}_{t+\Delta t} = \ddot{\mathbf{r}}_{t+\Delta\tau} - \ddot{\mathbf{r}}_t = \frac{1}{\beta(\Delta\tau)^2}\Delta\mathbf{r}_t - \frac{1}{\beta\Delta\tau}\dot{\mathbf{r}}_t - \frac{1}{2\beta}\ddot{\mathbf{r}}_t \tag{7.24}$$

7.2.2 HHT-α Method

Hileber-Hughes-Taylor method (HHT -α method) is a generalization of Newmark's method. The relation between displacement, velocity and acceleration vectors at time t and the next time step t + $\Delta\tau$:

$$\mathbf{r}_{t+\Delta\tau} = \mathbf{r}_t + \dot{\mathbf{r}}_t\Delta\tau + \frac{1}{2}(\Delta\tau)^2((1-2\beta)\ddot{\mathbf{r}}_t + 2\beta\ddot{\mathbf{r}}_{t+\Delta\tau} \tag{7.25}$$

$$\dot{\mathbf{r}}_{t+\Delta\tau} = \dot{\mathbf{r}}_t + (\mathbf{1}-\gamma)\ddot{\mathbf{r}}_t\Delta\tau + \gamma\ddot{\mathbf{r}}_{t+\Delta\tau}\Delta\tau \tag{7.26}$$

For a linear undamped system, the HHT -α method is unconditionally stable if:

$$-\frac{1}{3} < \alpha < 0 \tag{7.27}$$

$$\gamma = \frac{1}{2}(1-\alpha) \tag{7.28}$$

$$\beta = \frac{1}{4}(1-\alpha)^2 \tag{7.29}$$

7.2.3 Nonlinear Dynamic Analysis in RIFLEX

The nonlinear incremental dynamic equation of motion is solved by using linearization at each load incremental step. By computing the tangent of the mass, damping and the stiffness matrices $\mathbf{M}_t, \mathbf{C}_t$ and $\mathbf{K}_t$ for each increment, the linearized dynamic equation is given by (rif, 2011):

$$\mathbf{M}_t \Delta \ddot{\mathbf{r}}_t + \mathbf{C}_t \Delta \dot{\mathbf{r}}_t + \mathbf{K}_t \Delta \mathbf{r}_t = \Delta \mathbf{R}_t^E \tag{7.30}$$

where $\Delta\ddot{\mathbf{r}}_t$, $\Delta\dot{\mathbf{r}}_t$, and $\Delta\mathbf{r}_t$ are the incremental acceleration, velocity and displacements vectors respectively and $\Delta\mathbf{R}_t^E$ is the incremental external force vector between step t and t+$\Delta\tau$.

The linearization of the equation of motion gives rise to an unbalanced force vector. The unbalance is caused by the change in the nonlinear mass, damping and stiffness over the time increment. Thus, the dynamic equilibrium is not satisfied. The residual force vector for the previous step is given by:

$$\delta \mathbf{R}_{t-\Delta\tau} = \mathbf{R}_t^E - (\mathbf{R}_t^I + \mathbf{R}_t^D + \mathbf{R}_t^S) \tag{7.31}$$

The equilibrium correction Eq. 7.31 is be added to the equilibrium equation at the current step, t, to avoid large errors::

$$\mathbf{M}_t \Delta \ddot{\mathbf{r}}_t + \dot{\mathbf{C}}_t \Delta \mathbf{r}_t + \mathbf{K}_t \Delta \mathbf{r}_t = \mathbf{R}_{t+\Delta\tau}^E - (\mathbf{R}_t^I + \mathbf{R}_t^D + \mathbf{R}_t^S) \tag{7.32}$$

By inserting Eq. 7.23 and 7.24 into Eq. 7.31 at the time interval $t + \Delta\tau$ gives:

$$\hat{\mathbf{K}}_t \Delta \mathbf{r}_t = \Delta \hat{\mathbf{R}}_t \tag{7.33}$$

where $\hat{\mathbf{K}}_t$ and $\Delta\hat{\mathbf{R}}_t$ is the effective stiffness and effective incremental vector respectively. These are expressed as:

$$\hat{\mathbf{K}}_t = \frac{1}{\beta(\Delta\tau)^2}\mathbf{M}_t + \frac{\gamma}{\beta\Delta\tau}\mathbf{C}_t + \mathbf{K}_t \tag{7.34}$$

$$\Delta\hat{\mathbf{R}}_t = \Delta\mathbf{R}_{t+\Delta\tau}^E - (\mathbf{R}_t^I + \mathbf{R}_t^D + \mathbf{R}_t^S) + \mathbf{M}_t\Big(\frac{1}{\beta\Delta\tau}\dot{\mathbf{r}}_t + \frac{1}{2\beta\Delta}\ddot{\mathbf{r}}_t\Big) + \mathbf{C}_t\Big(\frac{\gamma}{\beta}\dot{\mathbf{r}}_t + \big(\frac{\gamma}{2\beta} - 1\big)\Delta\tau\ddot{\mathbf{r}}_\mathbf{t}\Big) \tag{7.35}$$

Between the load incrementation, iterations are performed so that dynamic equilibrium is obtained. The iteration procedure is based on Newton-Raphson procedure which gives the iterative equilibrium after iteration number i:

$$ {}^{i-1}\mathbf{R}^{I}_{t+\Delta\tau} + {}^{i-1}\mathbf{R}^{D}_{t+\Delta\tau} + {}^{i-1}\Delta\mathbf{R}^{S}_{t+\Delta\tau} = {}^{i-1}\Delta\mathbf{R}^{E}_{t+\Delta\tau} - \left({}^{i}\Delta\mathbf{R}^{I}_{t+\Delta\tau} + {}^{i}\mathbf{R}^{D}_{t+\Delta\tau} + {}^{i}\Delta\mathbf{R}^{S}_{t+\Delta\tau} \right) \tag{7.36} $$

The acceleration, velocity and displacement vector is given by:

$$ {}^{i}\ddot{r}_{t+\Delta\tau} = {}^{i-1}\ddot{r}_{t+\Delta\tau} + \frac{\gamma}{\beta(\Delta\tau)^2}\,{}^{i}\Delta_{\dot{r}} \tag{7.37} $$

$$ {}^{i}\dot{r}_{t+\Delta\tau} = {}^{i-1}\dot{r}_{t+\Delta\tau} + \frac{\gamma}{\beta\Delta\tau}\,{}^{i}\Delta_{r} \tag{7.38} $$

$$ {}^{i}r_{t+\Delta\tau} = {}^{i-1}r_{t+\Delta\tau} + {}^{i}\Delta_{r} \tag{7.39} $$

where ${}^{i}\Delta r$ is the displacement correction vector between two iteration step given by:

$$ {}^{i}\Delta_{r} = {}^{i}r_{t} + {}^{i-1}r_{t} \tag{7.40} $$

Eq. 7.36 may be reorganized and by use of Eqns. 7.23 and 7.24 the dynamical equilibrium may be expressed as:

$$ \left(\frac{1}{\beta(\Delta\tau)^2}\,{}^{i-1}\mathbf{M}_{t+\Delta\tau} + \frac{\gamma}{\beta\Delta\tau}\,{}^{i-1}\mathbf{C}_{t+\Delta\tau} + {}^{i-1}\mathbf{K}_{t+\Delta\tau} \right) {}^{i}\Delta_{r} = \mathbf{R}^{E}_{t+\Delta\tau} - \left({}^{i-1}\mathbf{R}^{I}_{t+\Delta\tau} + {}^{i-1}\mathbf{R}^{D}_{t+\Delta\tau} + {}^{i-1}\mathbf{R}^{S}_{t+\Delta\tau} \right) \tag{7.41} $$

where the inertia and damping matrix may be calculated by:

$$ {}^{i-1}\mathbf{R}^{I}_{t+\Delta\tau} = \mathbf{M}^{i-1}_{t+\Delta\tau}\ddot{\mathbf{r}}_{t+\Delta\tau} \tag{7.42} $$

$$ {}^{i-1}\mathbf{R}^{D}_{t+\Delta\tau} = \mathbf{C}^{i-1}_{t+\Delta\tau}\dot{\mathbf{r}}_{t+\Delta\tau} \tag{7.43} $$

The right-hand side of Eq. 7.41 involves the unbalance in inertia, damping and internal forces. Displacement, velocity and accelerations are update by use of Eqns. 7.37, 7.38 and 7.39.

For the iterative approach to be stable, a sufficiently small time step is applied. Incremental

steps are applied and corrected by ordinary Newton-Raphson procedure. The convergence criterion for the iteration is the same as for the static analysis.

7.2.4 Nonlinear Dynamic Analysis in SIMLA

Similar to the Newmark β-family, the HHT-α method has the same relations between displacements, velocity and acceleration vectors , see Eq. 7.23 and Eq. 7.24. In this method, however, the equilibrium equation for the system is modified by (Sævik, 2008):

$$\mathbf{M}\ddot{\mathbf{r}}_{t+\Delta\tau} + (1+\alpha)\mathbf{C}\dot{\mathbf{r}}_{t+\Delta\tau} - \alpha\mathbf{C}\dot{\mathbf{r}}_t + (1+\alpha)\mathbf{R}^S_{t+\Delta\tau} - \alpha\mathbf{R}^S_t = (1+\alpha)\mathbf{R}^E_{t+\Delta\tau} - \alpha\mathbf{R}^E_t \tag{7.44}$$

The modification is introduced to damp out higher modes without diminishing the 2nd order accuracy (Sævik, 2008). This is done by numerical damping by means of time averaging. The parameter α is introduced to control the damping level.

The higher frequency modes do not contribute to dynamic amplification, and thus, it is not of importance in dynamic analysis. In Newmark -β method applying numerical damping, the higher modes may be damped out in compensation of reduced accuracy from 2nd to 1st order. By increasing the damping ratio or by introducing Rayleigh-damping will generally damp out the medium modes while the lower and higher modes remain almost unchanged (Fylling et al., 1995).

The incremental dynamic equilibrium equation, Eq. 7.45, is obtained by subtracting the equilibrium equation at time step t from Eq. 7.44 and inserting the incremental acceleration and velocity derived in Newmark -β method:

$$\hat{\mathbf{K}}_t \Delta\ddot{\mathbf{r}}_{t+\Delta\tau} = \Delta\hat{\mathbf{R}}_{t+\Delta\tau} \tag{7.45}$$

where the effective stiffness matrix $\hat{\mathbf{K}}_t$ is given by:

$$\hat{\mathbf{K}}_t = a_0\mathbf{M} + c_0\mathbf{C} + b_0\mathbf{K_{T,t}} \tag{7.46}$$

$$a_0 = \frac{1}{\Delta\tau^2\beta} + (1+\alpha)\frac{\alpha_1\gamma}{\Delta\tau\beta} \tag{7.47}$$

$$c_0 = (1+\alpha)\frac{\gamma}{\Delta\tau\beta} \tag{7.48}$$

$$b_0 = (1+\alpha)\frac{\alpha_2\gamma}{\Delta\tau\beta} \tag{7.49}$$

where $\mathbf{K_T}$ is the global tangent stiffness matrix. The effective load vector $\Delta\hat{\mathbf{R}}_{t+1}$ is written as:

$$\Delta\hat{\mathbf{R}}_{t+\Delta\tau} = (1+\alpha)\left[\mathbf{R}^E_{t+\Delta\tau} - \mathbf{R}^E_t + \mathbf{C}\mathbf{b}_t\right] + \mathbf{M}\mathbf{a}_t + \mathbf{R}^E_t - \mathbf{R}^S_t - \mathbf{C}_t\dot{\mathbf{r}}_t \tag{7.50}$$

$$\mathbf{a}_t = \frac{1}{\Delta t\beta}\dot{\mathbf{r}}_t + \left(\frac{1}{2\beta} - 1\right)\ddot{\mathbf{r}}_t \tag{7.51}$$

$$\mathbf{b}_t = \left(\frac{\lambda}{\beta} - 1\right)\dot{\mathbf{r}}_t + \left(\frac{\lambda}{2\beta} - 1\right)\Delta\tau\ddot{\mathbf{r}}_t \tag{7.52}$$

Eq. 7.50 considers the unbalanced forces at time step t. The displacement at time step t + $\Delta\tau$ is found by solving Eq. 7.46.

In general the dynamic equation will not be fulfilled so that equilibrium iteration must be performed before a new load step is introduced. Newton-Raphson iteration procedure is adopted. The dynamic equilibrium may be written as:

$$\hat{\mathbf{K}}^i\Delta_r = (1+\alpha)\left[\mathbf{R}^E_{t+\Delta\tau} - {}^{i-1}\mathbf{R}^S_{t+\Delta\tau} - {}^{i-1}\mathbf{C}\dot{\mathbf{r}}_{t+\Delta\tau}\right] - {}^{i-1}\mathbf{M}\ddot{\mathbf{r}}_{t+\Delta\tau} - \alpha\left(\mathbf{R}^E_t - \mathbf{R}^S_t - {}^{i-1}\mathbf{C}\dot{\mathbf{r}}_t\right) \tag{7.53}$$

The iteration procedure and the convergence criteria are the same as used in RIFLEX.

Chapter 8

Implementation of Vertical Degradation Soil Model

A vertical degradation soil model was developed. The model named AUBENY-d was implemented in the programming languages FORTRAN and MATLAB. It is based on the non-degradation model developed by Aubeny et al. (2006) and the degradation rule by Aubeny et al. (2008), see Sec. 4.2 and Sec. 4.3 respectively.

The code is described in the Sec. 8.1 below and can be found in the appendix in the programming languages FORTRAN and MATLAB, see App A.3 and A.4.

8.1 Vertical Soil Degradation Model

The flowchart in Fig. 8.1 describes the structure of the code AUBENY-d. The code computes the soil resistance and stiffness by main inputs like z-coordinate of a riser, IOP and LSNUM. The z-coordinate is defined positive downwards into the soil. IOP is the identifier operator for deciding whether the self-embedment is linear or has the shape of the backbone curve developed by Aubeny et al. (2006). The linear case is only a simplification. It predicts the reality well as long as the soil is soft. LSNUM is the load step number that starts counting as soon as the code is executed. Input parameters are stored in the input_array.

A 1x23 dimensional array, denoted work_array, are updated every load step. The array keeps track of the parameters necessary to model the riser-soil interaction. The values from the previous load step are transferred to the next step. One of the ”memory” parameters is the path identifier that remembers the path-formulation that was used in the previous step. There are seven such path identifiers, and an explanation of them are listed in Tab. 8.1. If a reversal occurs from either inside or along the bounding loop or if hits the boundary requirements, the path identifier is changed.

Table 8.1: Path Identifier of Vertical Soil Model

PATH ID	Path Description
0	Backbone curve
12	Elastic rebound curve
23	Partial soil-riser separation curve
30	Full soil separation
321	Re-contact curve and reloading from path 23
122	Unloading from path 31 or from an arbitrary point within the loop on path 121
	Elastic rebound curve and partial soil-riser separation curve outside bounding loop
121	Reloading from path 12 or from an arbitrary point within the loop on path 122

The output of the subroutines is the soil force, F_z, and the soil stiffness, K_z, at the given penetration depth, z. These are stored in the output_array.

There are assumptions related to the model developed. The trench width is assumed to be w/D = 1 such that the backbone parameters are more easily obtained.

A summary of the code is described below containing these following steps:

1. Read the riser - and soil properties in the input_array. There are two soil properties, shear strength at mudline s_u and the shear strength gradient s_{ug}, two backbone parameters, and b and the riser diameter for calculation of the backbone curve. Four bounding loop parameters, k_0, ω, ϕ, ψ are used to calculate some characteristic points that define the bounding loop (z_2, P_2, P_3). There are two degradation parameters, α, β stored in the input array.

2. Read the intermediate parameters stored in the work_array.

3. If IOP=1, the linear spring model is activated to calculate the penetration into virgin soil by assuming the penetration to be static. If IOP =2, the nonlinear approach is selected.

4. When the nonlinear degradation model is executed a local load step counter is activated (counts the number of incremental loading steps in the non-degradation model). If the step counter is equal to zero, the transition from linear to nonlinear must be checked. If there is no contact in the transition zone, the code is stopped.

5. The degradation control point (z_1^*, F_{z1}^*) is calculated as the deflection increment are accumulated.

6. For each new loading load step, the code assumes that the previous path is governing. Requirements for each path decides whether or not the path is changed. Once one of the requirement are fulfilled there is a change of path.

7. The soil force F_z and soil stiffness K_z are determined for each loading cycle and is stored in the output_array.

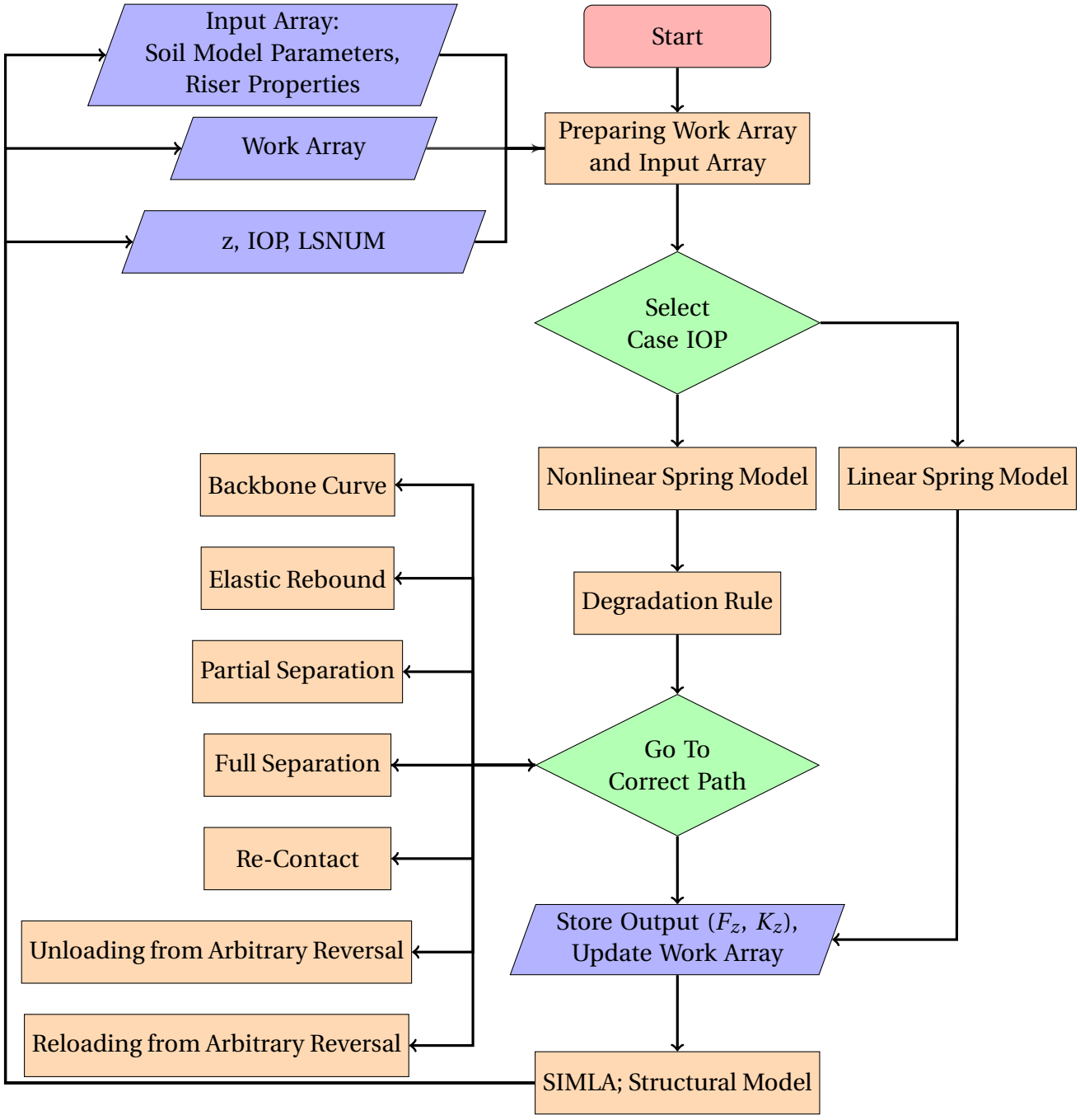

Figure 8.1: Flowchart of Vertical Soil Degradation Model

8.1.1 Linear Model

AUBENY- subroutine includes an option for a linear model for calculation of the penetration into virgin soil. This model is computed if the user defined parameter IOP=1. The soil force may

be determined by:

$$F_z = K_s z \tag{8.1}$$

where K_s is the static soil stiffness which is taken as the secant stiffness on the backbone curve. The soil stiffness K_z is then defined by:

$$K_z = K_s \tag{8.2}$$

8.1.2 Degradation Rule

Due to the cyclic loading the soil will be experiencing degradation. The apparent maximum penetration, z_1^* is defined by:

$$z_1^* = z_{Fmax} + \alpha_d (\lambda_n)^{\beta_d} \tag{8.3}$$

where α_d and β_d are degradation control parameters and z_{Fmax} is the experienced penetration depth for maximum soil resistance. The accumulated displacement λ_n is increasing for unloading only along the bounding loop and for unloading from an arbitrary reversal point. When the deflection, z, becomes larger than the deflection in the control point, z_1^*, λ_n is reset. It can be calculated by:

$$\lambda_n = \sum_j^n |\Delta z_j| \tag{8.4}$$

where $|\Delta z_j|$ is the deflection per cycle, j, and n is the number of cycles between the resets. The maximum accumulated deflection per cycle is according to Nakhaee and Zhang (2010) given by:

$$\Delta z_j = z_1 - z_3 \tag{8.5}$$

The maximum apparent load, F_{z1}^* is always located on the backbone curve. Due to degradation of the soil, the backbone curve is modified, see Subsec. 8.1.3.

8.1.3 Backbone Curve

Path 0 represents the backbone curve. The computation of the soil resistance during initial soil penetration may be calculated by:

$$F_{zi} = a(z_i/d)^b(s_{u0} + s_{ug}z_i)D \tag{8.6}$$

where i is the current load step number. The soil stiffness is found by differentiation of Eq. 8.6:

$$K_{zi} = a * b * \frac{z_i}{D}(s_{u0} + s_{ug}z_i)D + a\left(\frac{z_i}{D}\right)^b s_{ug}D \tag{8.7}$$

When unloading occurs from backbone curve, the characteristic points, point 2 and point 3, on the bounding loop are calculated based on point 1 and soil parameters.

The backbone curve for the initial penetration, must be corrected for the degradation of the soil during the cyclic riser motions. The modification is introduced when reaching the degradation control parameter z_1 during reloading. The difference is found between the soil resistance of the previous backbone curve and the current soil resistance for the soil deflection at control point, as depicted in Fig. 8.2.

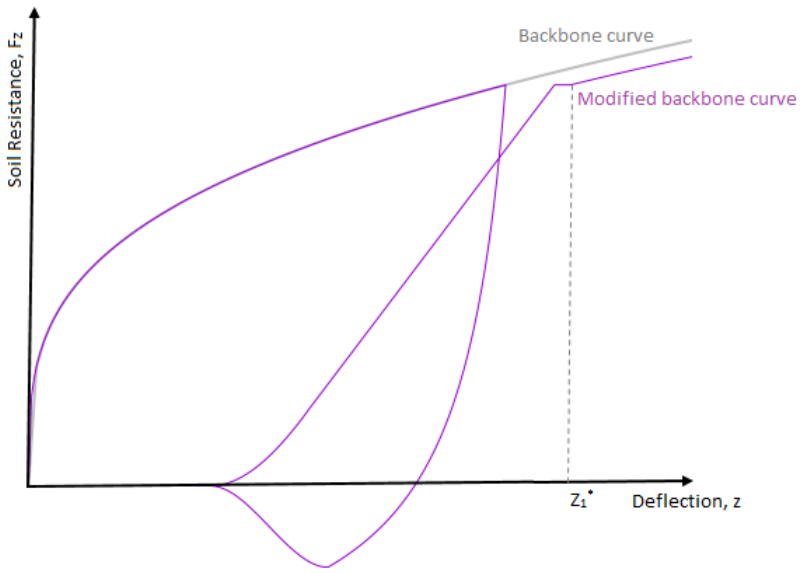

Figure 8.2: Modified Backbone Curve

The soil resistance is thus calculated as:

$$F_{zi} = a(z_i/d)^b(s_{u0} + s_{ug}z_i)D - dp_{backbone} \tag{8.8}$$

where $dp_{backbone}$ is the accumulated difference between the soil resistance of the previous backbone curve and the current soil resistance for the soil deflection at control point. The soil stiffness is determined by:

$$K_{zi} = a * b * \frac{z_i}{D}(s_{u0} + s_{ug}z_i)D + a\left(\frac{z_i}{D}\right)^b s_{ug}D \tag{8.9}$$

8.1.4 Bounding Loop

Point 1 on the backbone curve defines the maximum soil force obtained. When reversal occurs on the backbone, path 12 is initiated as the elastic rebound is entered. The soil force at the current load step is determined by:

$$F_{zi} = F_{z1} + \frac{z_i - z_1}{\frac{1}{k_0} + \chi\frac{z_i - z_1}{(1+\omega)F_{z1}}} \tag{8.10}$$

where the parameter χ is -1 for unloading. The soil stiffness is computed by differentiation of Eq. 8.10:

$$K_{zi} = \frac{1}{A} + \chi\frac{z_i - z_1}{(1+\omega)F_{z1}A^2} \tag{8.11}$$

$$A = \frac{1}{k_0} + \chi\frac{z_i - z_1}{(1+\omega)F_{z1}} \tag{8.12}$$

If further unloading occurs beyond the maximum suction limit, the pipe will move into path 321. The soil force and soil stiffness is computed by the following expressions respectively;

$$F_z = \frac{F_{z2}}{2} + \frac{F_{z2}}{4}\left[3\left(\frac{z_i - z_0}{z_m}\right) - \left(\frac{z_i - z_0}{z_m}\right)^3\right] \tag{8.13}$$

$$z_0 = \frac{z_2 + z_3}{2} \tag{8.14}$$

$$z_m = \frac{z_2 - z_3}{2} \tag{8.15}$$

$$K_{zi} = \frac{F_{z2}}{4}\left[\frac{3}{z_m} - \frac{3(z_i - z_0)^2}{z_m^3}\right] \tag{8.16}$$

The re-contact curve is included in path 321 and is modeled by:

$$F_{zi} = \frac{F_{z1}^* + F_{z3}}{2} + \frac{F_{z1}^* + F_{z3}}{4}\left[3\left(\frac{z_i - z_0}{z_m}\right) - \left(\frac{z_i - z_0}{z_m}\right)^3\right] \tag{8.17}$$

$$z_0 = \frac{z_1^* + z_3}{2} \tag{8.18}$$

$$z_m = \frac{z_1^* - z_3}{2} \tag{8.19}$$

$$K_{zi} = \frac{F_{z1}^* + F_{z3}}{4}\left[\frac{3}{z_m} - \frac{3(z_i - z_0)^2}{z_m^3}\right] \tag{8.20}$$

If the deflection is smaller than z_3, the full separation path is entered. There is no soil contact. F_z and K_z is, therefore, zero.

8.1.5 Reversal Cycles from Bounding Loop

There are three different formulations when a reversal starts from the bounding loop. Reloading from the elastic rebound curve 12 with an arbitrary reversal point (z_r, P_r), enters into the path 122 with soil force as follows (Jiao, 2007):

$$F_{zi} = F_{zr} + \frac{z_i - z_r}{\frac{1}{k_0} + \chi\frac{z_i - z_r}{(1+\omega)F_{z1}\xi}} \tag{8.21}$$

$$\xi = \frac{z_1^* - z_r}{F_{z1}^*(1+\omega)\left(\frac{z_1^* - z_r}{F_{z1}^* - F_{zr}} - \frac{1}{k_0}\right)} \tag{8.22}$$

where ξ is another degradation control parameter controlling the degree of degradation for this hyperbolic degradation curve. χ=1 for loading.

The soil stiffness is found by differentiation of Eq. 8.35:

$$K_{zi} = \frac{1}{A} + \chi \frac{z_r - z_i}{(1+w)F^*_{z1}\chi A^2} \tag{8.23}$$

$$A = \frac{1}{k_0} + \chi \frac{z_i - z_r}{(1+w)F^*_{z1}\xi} \tag{8.24}$$

Reloading from the partial soil separation curve 23 with an arbitrary reversal point (z_r, F_{zr}), enters into the path 121 with soil force and stiffness as follows:

$$F_{zi} = \frac{F^*_{z1} + F_{zr}}{2} + \frac{F^*_{z1} + F_{zr}}{4}\left[3\left(\frac{z_i - z_0}{z_m}\right) - \left(\frac{z_i - z_0}{z_m}\right)^3\right] \tag{8.25}$$

$$z_0 = \frac{z^*_1 + z_r}{2} \tag{8.26}$$

$$z_m = \frac{z^*_1 - z_r}{2} \tag{8.27}$$

$$K_{zi} = \frac{F^*_{z1} + F_{zr}}{4}\left[\frac{3}{z_m} - \frac{3(z_i - z_0)^2}{z^3_m}\right] \tag{8.28}$$

When unloading occurs below the maximum soil force from Re-Contact curve 31, path 122 is entered. The soil force is given by:

$$F_z = F_{zr} + \frac{z_i - z_r}{\frac{1}{k_0} + \chi\frac{z - z_r}{(1+\omega)F_{z1}}} \tag{8.29}$$

where the parameter χ is -1 for unloading. The soil stiffness is computed by differentiation of Eq. 8.29:

$$K_{zi} = \frac{1}{A} + \chi \frac{z_i - z_r}{(1+\omega)F_{z1}A^2} \tag{8.30}$$

$$A = \frac{1}{k_0} + \chi \frac{z_i - z_r}{(1+\omega)F_{z1}} \tag{8.31}$$

If reloading occurs within the bounding loop,the reloading path from path 23 works as a boundary. If the reversal occur from path 31 this path is taken as the boundary as depicted in Fig. 8.3.

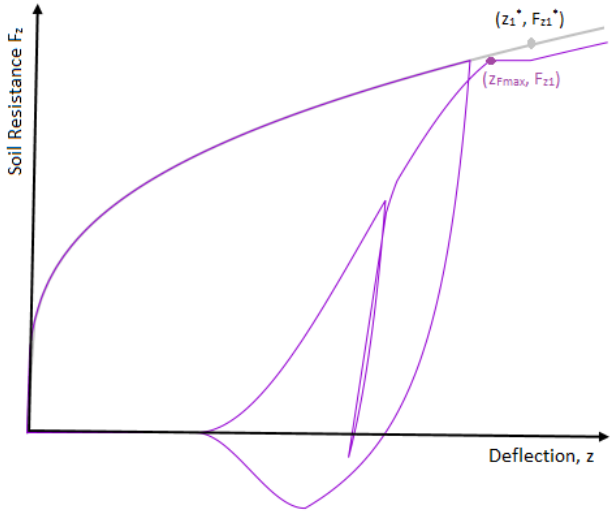

Figure 8.3: Reversals Inside Bounding Loop

One reference point is the maximum soil resistance force achieved, F_{z1}. When reloading occurs either on or within the bounding loop, the curve moves towards the degradation control point (z_1^*, F_{z1}^*). When the penetration depth passes the maximum soil force F_z1, a reversal here will create a new point 1 (z_1, F_{z1}) and enter into a new bounding loop. This is illustrated in Fig. 8.4. The characteristic bounding loop points, (z_2, F_{z2}, z_3) will be updated. If reloading occurs pass

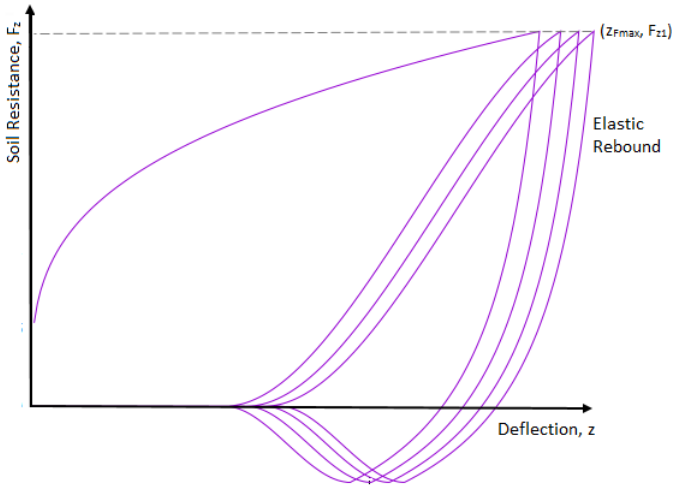

Figure 8.4: Elastic Rebound Curve

the point $(z_{\text{pmax}}, F_{z1})$, it is assumed to be constant until the deflection point z_1^* is reached. This is only an assumption as the reloading curves are not adapted for the developed model. If the

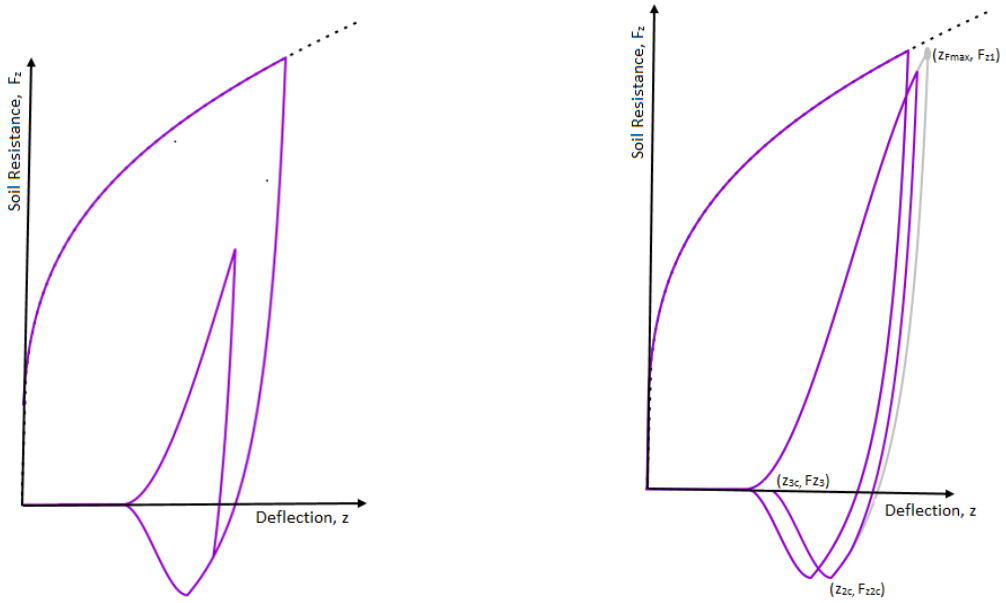

Figure 8.5: Reversals from Re-Contact Curve

penetration depth becomes equal to or larger than the point z_1^*, the calculation of the soil force and stiffness follows the modified backbone curve.

If an unloading from path 31 or an arbitrary reversal point come across the boundary of path 12 or path 23 with reference to the point on the bounding loop (z_1, F_{z1}), it will start to follow one of the two paths. If unloading occurs outside the bounding loop, it is necessary to locate the point $(z_{\text{Fmax}}, F_{z1})$ to establish boundaries. z_{Fmax} is the deflection corresponding to the maximum soil force on the last reloading curve. This parameter is found through iteration and is further used together with the point F_{z1} to calculate control points on the "boundary" bounding loop with corresponding characteristic control points $(z_{2c}, F_{z2c}, z_{3c})$. If the unloading curve touches one of the two boundaries, the path 121 is entered. Fig. 8.5 illustrates some outcomes.

8.1.6 Reversal Cycles within and Outside Bounding Loop

There are two model formulations used to determine the reversal loops within and outside the bounding loop. Example of loops outside the bounding loop is illustrated in Fig 8.6.

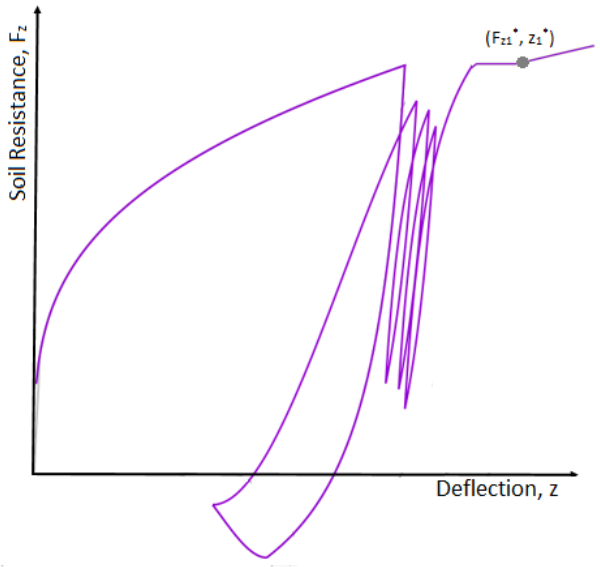

Figure 8.6: Reversal Cycles outside Bounding Loop

Path 122 include a unloading curve from an arbitrary point within or outside the bounding loop:

$$F_{zi} = F_{zr} + \frac{z_i - z_r}{\frac{1}{k_0} + \chi \frac{z_i - z_r}{(1+\omega)F_{z1}}} \tag{8.32}$$

where the parameter χ is -1 for unloading. The soil stiffness is computed by differentiation of Eq.8.32:

$$K_{zi} = \frac{1}{A} + \chi \frac{z_i - z_r}{(1+\omega)F_{z1}A^2} \tag{8.33}$$

$$A = \frac{1}{k_0} + \chi \frac{z_i - z_r}{(1+\omega)F_{z1}} \tag{8.34}$$

Reloading curves from an arbitrary point within or outside the bounding loop is incorporated in path 121 and has the form of Jiao (2007):

$$F_{zi} = F_{zr} + \frac{z_i - z_r}{\frac{1}{k_0} + \chi \frac{z_i - z_r}{(1+\omega)F_{z1}\xi}} \tag{8.35}$$

$$\xi = \frac{z_1^* - z_r}{F_{z1}^*(1+\omega)\left(\frac{z_1^* - z_r}{F_{z1}^* - F_{zr}} - \frac{1}{k_0}\right)} \tag{8.36}$$

where χ=1 for reloading. The soil stiffness is found by differentiation of Eq. 8.35:

$$K_{zi} = \frac{1}{A} + \chi \frac{z_i - z_1}{(1+\omega)F_{z1}A^2} \tag{8.37}$$

$$A = \frac{1}{k_0} + \chi \frac{z_i - z_1}{(1+\omega)F_{z1}} \tag{8.38}$$

8.2 Comments on the Degradation Model

The soil degrading model consists of empirical formulas formulated by conduction of tests and numerical methods. The backbone curve describing the initial penetration follows a power law function which is validated by Aubeny et al. (2005) through theoretical studies and test measurements by Dunlap et al. (1990). For the bounding loop, model simulations have been applied to validate the data measurements. The unloading paths, 12, 23 and the path from an arbitrary reversal point seem to be adequately described. However, the cubic degradation curve requires further study. The hyperbolic reloading curve from path 12 is not properly verified due to lack of data (Jiao, 2007). The unloading curve from a reversal within or from the bounding loop needs to be validated through laboratory test basin measurements (Aubeny and Biscontin, 2009).

Chapter 9

Integration of Vertical Soil Model in SIMLA

The Fortran subroutine, containing the linear model and vertical soil degradation model described in Ch. 8, were integrated inside SIMLA as a material model. Fig. 9.1 shows the flowchart of the communication between SIMLA and the soil model.

The model is acting through the cont126 element which is a contact element for pipe-soil interaction modeling on the original seabed. There is an exchange of data between the soil model and the riser motion through the contact element through mainly a work array. The work array stores soil model parameters, which are determined from the load history of the interaction. During every load step, the array is updated. Since the soil model is nonlinear, each load step yields an imbalance vector of the riser-soil interaction problem. In between each load step, an iteration procedure must, therefore, be performed. The work array from the last iterative step of the previous load step is copied to the subroutine for the next load step. Then the soil force and stiffness is calculated in the subroutine by use of this work array and an assumed riser deflection. The soil force and stiffness is computed iteratively until the corresponding deflection lies sufficiently close to the assumed riser deflection. At the end of the iterative equilibrium procedure, the work array is updated.

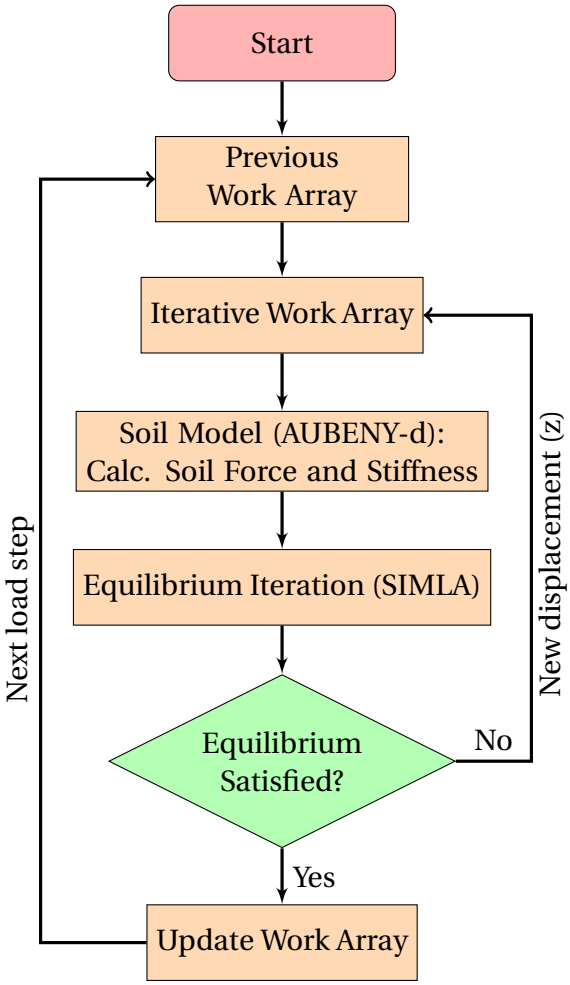

Figure 9.1: Flowchart of Soil Model in SIMLA (Irman, 2015)

Chapter 10

Validation of Vertical Soil Model

The validation process is a necessity to make sure that the code is able to reproduce a correct picture of the approximate physical soil behavior. Both the linear and non-linear soil model were validated in SIMLA.

10.1 Linear Soil Model

The initial penetration of the soil is simplified by using a linear spring. To validate the linear soil model, the commando TPOND in the SIMLA input file was put to a high value. This commando determines when the non-linear soil model is to be activated. The result is depicted in Fig. 10.1 for a soil stiffness taken as $K_s = 65\text{kN/m}$.

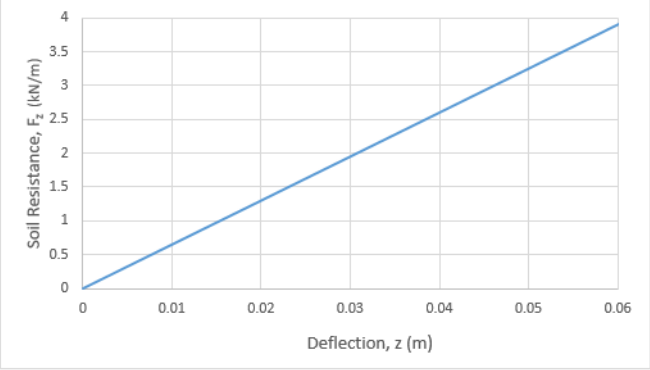

Figure 10.1: Linear Soil Model

10.2 Non-Linear Soil Model

In the published literature, there are some displacement-and load control test to compare with.

(Aubeny et al., 2008) used the degradation rule to simulate displacement controlled loading cycles. The result of the work is shown in Fig. 10.2. The soil input parameters used in the analysis are listed in Tab. 10.1.

Table 10.1: Soil Model Parameters for Validation of Vertical Soil Model (Aubeny et al., 2008)

Parameter	Description	Value
S_{u0}	Soil strength [kPa]	3.0
S_{ug}	Soil strength gradient [kPa/m]	1.3
a	Backbone Curve Coefficient	6.73 (z_1/D<0.5)
		6.15 (z_1/D>0.5)
b	Backbone Curve Exponent	0.29 (z_1/D<0.5)
		0.29 (z_1/D<0.5)
ω	Unload Large Deflections	0.53
ϕ	Unload Tension Limit	0.203
ψ	Soil-Riser Separatio	0.661
k_0/s_{u0}	Unload Initial Stiffness	660

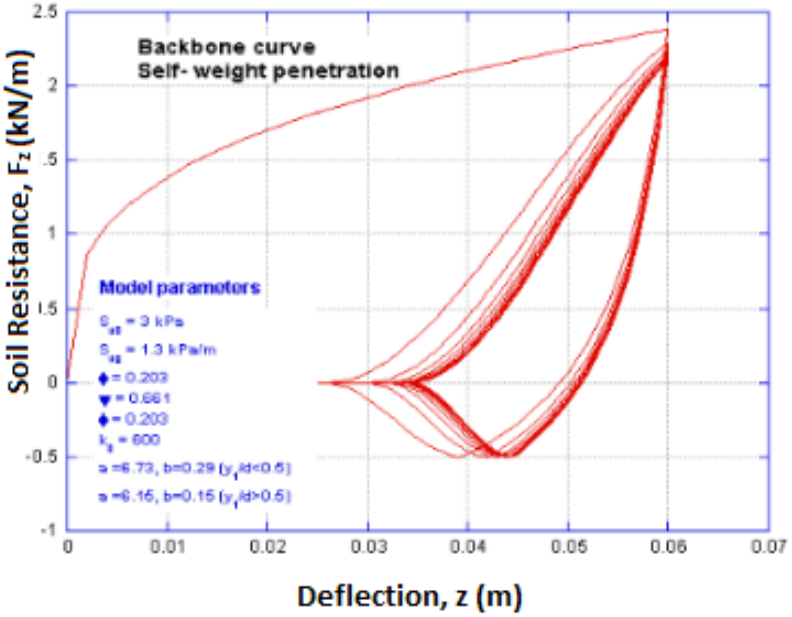

Figure 10.2: Cycles of Displacement Controlled loading into Soil (Aubeny et al., 2008)

By applying the same soil parameters, the implemented soil model gives the following result as depicted in Fig. 10.3 when running SIMLA. The two figures should be showing the same

soil behavior as both are based on Aubeny's Non-degradation model. However, there are some differences. First, the point of the suction limit between the two figures is somewhat different. This point is reached at approximately, (z, F_z) = (0.0394m -0.5 kN/m) for the case executed by Aubeny while the result of the implemented soil model is about (0.0377m, -0.48kN/m). The backbone curve is concluded to be similar after laborious comparison. As the maximum suction force is computed by the deflection of maximum soil force achieved, F_{z1}, and the soil stiffness parameter ψ, it is not easy to explain the discrepancy. The point where the pipe loses contact with the soil is also different as a result of accumulated "error".

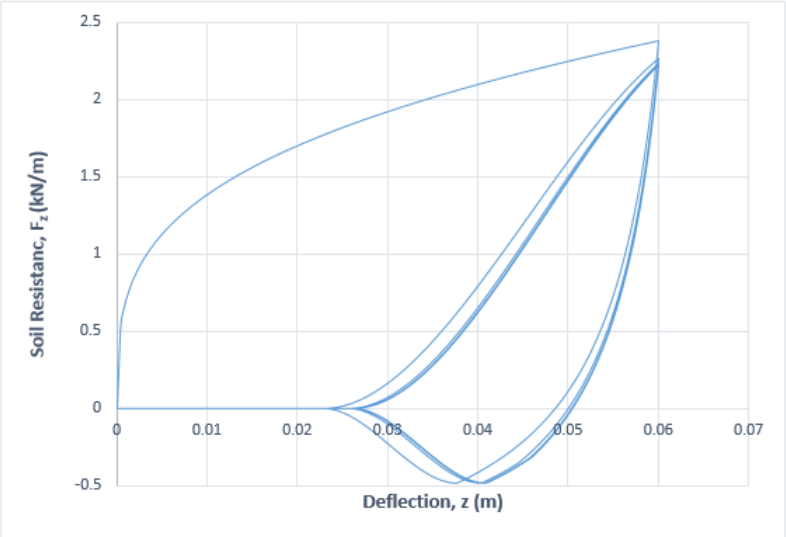

Figure 10.3: Cycles of Displacement Controlled Loading into Soil

The value of the degradation control parameters used seems to be the major difference between the two figures, as these are not listed in the conference paper (Aubeny et al., 2008). The way of computing the degradation should be the same as both are using the degradation rule by Jiao (2007). According to his work, the degradation is based on accumulated the deflection within each cycle, see sec 4.3. The α and β are taken as 0.009 and 0.03 respectively; this gives some discrepancies.

NGI performed large-scale model tests of soil-riser interaction in marine clay in the Gulf of Guinea (Langford et al., 2008). The experimental tests concentrated on the two-dimensional interaction of the soil behavior under various vertical riser velocities and amplitudes. A short, rigid pipe section was interacting with the soil under controlled conditions. The aim of the in-

vestigations was to calibrate soil models due to the interactions. Fig. 10.4 shows the result of large-cycle penetration tests for two different penetration velocities and penetration rate. For each loading cycle, the pipe was given a deflection under load-controlled response.

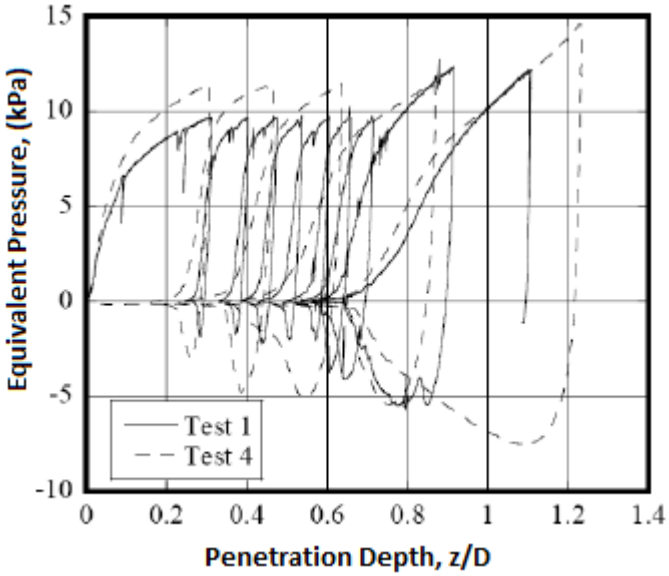

Figure 10.4: Soil Resistance under Load-Controlled Response (Langford et al., 2008)

By defining a constant level of soil resistance, the implemented soil model showed a similar trend in Fig. 10.5.

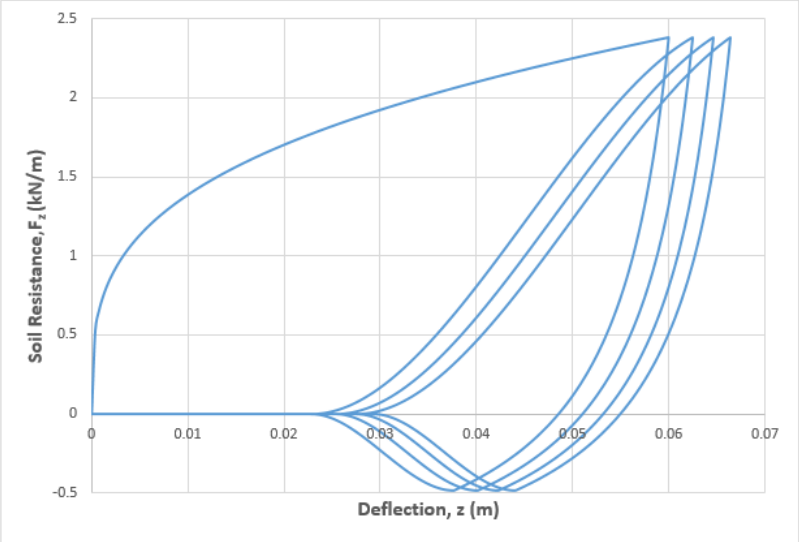

Figure 10.5: Soil Resistance under Load-Controlled Response

The bounding loop is translating along the horizontal axis for each loading cycle. The load-deflection loops are almost identical except for the deformation of the soil when β=0.5.

The literature contains few illustrations of other ways/directions the load-deflection curve can take. The specified boundary requirements during unloading outside the loop should only be considered tentative until validation is conducted. It is assumed that the soil degradation influences the backbone curve. Hence, the curve is given a load correction. This way of calculating further penetration into the virgin soil needs to be validated.

Chapter 11

Analysis of Vertical Riser-Soil Interaction

The effect of soil degradation on bending fatigue at the TDP of an SCR was studied. Only motions in the vertical plane were considered. Thus, interaction effects coupled to lateral motions were neglected. The procedure for examining the influence of soil degradation was divided into three phases. In the first phase, motion histories using an extreme sea state were obtained of an SCR in the vertical plain using RIFLEX. In the second phase, the same motions were prescribed to a truncated SIMLA model to obtain a trench profile. In the last phase, an elastic soil model was used to conduct an SCR analysis in SIMLA for a flat seabed and a similar analysis except the seabed being modeled by the obtained trench profile. The bending stresses of the two cases was assessed.

11.1 Phase 1: Motion Histories in RIFLEX

Two one-hour simulations were conducted to obtain horizontal and vertical motion histories of a point on the riser located approximately 200 m above the seabed. One environmental condition with the most extreme sea state in the scatter diagram with annual exceedance probability of 10^{-2} was conducted. The other analysis consisted of a less extreme sea state the scatter diagram. In both analysis, a current profile with annual exceedance probability of 0.63 was selected.

11.1.1 Simulation Setup

A local coordinate system was defined. The origin of this coordinate system is the reference to which all responses are computed. RAO's for the floating structure is measured/calculated at the sea surface, $z = 0$. These were imported to RIFLEX. As the waves were generated, the motions of the platform were described by the RAO's. The origin of the local coordinate system had to be placed at the sea surface. The hang-off point was (x,y,z) = (44.5,0,-35) from the origin of the local coordinate system.

The pipe was modeled as a beam in SIMA consisting of three segments. The segment around the TDP constituted of small elements with length 2.5 times the outer diameter. The other two segments had larger element length of approximately 4-5 meters. The anchor point of the pipe was fixed in all translations and the moment around the x-axis. This was to keep the motions in the vertical plane. The hang-off point at the semi-submersible was fixed in all translations while it was free to rotate in all directions. Thus, there were no moments at this end.

The different load types applied for the static analysis were volume forces, specified displacements, current forces and activation of bottom friction forces in the corresponding order.

The nonlinear time domain analysis was conducted with a simulation length of one hour with a time increment of 0.01 sec. The time increment needs to be sufficiently small to capture the interaction between the soil and the pipe. The time increment before updating the environmental data, i.e. the kinematics, was put to 0.16 sec.

11.1.2 Riser Properties

The calculated length of the riser was 1602.5 m, found by computation of the static catenary equations. The inelastic equations were used, so bending stiffness and elastic stiffness were neglected. The outer pipe diameter was specified to 355.6mm while its wall thickness is 28.575mm. A coating was applied on the outside and added up to an external diameter of 365.6mm. Input values are listed in Tab. 11.1.

Table 11.1: Riser Input Parameters

Parameter	Description	Value
T_0	Horizontal top tension [kN]	150
X-x	Dist. of pipe-soil contact [m]	250
h	Depth [m]	1280
D_o	Outer diameter (no coating) [mm]	355.6
t_{steel}	Steel wall thickness [mm]	28.575
E	Elastic modulus [N/m^2]	2.07×10^{11}
σ_Y	Yield stress [MPa]	450
ρ_{steel}	Steel density [kg/m^3]	7.8
ν	Poisson's ratio[-]	0.20
$t_{coating}$	Coating thickness [mm]	5
$\rho_{coating}$	Coating density [kg/m^3]	8.1
ρ_i	Internal fluid density [kg/m^3]	135

Table 11.2: Calculated Riser Parameters

Paramenter	Description	Value
L	Riser length [m]	1602.5
EA	Axial stiffness [N]	6.08×10^9
EI	Bending stiffness[Nm^2]	81.85×10^6
GJ/L	Torsional stiffness [Nm]	3.92×10^4
G	Shear modulus [-]	7.96×10^{10}
ω_s	Submerged weight [N/m]	1336

11.1.3 Soil Input Parameters

The interaction between the soil and the riser is based on the penalty formulation, saying that bodies can not penetrate each other. The axial and lateral soil stiffness was not provided by STATOIL, so these were just approximate values. The axial and lateral stiffness were calculated using the Coulomb friction model. By assuming an adequate displacement of 0.01m and 0.1m in the axial and lateral direction respectively the stiffnesses are found. Tab. 11.3 and Tab. 11.4 list the soil parameters.

Table 11.3: Soil Input Parameters in RIFLEX

Paramenter	Description	Value
K_z	Vertical soil stiffness [N/m/m]	600 000
μ_y	Lateral friction coefficient [-]	1.0
μ_x	Axial friction coefficient [-]	0.2

Table 11.4: Calculated Soil Input Parameters in RIFLEX

Paramenter	Description	Value
K_x	Axial soil stiffness[N/m/m]	26719
K_y	Lateral soil stiffness[N/m/m]	13359

11.1.4 Environmental Description

From a scatter diagram of the significant wave height, H_s and spectral peak period, T_p of hundred years, some sea states were selected (the approach is described in Ch. 2.2). The wave spectrum, JONSWAP-3 parameter spectrum which describes pure wind driven sea, were chosen.

$$S(f) = \frac{5}{16} H_S^2 T_p \Big(\frac{f}{f_p}\Big)^{-5} exp\Big\{-\frac{5}{4}\Big(\frac{f}{f_p}\Big)^{-4}\Big\}(1-0.287\ln(\gamma_J))\gamma_J^{\exp\Big\{-0.5\Big(\frac{f-fp}{fp\sigma}\Big)^2\Big\}} \tag{11.1}$$

where f_p is the spectral peak frequency and σ is a parameter that describes the relative width of the peak.

$$\sigma = \begin{cases} 0.07 & \text{if } f <= fp \\ 0.09 & \text{if} f >= fp \end{cases}$$

The peak-enhancement factor γ_J is given by:

$$\gamma_J = 42.2\Big(\frac{2\pi H_s}{g T_p^2}\Big)^{6/7} \tag{11.2}$$

where g is the acceleration of gravity.

The two different sea state used in the analysis are listed in Tab. 11.7 and Tab. 11.6 .

Table 11.5: The Most Extreme Sea State in the Scatter Diagram with Annual Exceedance Probability of 10^{-2}

Paramenter	Description	Value
H_s	Significant wave height [m]	16.5
T_p	Spectral peak period [s]	18.5

Table 11.6: A Lower Extreme Sea State in the Scatter Diagram with Annual Exceedance Probability of 10^{-2}

Paramenter	Description	Value
H_s	Significant wave height [m]	16.5
T_p	Spectral peak period [s]	18.5

Table 11.7: The most extreme sea state in the scatter diagram with annual exceedance probability of 10^{-2}

Paramenter	Description	Value
H_s	Significant wave height [m]	16.5
T_p	Spectral peak period [s]	18.5

The current profile was based on the extreme values for omni-directional current speed at varying depths, see App. A.2.

The loads on the riser were determined by use of Morison's equation for a small volume structure. The mass coefficient used in the analysis has a value of C_m =2, which is the theoretical value for a smooth cylinder. The drag coefficient depends on many parameters such as the Reynolds number. Fig. 11.1 shows the drag coefficient for a circular cylinder with different roughnesses and Reynolds number in a steady flow. The varying surface roughness k_r are listed in Tab. 11.8. In the analysis, painted steel was used.

Table 11.8: Surface Roughness (DNV, 2007b)

Material	k_r [meters]
Steel, new uncoated	$5 \times 10-5$
Steel painted	5×10^{-6}
Steel, highly corroded	$3 \times 10-3$
Concrete	$3 \times 10-3$
Marine growth	$5 \times 10^{-3} - 5 \times 10^{-2}$

Based on the current profile from the metocean report, the Reynolds number was calculated. The calculation gave Reynolds numbers between 1.0×10^5 to 1.7×10^5 for different water depths and various annual exceedance probability of the current profile. From Fig. 11.1, the drag coefficient was found to be below 0.7. According to the DNV rules (DNV, 2007b), the C_d shall not be less than 0.7 for a smooth oscillating circular cylinder. Including roughness, C_d should be even higher. In the analysis, the drag coefficient was therefore given by 0.7.

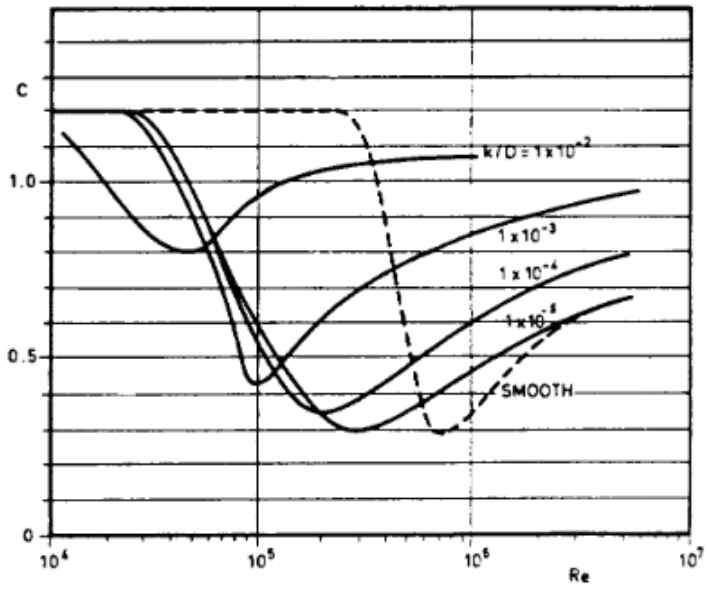

Figure 11.1: Drag Coefficient for Fixed Circular Cylinder for Steady Flow in Critical Regime (DNV, 2007b)

The hydrodynamic coefficients are listed in Tab. 11.9.

Table 11.9: Hydrodynamic Parameters

Paramenter	Description	Value
C_m	Mass coefficient in normal dir. [-]	2.0
C_d	Drag coefficient in normal dir. [-]	0.7

11.2 Phase 2: Trench Profile in SIMLA

In the analysis of the riser-soil interaction the bending stresses that arise at the TDP were obtained. A truncated riser configuration was developed in SIMLA with the same properties as listed in Sec. 11.1.2. The effective bottom tension and static configuration from the motion histories were found in RIFLEX. The top point of the truncated model was located 198 m above the seabed, such that the soil interaction effects were captured. The most extreme motion histories from the RIFLEX analysis were prescribed to the top point of the truncated model. The developed soil model was used in the analysis to obtain a trenched seabed profile.

The duration of the analysis was one hour with the most extreme sea state such that a proper

trench profile could be established.

11.2.1 Simulation Setup

In SIMLA, the pipe was modeled utilizing PIPE31 element. This element is a 3D two-node beam with linear elastic properties.

The contact between the pipe and the soil was modeled by the element CONT126. These elements work as vertical linear springs that represent the vertical stiffness. The degradation soil model is acting through this element. The contact elements are attached to all nodes at the riser.

A static and dynamic analyses were performed for analyzing the soil-riser interaction. In the static analysis, the model obtains its static configuration from a stress-free condition using the stressfree command. The position of the top point of the truncated model was taken from the full RIFLEX model. When the riser adjusted to the static configuration, the anchor point will slide along the seabed. Comparing with RIFLEX, the difference of the location of the end point is 0.5 m. The dynamic analysis was performed by RESTART command. During the dynamic analysis, the nonlinear degradation model was activated.

The static configuration of the truncated model is shown in Fig. 11.2 with a trench profile.

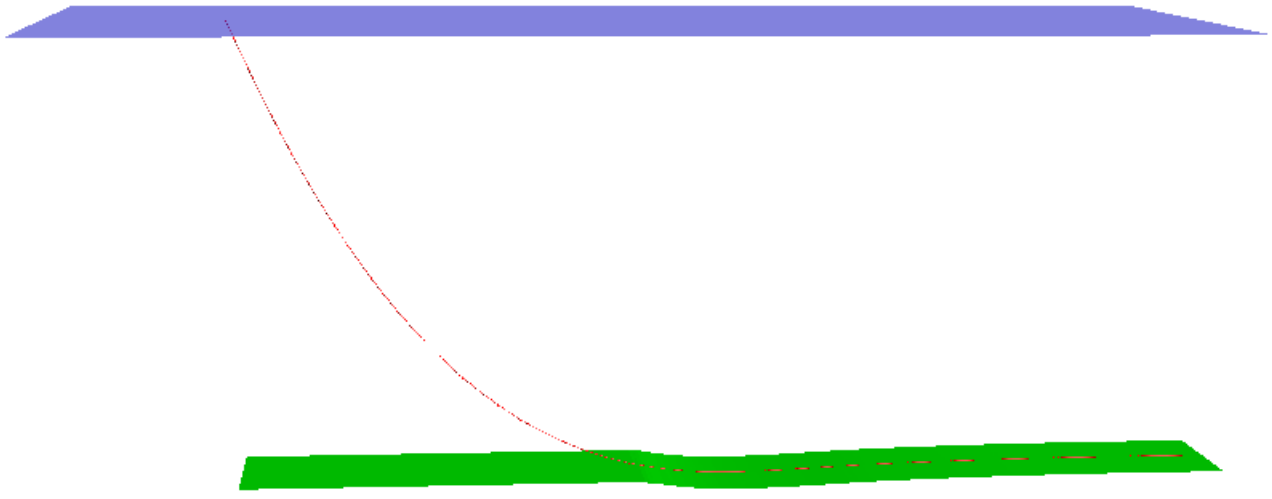

Figure 11.2: Truncated Riser Model in SIMLA

11.2.2 Riser Properties

Node 615 at the middle segment of the full riser configuration in RIFLEX was represented as the top point in the truncated SIMLA model. The length of the riser was calculated based on the input data in RIFLEX and found to be L = 538 m. The riser properties remained the same as in the RIFLEX analysis.

The coordinate system was located at 198 m above the seabed and the riser lies symmetrically about the vertical axis. The anchor point was found after executing the stress-free input file and plot function GNPLOT. Some details about the truncated riser model are listed in Tab. 11.10.

Table 11.10: Truncated Riser Model

Paramenter	Description	Value
(x_0, z_0)	Anchor coordinate [m]	(-269.1, -198.02)
(x, z)	Top coordinate [m]	(172.5, -0.53)
	Element length [m]	2
L	Riser Length [m]	538

11.2.3 Soil Input Parameters

The soil was modeled using the implemented vertical soil degradation model. Following soil model parameters ω, ϕ and ψ were taken from Dunlap et al. (1990) test data, the value of the parameters a and b are for rough condition and the degrading parameters α_d and β_d were found in the article (Aubeny et al., 2008), see Fig. 11.11.

Table 11.11: Soil Model Parameters for SIMLA Analysis (Aubeny et al., 2008)

Parameter	Description	Value
a	Backbone Curve Coefficient	6.73
b	Backbone Curve Exponent	0.29
α_d	Soil Degradation Parameter	0.007
β_d	Soil Degradation Parameter	0.03
k_0	Unload Initial Stiffness	660
ω	Unload Large Deflections	0.53
ϕ	Unload Tension Limit	0.203
ψ	Soil-Riser Separation	0.661
S_{u0}	Shear strength at mudline	3.0 kPa
S_{ug}	Shear strength gradient	1.3kPa/m

The linear stiffness used for initial penetration were calculated from the deflection and contact forces found from the stress-free analysis. The value of the linear stiffness was found to be K_z=65 kN/m/m.

11.3 Phase 3: SCR analysis with Two Seabed Profiles in SIMLA

Two SCR analysis was conducted with an elastic soil model with different seabed profile. The first analysis used a flat seabed, while the second analysis used the obtained trench profile from phase two. In the latter analysis the static riser configuration was changed with respect to the specified geometry due to the occurrence of the trench. The difference was accounted for by adding a new static analysis in the restart analysis. The command TPOND was set to a high value to avoid activation of the nonlinear model. Time series of 500 sec of bending moments around the lateral axis and the axial force were computed at ten different points along the truncated riser model in the vicinity of TDP. The time series were computed by using the command DYNRES_E for specific elements. From the series of bending moments and axial force the stresses histories at the outer fiber were calculated for a thick-walled pipe. By use of rain flow counting, see sub-section 2.2.3, the stress history was reduced into stress ranges with the corresponding number of stress cycles. A code in MATLAB developed by Irvine (2012) was applied.

Stress histograms were obtained by use of rain flow counting method, and tables of the stress ranges and the corresponding number of cycles can be found in the appendix. At 24 elements at the riser in the vicinity of TDP, these histograms were plotted for both SCR analyses. The relative fatigue damage using Miner's sum were calculated for each section and compared for the two cases: $D_{fat} = (\Delta S)^m N$. m is the negative inverse slope of the S-N curve and is taken as 4. The The number of cycles for the lowest stress ranges were neglected. The effect of soil degradation on bending fatigue is assessed in this section.

11.4 Result and Discussion

Fig. 11.3 and Fig. 11.4 show the vicinity of the TDP in static configuration. The riser configuration will vary when the motion histories are exerted at the top point of the riser. Therefore, the figures can be a reference when looking at the element stress of time. Coordinates of the first node at each element are presented in Tab. 11.12 and 11.13 below for the two cases.

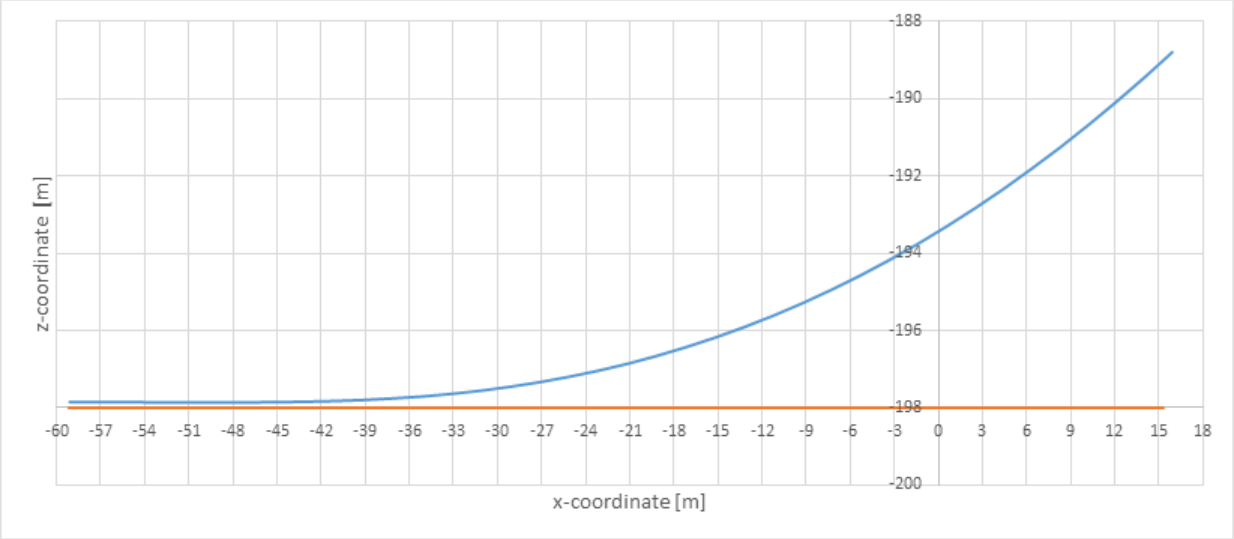

Figure 11.3: Static of Riser Configuration in the Vicinity of TDP with flat sea bottom

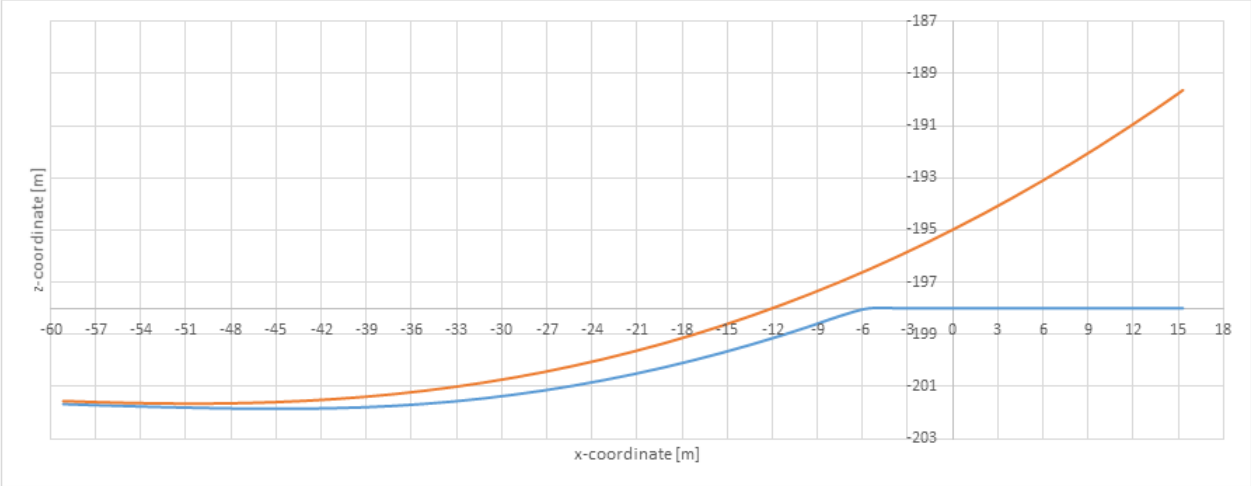

Figure 11.4: Static of Riser Configuration in the Vicinity of TDP with trench profile

Table 11.12: Coordinates of the Riser Elements in Static Analysis (Flat Seabed)

Element nr.:	117	118	119	120	121	122	123	124	125	126	127	128
x- coordinate	-37	-35	-33	-31	-29	-27	- 25	-23	-21	-19	-17	-15
z - coordinate	-197.8	-197.8	-197.7	-197.6	197.6	-197.5	-197.3	-197.2	-197	-196.9	-196.7	-196.4
Element nr.:	129	130	131	132	133	134	135	136	137	136	139	140
x- coordinate	-13	-11	-9	-7	-5	- 3	-1	- 0.6	3	5	6	8.3
z - coordinate	-196.2	-195.9	-195.6	-195.3	-195	194.6	-194.2	-193.8	-193.3	-192.8	-192.3	-191.8

Table 11.13: Coordinates of the Riser Elements in Static Analysis (Trench Profile)

Element nr.:	117	118	119	120	121	122	123	124	125	126	127	128
x- coordinate	-37	-35	-33	-31	-29	-27	- 25	-23	-21	-19	-17	-15
z - coordinate	-201.3	-201.2	-201.0	-200.8	-200.7	-200.4	200.2	-200.0	-199.9	-199.7	-199.4	-199.0
Element nr.:	129	130	131	132	133	134	135	136	137	136	139	140
x- coordinate	-13	-11	-9	-8	-6	- 4	-2	- 0.2	2	4	6	7.5
z - coordinate	-198.7	-198.3	-197.9	-197.4	-197.0	196.5	-196.0	-195.5	-194.9	-194.3	-193.7	-193.1

The number of cycles is plotted along the vertical axis against the decreasing stress range along the horizontal axis. The values are listed in the corresponding tables. The lowest stress ranges are neglected.

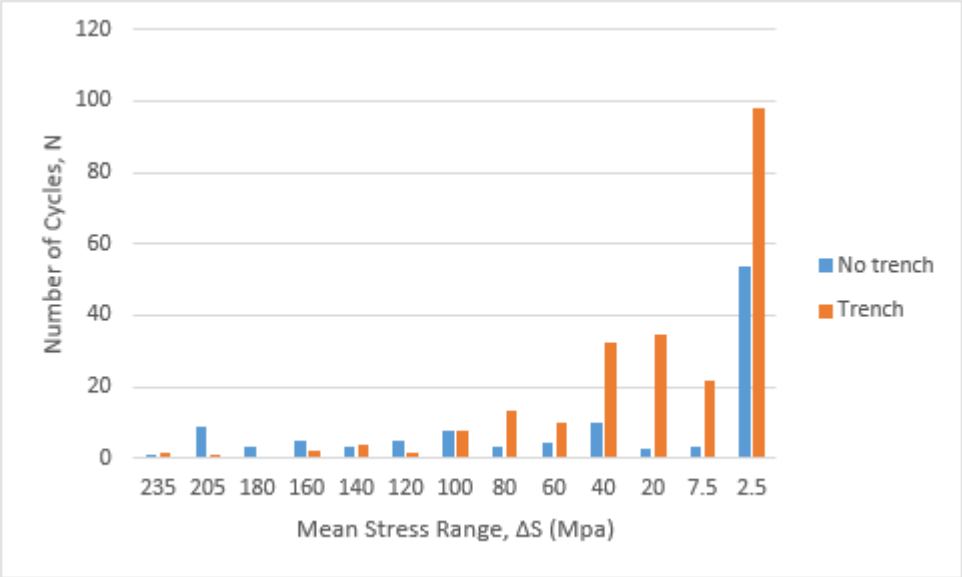

Figure 11.5: Stress Histogram of Riser Element 117

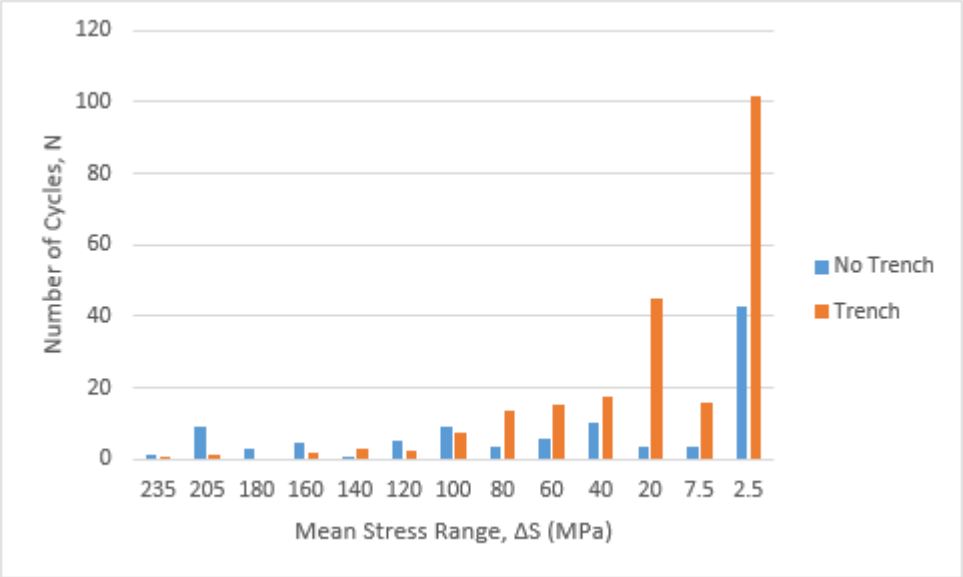

Figure 11.6: Stress Histogram of Riser Element 118

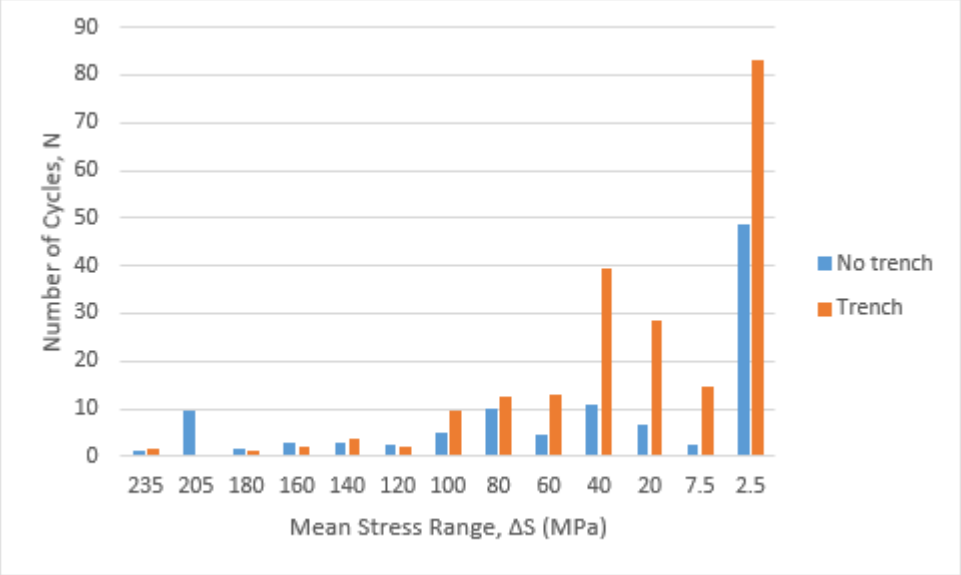

Figure 11.7: Stress Histogram of Riser Element 119

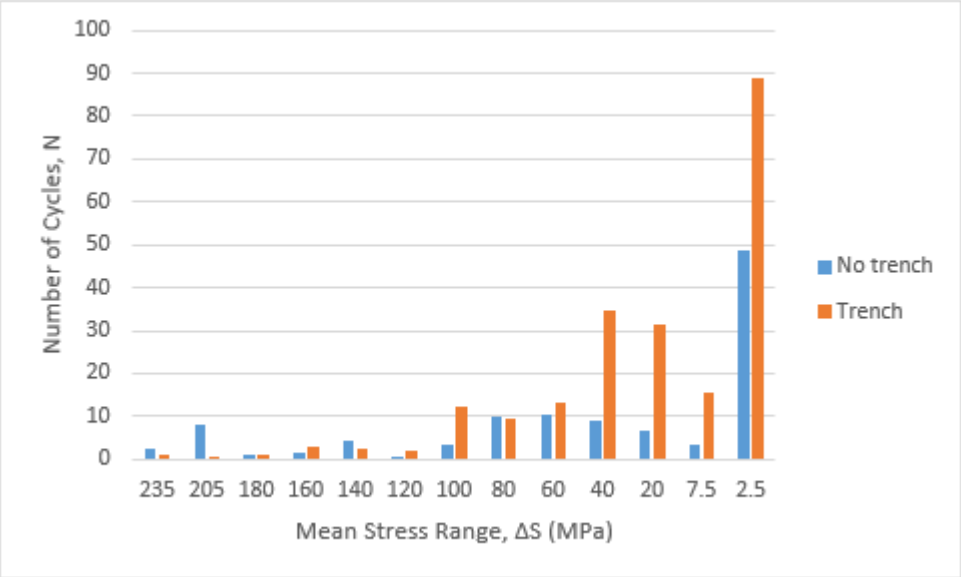

Figure 11.8: Stress Histogram of Riser Element 120

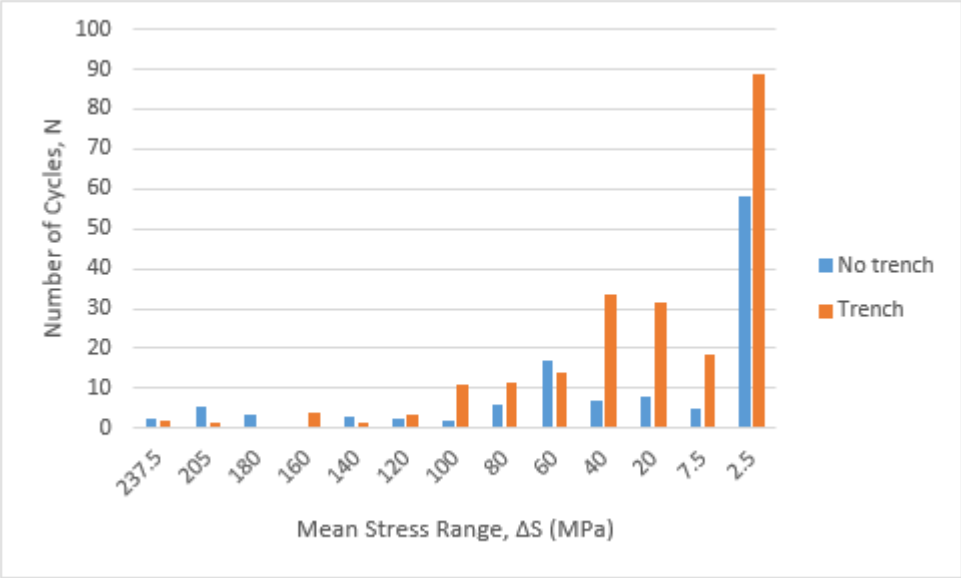

Figure 11.9: Stress Histogram of Riser Element 121

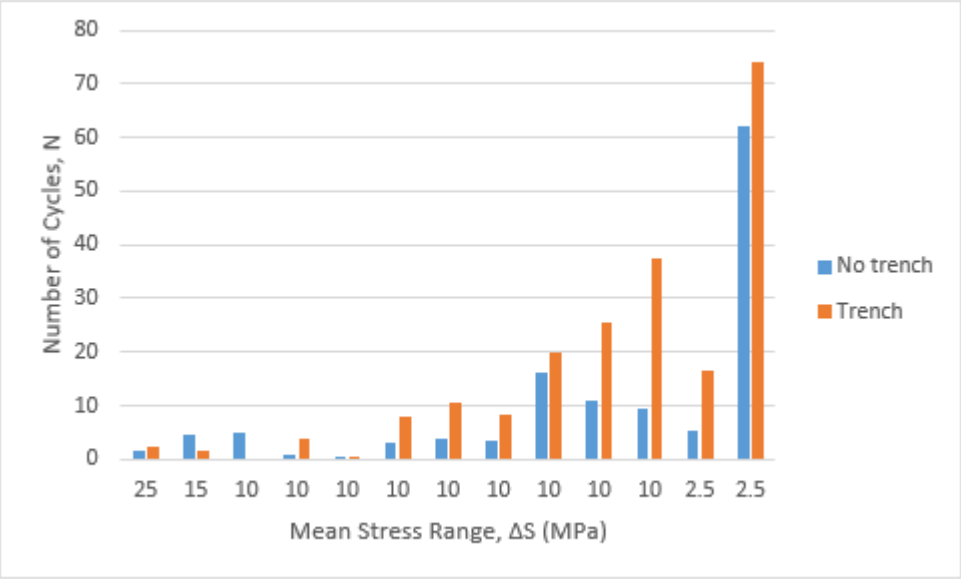

Figure 11.10: Stress Histogram of Riser Element 122

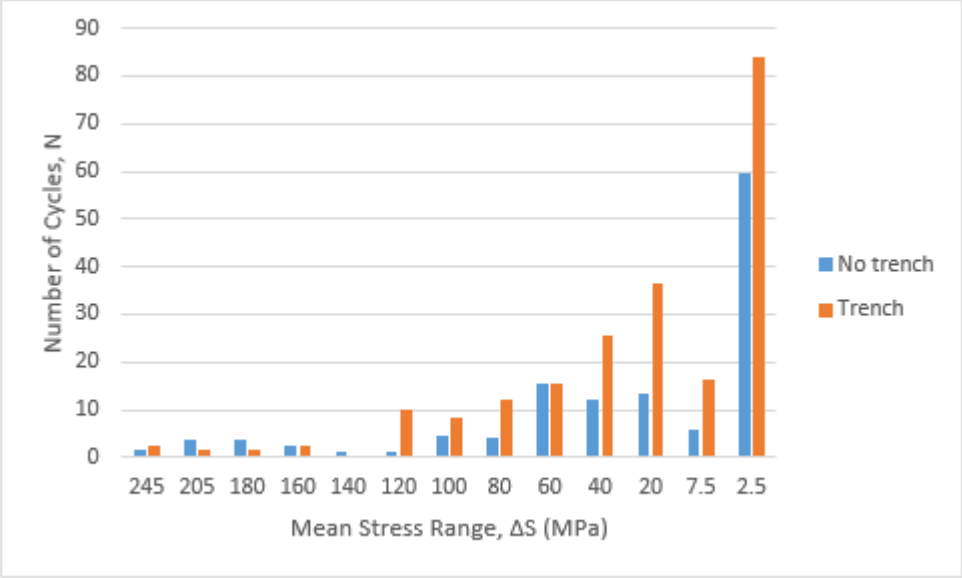

Figure 11.11: Stress Histogram of Riser Element 123

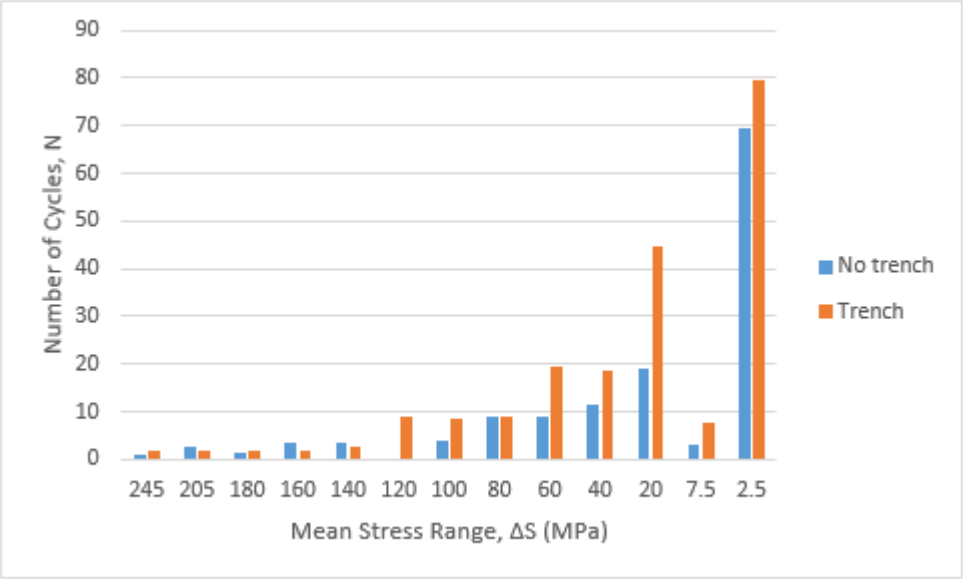

Figure 11.12: Stress Histogram of Riser Element 124

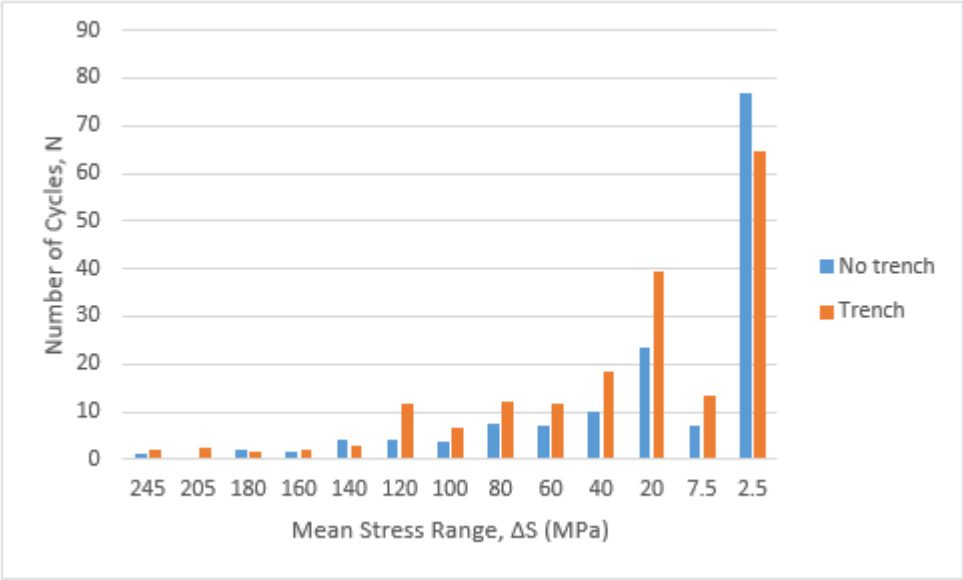

Figure 11.13: Stress Histogram of Riser Element 125

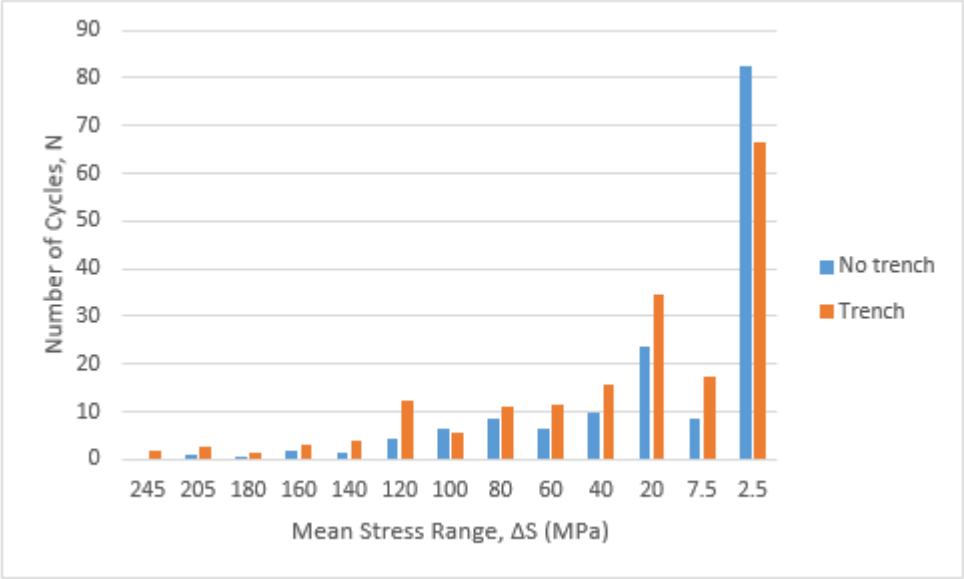

Figure 11.14: Stress Histogram of Riser Element 126

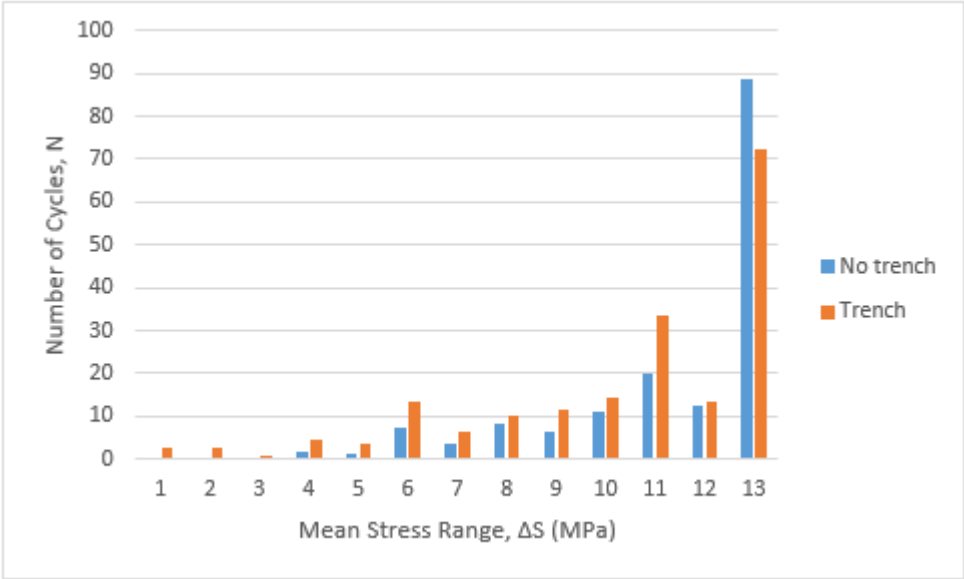

Figure 11.15: Stress Histogram of Riser Element 127

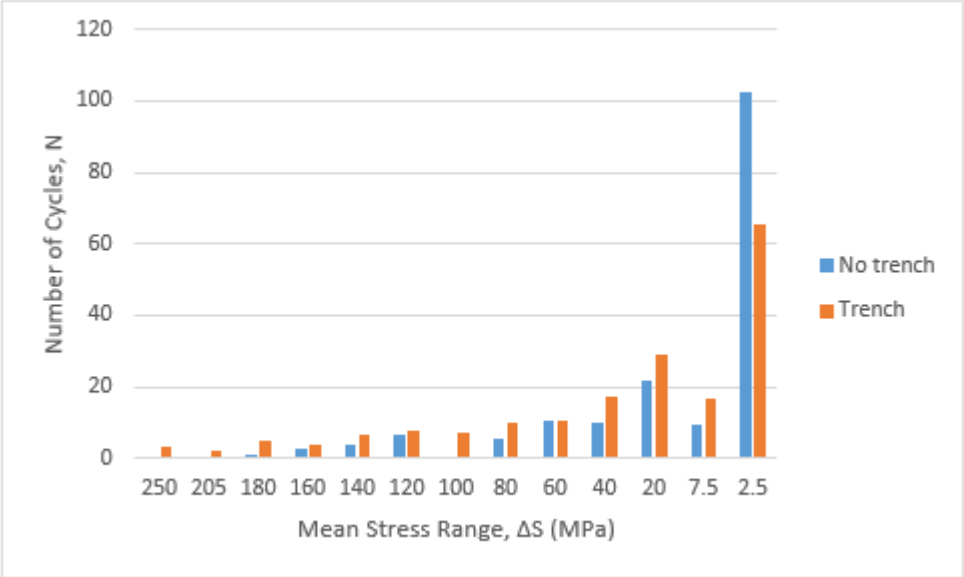

Figure 11.16: Stress Histogram of Riser Element 128

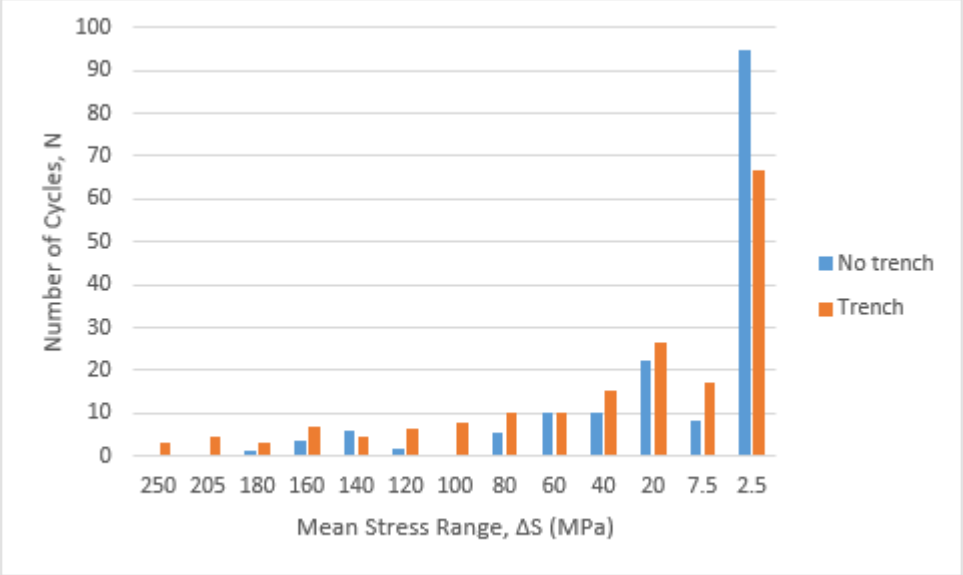

Figure 11.17: Stress Histogram of Riser Element 129

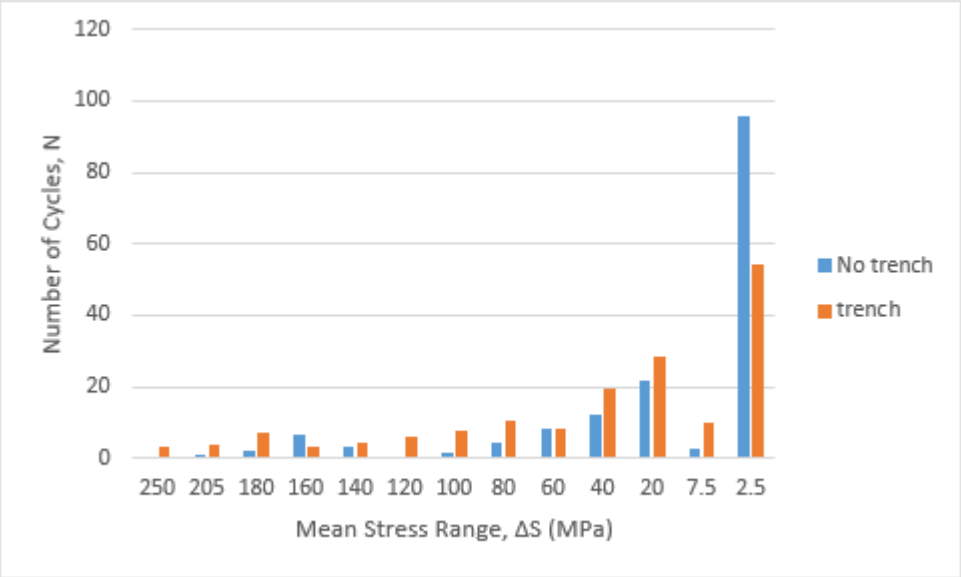

Figure 11.18: Stress Histogram of Riser Element 130

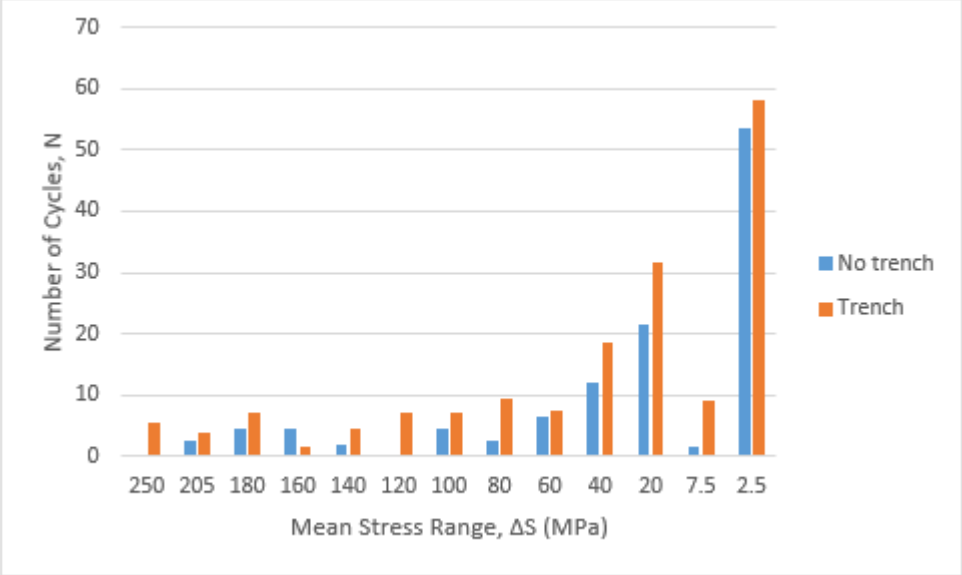

Figure 11.19: Stress Histogram of Riser Element 131

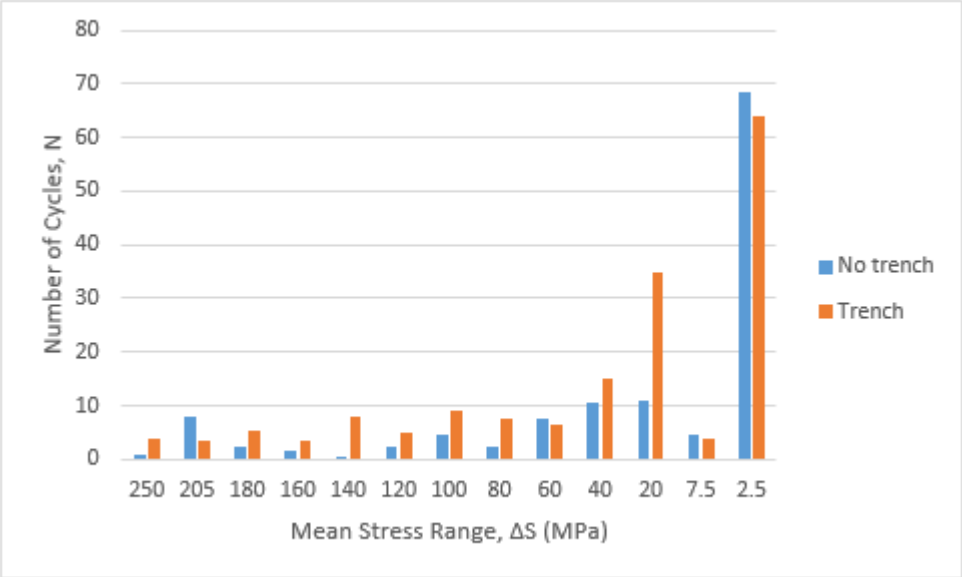

Figure 11.20: Stress Histogram of Riser Element 132

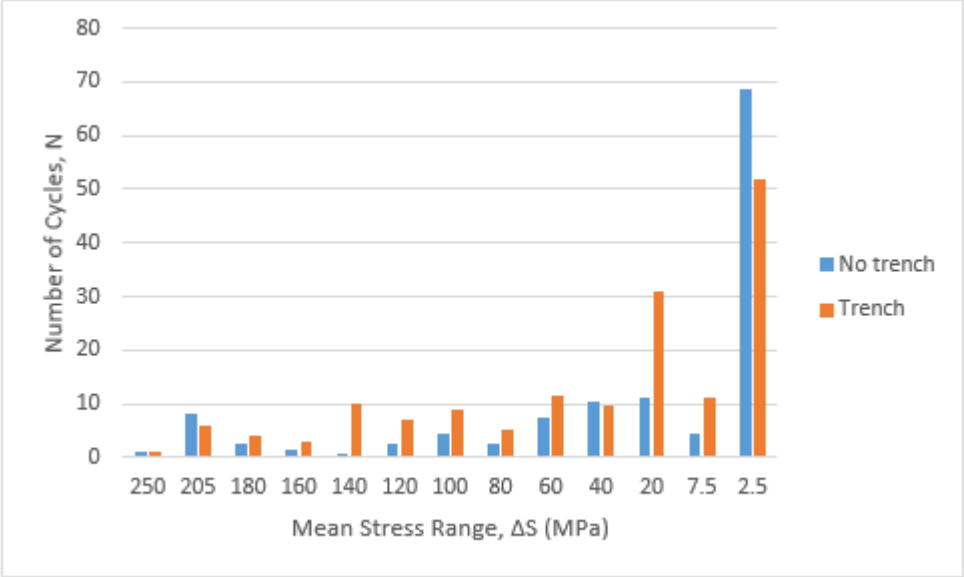

Figure 11.21: Stress Histogram of Riser Element 133

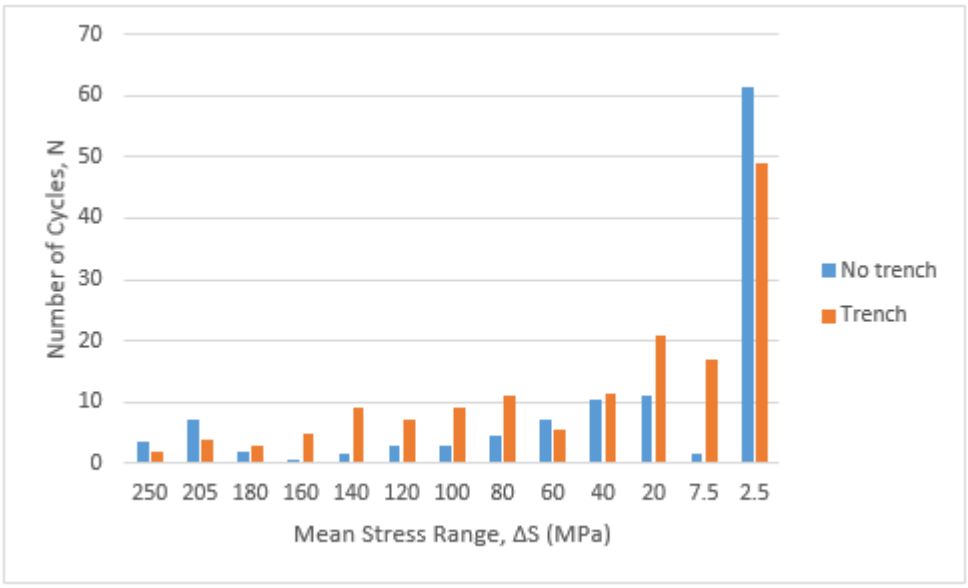

Figure 11.22: Stress Histogram of Riser Element 134

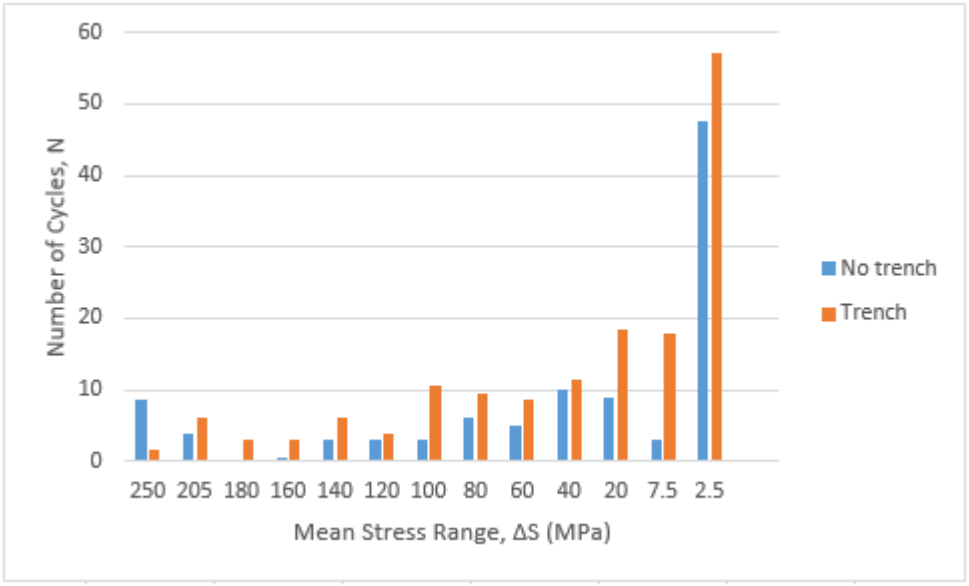

Figure 11.23: Stress Histogram of Riser Element 135

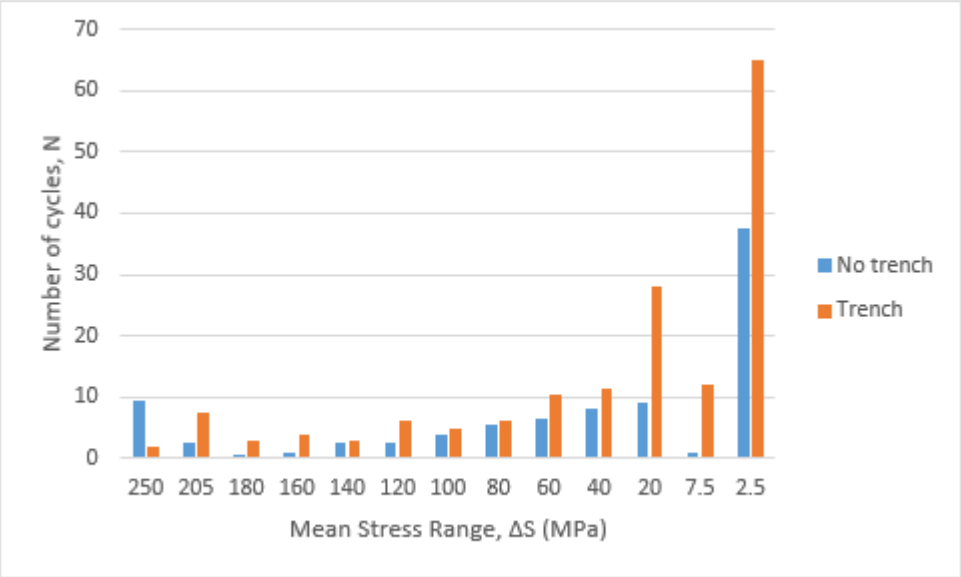

Figure 11.24: Stress Histogram of Riser Element 136

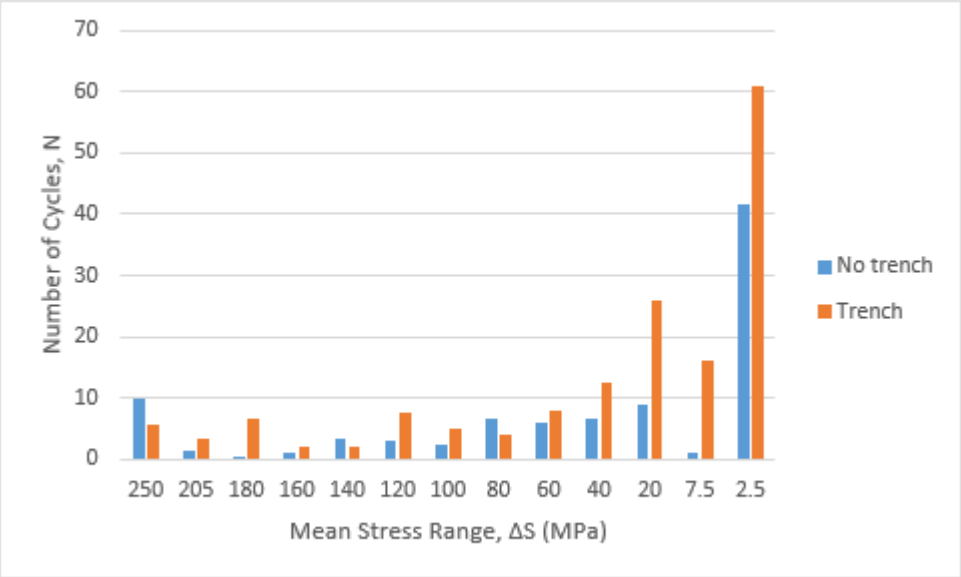

Figure 11.25: Stress Histogram of Riser Element 137

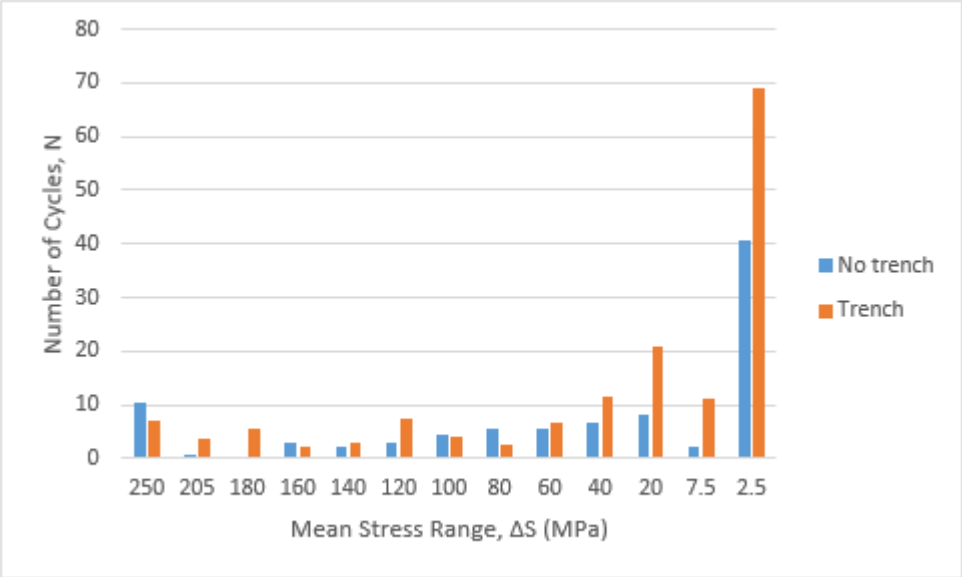

Figure 11.26: Stress Histogram of Riser Element 138

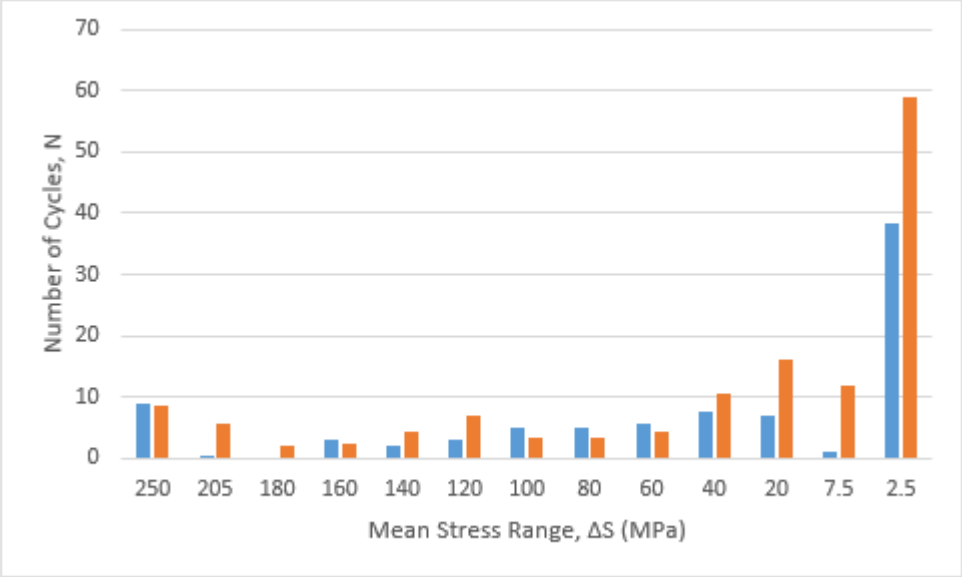

Figure 11.27: Stress Histogram of Riser Element 139

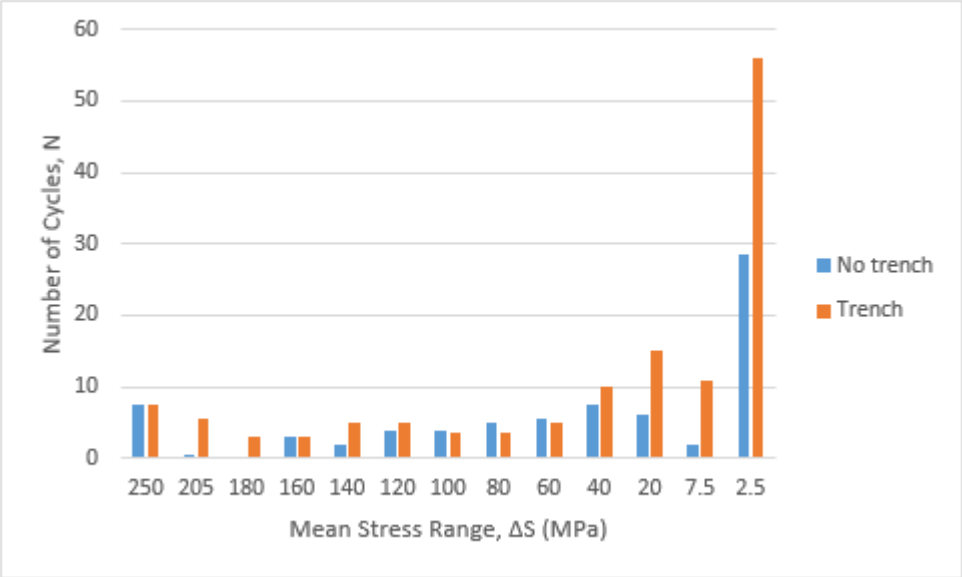

Figure 11.28: Stress Histogram of Riser Element 140

Tab. 11.14 tabulated the relative damage sum for cross-sections in the vicinity of TDP for both cases. The value of the damage sum were scaled by a factor of 10^{10}.

Table 11.14: Approximate Coordinates of the Riser Elements in Static Analysis

Element nr.:	117	118	119	120	121	122	123	124	125
D_{fat} (no trench)	2.928	2.914	2.604	2.654	2.403	2.085	1.834	1.415	1.071
D_{fat} (trench)	1.102	1.024	1.131	1.023	1.478	1.785	1.874	1.850	1.939
Element nr.:	126	127	128	129	130	131	132	133	134
D_{fat} (no trench)	0.622	0.566	0.613	0.786	1.047	1.353	2.303	1.887	3.026
D_{fat} (trench)	2.049	2.356	2.943	3.186	3.631	4.130	3.532	2.724	2.767
Element nr.:	135	136	137	138	139	140			
D_{fat} (no trench)	4.301	4.492	4.547	4.602	4.019	3.444			
D_{fat} (trench)	2.629	3.014	4.034	4.394	5.042	4.767			

There is no clear pattern for which effect the soil degradation may have. The highest value of the relative damage sum at the cross-sections oscillates between the two cases. The conclusion can not be drawn by looking at cross-section for the cross-section. The full picture of must is studied as the riser behaves differently for the two cases. The relative damage sum for the case with a trench profile is considerably higher than for the case with flat seabed in the elements 124-133. The distance these elements spans covers the transition zone where the trench profile turns to a flat seabed.

The largest relative fatigue damage of all cross-sections is element 139 for the case with trench profile. This element is the most critical regarding fatigue. Thus, the analyses may indicate that the soil degradation has no influence on the riser fatigue life.

Chapter 12

Conclusion

Soft clay at deep water introduces sensitive parameters in the modeling of pipe-soil interaction. The soil provides stiffness which is hard to determine due to the complexity of the cohesive soil. There exist empirical models of the soil in the vertical and lateral directions that are frequently employed. The formulations of the pipe-soil interactions may be given by a force-displacement curve. These are often based on numerical model and test data.

The soil behavior is history dependent due to the nonlinearities. For extreme loading cycles, the vertical soil behavior may be described by four main paths/curves. The backbone curve considers the initial penetration into the virgin soil, while elastic rebound curve models the soil resistance when the pipe is uplifted. Partial pipe-soil separation curve describes the reduction of soil resistance after maximum suction force until the pipe is fully separated. The re-contact curve defines the re-loading of the riser into the soil. This enclosed loop is denoted the backbone curve. The bounding loop represents cases where extreme motion leads to full separation during uplifting. However, arbitrary reversals may occur if the motions are not large enough.

A nonlinear degradation soil model is implemented in the two programming languages FORTRAN and MATLAB to describe the behavior of soft clay. The code showed respectable correspondence when comparing some cases with similar published literature. The literature contains few illustrations of the different paths the force-displacement curve can enter. The boundary requirements during unloading outside the bounding loop should only be considered as

tentative until validation is conducted. It is assumed that the soil degradation influences the backbone curve. The backbone curve is thus implemented such that for extreme reloading, the curve is given a load correction. This way of calculating further penetration into virgin soil needs to be validated.

The soil degradation is beneficial for the fatigue life of the riser at the TDP. The soil stiffness reduces during complex loading, due to effects such as self-burying and plastic deformation. The SCR analysis of a truncated model using a trench soil profile and a flat seabed showed different results. The effect of the soil degradation did not positively influence the fatigue life of the riser. Of 24 plots of the bending stresses, the critical cross-section regarding fatigue was in the case using a trench profile. The analysis should be studied further to give a proper conclusion to the effect the soil degradation may have. The duration of the analysis was 500 sec. By applying a longer simulation time, the result would be more representative. Also, the value of the degradation parameters may have an effect on the result. By introducing a higher degree of soil degradation, its effect could give more prominent indications it will have on the fatigue life of the riser.

Chapter 13

Further Work

- Soil Degradation Model: The accuracy of the hyperbolic reloading curve needs to be validated against laboratory measurements. The flat reloading plateau is only a simplification in order to modify the backbone curve. An adequate formulation to describe the reloading should be studied further. The coupled effects between the lateral and vertical deflection should be incorporated into the soil model. The effect of strain rate effects, trench width, and pipe surface roughness on the backbone curve are not included in the model.
- Fatigue Analysis: A more thorough research needs to be done to give a more consistent conclusion of the effect of soil degradation. SCR analysis should be conducted for a number of degradation parameters to investigate the effect it may have on fatigue life. Also, a longer simulation time may be applied.

Bibliography

Riser system analysis program. https://www.sintef.no/globalassets/upload/marintek/pdf-filer/factsheets/riflex.pdf. Accessed: 2016-05-31.

Simla - simulation of pipelaying. https://www.sintef.no/globalassets/upload/marintek/pdf-filer/sofware/simla.pdf. Accessed: 2016-05-31.

(2011). *RIFLEX theory manual*. MARINTEK, v3.6 rev2 edition.

Aubeny, C. P. and Biscontin, G. (2009). Seafloor-riser interaction model. *International Journal of Geomechanics*, 9(3):133–141.

Aubeny, C. P., Biscontin, G., and Zhang, J. (2006). Seafloor interaction with steel catenary risers. *Final Project Report to Minerals Management Service, Offshore Technology Research Centre Industry Consortium, Texas A&M University, College Station, Houston, TX, OTRC Library*, (9/06A173).

Aubeny, C. P., Shi, H., and Murff, J. D. (2005). Collapse Loads for a Cylinder Embedded in Trench in Cohesive Soil. *International Journal of Geomechanics*, 5(4):320–325.

Aubeny, C. P., You, J., and Biscontin, G. (2008). Seafloor interaction with steel catenary risers. In *The Eighteenth International Offshore and Polar Engineering Conference*. International Society of Offshore and Polar Engineers.

Bridge, C., Laver, K., Clukey, E., Evans, T., et al. (2004). Steel catenary riser touchdown point vertical interaction models. In *Offshore Technology Conference*. Offshore Technology Conference.

Bridge, C. and Willis, N. (2002). Steel catenary risers–results and conclusions from large scale simulations of seabed interaction. In *Proc. of the Int. Conf. on Deep Offshore Technology*.

Bruton, D., Bolton, M., Carr, M., and White, D. (2008). Pipe-Soil Interaction With Flowlines During Lateral Buckling and Pipeline Walking - The SAFEBUCK JIP. Offshore Technology Conference.

Bruton, D., White, D., Cheuk, C., Bolton, M., and Carr, M. (2006). Pipe/Soil Interaction Behavior During Lateral Buckling, Including Large-Amplitude Cyclic Displacement Tests by the Safebuck JIP. Offshore Technology Conference.

Clukey, E., Housterman s, L., and Dyvik, R. (2005). Model tests to simulate riser-soil interaction in touch-down point region. pages 651–658. Frontiers in Offshore Geotechnics.

DNV (2007a). DNV-RP-C203: Fatigue Design of Offshore Steel Structures. Technical report, DNV, Høvik.

DNV (2007b). DNV-RP-F110: Environmental Conditions and Environmental Loads. Technical report, DNV, Høvik.

DNV (2007c). DNV-RP-F110: Global Buckling of Submarine Pipelines. Technical report, DNV, Høvik.

DNV (2010). DNV-RP-C203: Fatigue Design of Offshore Steel Structures. Technical report, DNV, Høvik.

DNV (2011). DNV-RP-F109: On-Bottom Stability Design of Submarine Pipelines.

DNV (2012). DNV-OS-F101: Submarine Pipeline System. Technical report, DNV, Høvik.

Dunlap, W., Bhojanala, R., Morris, D., et al. (1990). Burial of vertically loaded offshore pipelines in weak sediments. In *Offshore Technology Conference*. Offshore Technology Conference.

Elosta, H., Huang, S., and Incecik, A. (2013). Dynamic response of steel catenary riser using a seabed interaction under random loads. *Ocean Engineering*, 69:34–43.

Fontaine, E., Nauroy, J., Foray, P., Roux, A., Gueveneux, H., et al. (2004). Pipe-soil interaction in soft kaolinite: Vertical stiffness and damping. In *The Fourteenth International Offshore and Polar Engineering Conference*, pages 23–28. International Society of Offshore and Polar Engineers.

Fylling, I., Larsen, C. M., Sødahl, N., Ormberg, H., Engseth, A., Passano, E., and Holthe, H. (1995). *RIFLEX - theory manual*. Technical Report STF70-F95219, SINTEF Structural Engineering.

Fyrileiv, O. and Collberg, L. (2005). Influence of Pressure in Pipeline Design: Effective Axial Force. pages 629–636. American Society of Mechanical Engineers.

Gaul, L. and Nitsche, R. (2001). The Role of Friction in Mechanical Joints. *Applied Mechanics Reviews*, 54(2):93–106.

Giertsen, E., Verley, R., and Schroder, K. (2004). Carisima: A catenary riser/soil interaction model for global riser analysis. In *ASME 2004 23rd International Conference on Offshore Mechanics and Arctic Engineering*, pages 633–640. American Society of Mechanical Engineers.

Idriss, I. M., Dobry, R., and Sing, R. D. (1978). Nonlinear Behavior of soft clays during cyclic loading. *Journal of Geotechnical and Geoenvironmental Engineering*, 104(GT12):1427–1447.

Irman, A. A. (2015). Non-linear soil models for pipeline and riser analysis.

Irvine, T. (2012). Rainflow Fatigue Cycle Counting.

Jiao, Y. (2007). Non-linear load-deflection models for seafloor interaction with steel catenary risers.

Langford, T., Aubeny, C. P., et al. (2008). Model tests for steel catenary riser in marine clay. In *Offshore Technology Conference*. Offshore Technology Conference.

Mathisen, K. M. (2014). Lecture notes. Course: TMR4190 Elementmetoden.

Moan, T. (2003). *Finite Element Modelling and Analysis of Marine Structures*. TMR4190, Department of Marine Technology, NTNU.

Murff, J., Wagner, D., and Randolph, M. (1989). Pipe penetration in cohesive soil. *Géotechnique*, 39(2):213–229.

Nakhaee, A. and Zhang, J. (2010). Trenching effects on dynamic behavior of a steel catenary riser. *Ocean Engineering*, 37(2):277–288.

Nakhaee, A., Zhang, J., et al. (2008). Effects of the interaction with the seafloor on the fatigue life of a scr. In *The Eighteenth International Offshore and Polar Engineering Conference*. International Society of Offshore and Polar Engineers.

Sævik, S. (2008). *SIMLA - Theory Manual*. MARINTEK, Trondheim.

Theti, R. and Moros, T. (2001a). Soil interaction effects on simple catenary riser response. *Pipes and Pipelines International*, 46(3):15–24.

Theti, R. and Moros, T. (2001b). Soil interaction effects on simple-catenary riser response. *Pipes and Pipelines International*, 46(3):15–24.

Wang, Y., Cao, J., Sha, Y., Duan, M., Wang, D., Dong, Y., Zhou, Y., et al. (2011). Scr hang-off system selection considerations and criteria. In *The Twenty-first International Offshore and Polar Engineering Conference*. International Society of Offshore and Polar Engineers.

Willis, N., West, P., et al. (2001). Interaction between deepwater catenary risers and a soft seabed: large scale sea trials. In *Offshore Technology Conference*. Offshore Technology Conference.

Appendix A

Additional Information

A.1 Scatter diagram

	Spectral peak period (T_p) - (s)																						
H_S (m)	0-3	3-4	4-5	5-6	6-7	7-8	8-9	9-10	10-11	11-12	12-13	13-14	14-15	15-16	16-17	17-18	18-19	19-20	20-21	21-22	22-23	23-24	24-25
0-1	16	327	1563	3231	4022	3634	2662	1694	979	529	273	137	67	32	15	7	3	2	1				
1-2	1	81	1208	5680	12957	18379	18883	15493	10829	6740	3852	2068	1059	524	253	120	56	26	12	5	3	1	1
2-3		2	97	1093	4715	10664	15409	16182	13475	9452	5829	3260	1693	830	390	177	78	34	14	6	3	1	
3-4			2	78	718	2839	6191	8772	9040	7337	4965	2921	1542	748	339	146	60	24	9	4	1	1	
4-5				2	58	454	1650	3407	4616	4541	3490	2215	1209	585	258	105	40	15	5	2	1		
5-6					2	45	308	1019	1960	2482	2274	1615	937	463	201	78	28	9	3	1			
6-7						3	38	223	664	1164	1348	1123	720	373	163	62	21	6	2				
7-8							3	31	159	417	653	676	501	284	129	49	16	5	1				
8-9								3	26	110	250	341	309	200	98	38	12	3	1				
9-10									3	21	73	140	163	127	70	29	10	3	1				
10-11										3	16	45	72	70	46	22	8	2					
11-12											3	11	25	33	27	15	6	2					
12-13												2	7	13	14	9	4	1					
13-14													2	4	6	5	3	1					
14-15														1	2	2	2	1					
15 16															1	1	1						
16-17																	1						
Sum	**16**	**410**	**2869**	**10084**	**22472**	**36019**	**45143**	**46824**	**41750**	**32794**	**23025**	**14554**	**8306**	**4287**	**2011**	**866**	**349**	**135**	**52**	**20**	**8**	**3**	**1**

Figure A.1: Expected scatter diagram of significant wave height (H_s) and spectral peak period (T_p) for a period of 100 years at Aasta Hansteen field. Duration of sea state is 3 hour

A.2 Current Profile

Table 4.26 Extreme values for the omni-directional distributions of current speed at different depths at Aasta Hansteen Field. Duration of extreme event is 10 minutes.

Depth	Annual probability of exceedance		
	0.63	10^{-1}	10^{-2}
	cm/s	cm/s	cm/s
20	98	116	132
50	89	106	121
100	82	99	115
200	75	92	108
300	63	75	87
400	72	91	110
600	46	55	63
800	46	55	62
1000	45	57	67
1200	44	55	66
3m asb	41	49	57

Figure A.2: Extreme values for omni-directional distributions of current speed at 50 m depth at Aasta Hansteen field. Duration of extreme event is 10 minutes.

A.3 Vertical Soil Degradation Model - FORTRAN90

```
!-----------------------------------------------------------------------%
! VERTICAL RISER-SOIL MODEL (AUBENY-d)
!-----------------------------------------------------------------------%
!Penetration, z, positive downwards

subroutine aubeny(z, lsnum, LPU, IOP, input_array, work_array, res_array)
    implicit none

        !Declare input parameters
        integer :: IOP, LPU, lsnum
        double precision,intent(in), dimension(12) :: input_array
        double precision :: z
        double precision :: ks, d, strength_mudline, strength_grad, a_back, b_back, alpha_deg, beta_deg
        double precision :: k0, w_soil , phi_soil, psi_soil

        !Declare intermediate parameters
        integer :: i, lstart, path, path_dir
        double precision, intent(inout), dimension(25) :: work_array
        double precision :: z_prev, z_1bound, z_2bound, z_3bound, z_lastRev, z_cubicRev
        double precision :: z_1deg, z_1controlDeg, z_pmax, z_2boundc, z_3boundc
        double precision :: p_prev, p_1bound, p_2bound, p_3bound, p_lastRev, p_1controlDeg, p_2boundc,
             p_cubicRev, deltap_backbone, lambda

        !Declare internal variables
        integer :: ierr, lastpath_dir
```

```
double precision :: dz, p_bound, p_path12, p_path12c, p_path23
double precision :: p_reloadcubic, kz_reloadcubic, p_reloadHyperbolic, kz_unloadHyperbolic
double precision :: p_unloadHyperbolic, kz_reloadHyperbolic, iterationCubic, iterationHyperbolic

!Declare output
double precision, intent(out), dimension(2) :: res_array
double precision :: p, kz

!Input parameters
d = input_array(1)     !Riser diameter
phi_soil = input_array(2)   !Unload tension limit
strength_mudline = input_array(3) !Shear strength at mudline
strength_grad = input_array(4)  !Shear strength gradient
ks = input_array(5)     !Elastic stiffness
k0 = input_array(6)     !k0=660*strength_mudline
w_soil = input_array(7)    !Unload large deflections
psi_soil = input_array(8)   !Riser-soil separation parameter
a_back = input_array(9)    !Backbone curve coefficient
b_back = input_array(10)   !backbone curve exponent
alpha_deg = input_array(11)   !Degradation parameter for calculation of new z_1bound
beta_deg = input_array(12)   !Degradation parameter for calculation of new z_1bound

!Internal variables
path = int(work_array(1))   !Path identifier
i = int(work_array(2))    !Local load step counter when activating the nonlinear model
lstart = int(work_array(3))   !Load step nr. when nonlinear model is a activated
path_dir = int(work_array(4))   ! -1 for unloading and 1 for loading
z_prev = work_array(5)    !Previous deflection
z_1bound = work_array(6)   !Point on backbone curve
z_2bound = work_array(7)   !Deflection at maximum suction
z_3bound = work_array(8)   !Deflection at full separation
z_lastRev = work_array(9)   !Last arbitrary reversal
z_cubicRev = work_array(10)   !Deflection reversal on partial soil-separation curve
z_1deg = work_array(11)    !Deflection at initial penetration due to selfweight
z_1controlDeg = work_array(12)  !Degradation control parameter
z_pmax = work_array(13)    !Control parameter at maximum soil resistance
z_2boundc = work_array(14)   !Control parameter z_2bound by use of z_pmax
z_3boundc = work_array(15)   !Control parameter z_3bound by use of z_pmax
p_prev = work_array(16)    !Soil resistance at previous load step
p_1bound = work_array(17)   !Maximum soil resistance
p_2bound = work_array(18)   !Maximum soil suction
p_3bound = work_array(19) !Soil resistance at full separation
p_lastRev = work_array(20)   !Soil resistance at last arbitrary reversal
p_cubicRev = work_array(21)   !Soil resistance at corresponding z_cubicRev
p_1controlDeg = work_array(22)  !Degradation control parameter
```

```
p_2boundc = work_array(23)   !Control parameter p_2bound by use of z_pmax
deltap_backbone = work_array(24) !Load correction of backbone curve due to degradation
lambda = work_array(25)    !Accumulated displacement


select case(IOP)
        case(1) !Initial linear springs
        p = ks*z
        kz = ks
        path = 100
        !No suction is considered when loss of contact
        if (z<0.0d0) then
                path = 101
        end if

        case(2) !Nonlinear Soil Model
        if (i<=0) then
                !Initial calculation, there is no static approximation
                p_prev = a_back*(z_prev/d)**b_back*(strength_mudline+strength_grad*z_prev)*d
                lstart = lsnum
                path = 0
        end if

        !Check transition from linear to non-linear
        if (i==0) then
                if (z < 0.0d0) then
                        write(*,*) 'There is no soil contact, try reducing the starting time'
                        write(LPU,*) 'There is no soil contact, try reducing the starting time'
                        ierr = ierr-1
                        STOP
                end if
        end if

        !Load step
        i = lsnum - (lstart-1)

        lastpath_dir = path_dir
        if (z>z_prev)then
                path_dir = 1
        elseif (lastpath_dir == 1 .and. z==z_prev) then
                path_dir = 1
        else
                path_dir = -1
        end if
```

```
!--------------------------------- Define Degradation Control Point --------------------------------
               !Define reversals
               if (path_dir /= lastpath_dir) then
                      z_lastrev = z_prev
                      p_lastRev = p_prev
               end if

               !Reset degradation rule when z_1controlDeg is exceeded
               if (z>z_1controlDeg .and. z<z_prev) then
                      z_1deg= z_prev
                      lambda = 0.0d0
               end if

               if (z>=z_3bound .and. path_dir == -1) then
                      dz = abs(z-z_prev)
               elseif (z<z_3bound .and. z_3bound<z_prev) then
                      dz = abs(z_3bound-z_prev)
               end if
               lambda = lambda + dz
               z_1controlDeg = z_1deg + alpha_deg*(lambda)**beta_deg
               p_1controlDeg = a_back*(z_1controlDeg/d)**b_back*(strength_mudline+strength_grad*
                    z_1controlDeg)*d - deltap_backbone

!---------------------------- Calculation of Soil Resistance and Stiffness ---------------------------
               !Backbone curve
               !Define characteristic along bounding loop
10  if (path==0) then
                     p = a_back*(z/d)**b_back*(strength_mudline + strength_grad*z)*d
                     p = p-deltap_backbone
                     kz = a_back*b_back *(strength_mudline + strength_grad*z)*(z/d)**(b_back-1) + d*
                          a_back*strength_grad*(z/d)**b_back
                     if (z<z_prev .and. i>=1) then
                            z_1bound = z_prev
                            p_1bound = p_prev
                            call revboundingloop(z_1bound, p_1bound, phi_soil, k0, w_soil, psi_soil,
                                 z_2bound, p_2bound, z_3bound)
                            if (z<z_2bound .and. z>z_3bound) then
                                   path = 23
                                   go to 2
                            elseif (z<z_3bound) then
                                   path = 30
                                   go to 3
                            else
                                   path = 12
                                   go to 1
```

```
                        end if
                end if
        end if

        !Path 1-2; Elastic rebound
1 if (path == 12) then
        p = p_unloadHyperbolic(z, path_dir, z_1bound, p_1bound, p_1bound, k0, w_soil)
        kz = kz_unloadHyperbolic(z, path_dir, z_1bound, p_1bound, k0, w_soil)
        if (z <= z_2bound) then
                path = 23
                go to 2
        end if
        if (z>z_prev) then !Arbitrary reversal point on path 1-2
        path = 121
                go to 6
        end if
    end if

        !Path 2-3; Partial soil-separation
2 if (path == 23) then
        p = p_reloadcubic(z, z_2bound, z_3bound, p_2bound, p_3bound)
        kz = kz_reloadcubic(z, z_2bound, z_3bound, p_2bound, p_3bound)
        if (z > z_prev) then
                z_cubicRev = z_prev
                p_cubicRev = p_prev
                path = 321
                go to 4
        end if
        if (z<z_3bound) then
                path = 30
                go to 3
        end if
    end if

        !Path 3-0; Full separation
3 if (path == 30) then
        p = 0.0d0
        kz = 0.0d0
        if (z>=z_3bound) then
                z_cubicRev = z_3bound
                p_cubicRev = 0.0d0
                path = 321
                go to 4
        end if
    end if
```

```
        !Path 3-2-1; Re-loading after full separation and reversal from partial soil separation curve
4 if (path==321) then
                p = p_reloadcubic(z, z_1controlDeg, z_cubicRev, p_1controlDeg, p_cubicRev)
                kz = kz_reloadcubic(z, z_1controlDeg, z_cubicRev, p_1controlDeg, p_cubicRev)
                if (z >= z_1controlDeg) then
                        deltap_backbone = deltap_backbone + (p_1controlDeg-p_1bound)
                        path = 0
                        go to 10
                end if
                if (p>p_1bound) then
                        p = p_1bound
                        kz = 0.0d0
                end if
                if (z<z_prev) then
                        if (p_lastRev>=p_1bound) then
                                z_1bound = z_lastRev
                                p_1bound = p_lastRev
                                call revboundingloop(z_1bound, p_1bound, phi_soil, k0, w_soil, psi_soil,
                                     z_2bound, p_2bound, z_3bound)
                                path = 12
                                go to 1
                        end if
                        z_pmax = iterationCubic(z_1controlDeg, z_3bound, p_1controlDeg, p_3bound, p_1bound
                             )
                        call revboundingloop(z_pmax, p_1bound, phi_soil, k0, w_soil, psi_soil, z_2boundc,
                             p_2boundc, z_3boundc)
                        path = 122
                        go to 5
                end if
        end if

        !Path 1-2-2; Unloading from path 3-1 or from an arbitrary reversal within bounding loop
5 if  (path == 122) then
                p = p_unloadHyperbolic(z, path_dir, z_lastRev, p_lastRev, p_1bound, k0, w_soil)
                kz = kz_unloadHyperbolic(z, path_dir, z_lastRev, p_1bound, k0, w_soil)
                if (z>z_prev) then
                        path = 121
                        go to 6
                else
                        p_path12c = p_unloadHyperbolic(z_lastRev, -1, z_1bound, p_1bound, p_1bound, k0,
                             w_soil)
                        if (z_2bound<z .and. z_lastRev<=z_1bound .and. p_lastRev>=p_path12c) then
                        p_path12 = p_unloadHyperbolic(z, -1, z_1bound, p_1bound, p_1bound, k0, w_soil)
                                if (p<=p_path12) then
```

```
                                path = 12
                                go to 1
                        end if
                elseif (z_3bound<z .and. z<=z_2bound .and. z_lastRev<z_1bound .and. p_lastRev>=
                    p_path12c) then
                        p_path23 = p_reloadcubic(z, z_2bound, z_3bound, p_2bound, p_3bound)
                        if (p<=p_path23) then
                                path = 23
                                go to 2
                        end if
                elseif (z_pmax>=z .and. z>z_2boundc) then
                        p_path12 = p_unloadHyperbolic(z, -1, z_pmax, p_1bound, p_1bound, k0, w_soil
                            )
                        if (p<=p_path12) then
                                p = p_unloadHyperbolic(z, -1, z_pmax, p_1bound, p_1bound, k0, w_soil
                                    )
                        end if
                elseif(z_2boundc> z.and. z>z_3boundc) then
                        p_path23 = p_reloadcubic(z, z_2boundc, z_3boundc, p_2boundc, p_3bound)
                        if (p<=p_path23) then
                                p = p_reloadcubic(z, z_2boundc, z_3boundc, p_2boundc, p_3bound)
                                call revboundingloop(z_pmax, p_1bound, phi_soil, k0, w_soil,
                                    psi_soil, z_2bound, p_2bound, z_3bound)
                        end if
                elseif (z<=z_3bound) then
                        path = 30
                        go to 3
                end if
        end if
    end if

        !Path 1-2-1; Reloading from path 2-3, 1-2 or from an arbitrary reversal within bounding loop
6 if (path == 121) then
        if (z>=z_prev) then
                if (z >= z_1controlDeg) then
                        deltap_backbone = deltap_backbone + (p_1controlDeg- p_1bound)
                        path = 0
                        go to 10
                end if
                p = p_reloadHyperbolic(z, path_dir, z_lastRev, z_1controlDeg, p_lastRev,
                    p_1controlDeg, k0, w_soil)
                kz = kz_reloadHyperbolic(z, path_dir, z_lastRev, z_1controlDeg, p_lastRev,
                    p_1controlDeg, k0, w_soil)
                p_bound = p_reloadcubic(z, z_1controlDeg, z_cubicRev, p_1controlDeg, p_cubicRev)
                if (p>=p_bound) then
```

```
                        path = 321
                        go to 4
                    end if
                    if (p_lastRev == p_prev) then
                        z_pmax = iterationHyperbolic(z_1controlDeg, z_lastRev, p_1controlDeg,
                            p_lastRev, p_1bound, k0, w_soil)
                    end if
                    if (p>p_1bound) then
                        p=p_1bound
                        kz = 0.0d0
                    end if
                else
                if (p_prev>=p_1bound) then
                    z_1bound = z_lastRev
                    p_1bound = p_lastRev
                    call revboundingloop(z_1bound, p_1bound, phi_soil, k0, w_soil, psi_soil, z_2bound,
                        p_2bound, z_3bound)
                    path = 12
                    go to 1
                end if
                call revboundingloop(z_pmax, p_1bound, phi_soil, k0, w_soil, psi_soil, z_2boundc,
                    p_2boundc, z_3boundc)
                path = 122
                go to 5
                end if
            end if

!-----------------------------------------------Updating parameters-----------------------------------
                work_array(1) = real(path)
                work_array(2) = real(i)
                work_array(3) = real(lstart)
                work_array(4) = real(path_dir)
                work_array(5) = z !z_prev
                work_array(6) = z_1bound
                work_array(7) = z_2bound
                work_array(8) = z_3bound
                work_array(9) = z_lastRev
                work_array(10) = z_cubicRev
                work_array(11) = z_1deg
                work_array(12) = z_1controlDeg
                work_array(13) = z_pmax
                work_array(14) = z_2boundc
                work_array(15) = z_3boundc
                work_array(16) = p !p_prev
                work_array(17) = p_1bound
```

```
                work_array(18) = p_2bound
                work_array(19) = p_3bound
                work_array(20) = p_lastRev
                work_array(21) = p_cubicRev
                work_array(22) = p_1controlDeg
                work_array(23) = p_2boundc
                work_array(24) = deltap_backbone
                work_array(25) = lambda

        end select

!--------------------------------------- Updating result array ----------------------------------
        res_array(1:2)=(/p,kz/)

end subroutine aubeny

!-------------------------------------------------------------------------------------------------
!Calculate characteristic points on bounding loop
subroutine revboundingloop(z_1bound, p_1bound, phi_soil, k0, w_soil, psi_soil, z_2bound, p_2bound,
     z_3bound)
        implicit none
        double precision, intent(in) :: z_1bound, p_1bound, phi_soil, k0, w_soil, psi_soil
        double precision, intent(out) :: z_2bound, p_2bound, z_3bound

        z_2bound = z_1bound - ((1+w_soil)*p_1bound)/k0 * (1+phi_soil)/(w_soil-phi_soil)
        p_2bound = -phi_soil*p_1bound
        z_3bound = z_2bound - psi_soil*(z_1bound-z_2bound)

END subroutine revboundingloop


FUNCTION p_reloadHyperbolic(z, path_dir, z_lastRev, z_1controlDeg, p_lastRev, p_1controlDeg, k0, w_soil)
IMPLICIT NONE

        INTEGER, INTENT(IN) :: path_dir
        DOUBLE PRECISION, INTENT(IN) :: z, z_lastRev, z_1controlDeg, p_lastRev, p_1controlDeg, k0,
             w_soil
        DOUBLE PRECISION :: z0, zm, b, xi_controlP, p_reloadHyperbolic

        b = (z_1controlDeg - z_lastRev)/(p_1controlDeg - p_lastRev)- 1.0d0/k0
        xi_controlP = (z_1controlDeg - z_lastRev)/(p_1controlDeg*(1+w_soil)*b)
        p_reloadHyperbolic = p_lastRev + (z - z_lastRev) / (1.0d0/k0 + path_dir*(z-z_lastRev)/((1+w_soil
             )*p_1controlDeg*xi_controlP))

END FUNCTION p_reloadHyperbolic
```

```
FUNCTION kz_reloadHyperbolic(z, path_dir, z_lastRev, z_1controlDeg, p_lastRev, p_1controlDeg, k0, w_soil
    )
IMPLICIT NONE

       INTEGER, INTENT(IN) :: path_dir
       DOUBLE PRECISION, INTENT(IN) :: z, z_lastRev, z_1controlDeg, p_lastRev, p_1controlDeg, k0,
           w_soil
       DOUBLE PRECISION :: z0, zm, a, b, xi_controlP, kz_reloadHyperbolic

       b = (z_1controlDeg - z_lastRev)/(p_1controlDeg - p_lastRev)- 1.0d0/k0
       xi_controlP = (z_1controlDeg - z_lastRev)/(p_1controlDeg*(1+w_soil)*b)
       a = 1.0d0/k0 + path_dir*(z-z_lastRev)/((1+w_soil)*p_1controlDeg*xi_controlP)
   kz_reloadHyperbolic = 1.0d0/a + path_dir*(z_lastRev -z)/((1+w_soil) *p_1controlDeg*xi_controlP*a**2)

END FUNCTION kz_reloadHyperbolic

!-----------------------------------------------------------------------------------------------------
FUNCTION p_unloadHyperbolic(z, path_dir, z1, p1, p2, k0, w_soil)
       IMPLICIT NONE

       INTEGER, INTENT(IN) :: path_dir
       DOUBLE PRECISION, INTENT(IN) :: z, z1, p1, p2
       DOUBLE PRECISION :: k0, w_soil, p_unloadHyperbolic

       p_unloadHyperbolic = p1 + (z-z1)/(1.0d0/k0 + path_dir*(z-z1)/((1+w_soil)*p2))

END FUNCTION p_unloadHyperbolic

FUNCTION kz_unloadHyperbolic(z, path_dir, z1, p2, k0, w_soil)
       IMPLICIT NONE

       INTEGER, INTENT(IN) :: path_dir
       DOUBLE PRECISION, INTENT(IN) :: z, z1, p2, k0, w_soil
       DOUBLE PRECISION :: A, kz_unloadHyperbolic

       A = 1.0d0/k0 + path_dir*(z-z1)/((1+w_soil)*p2)
   kz_unloadHyperbolic = 1.0d0/A+ path_dir*(z1-z)/((1+w_soil)*p2*A**2)

END FUNCTION kz_unloadHyperbolic

!-----------------------------------------------------------------------------------------------------
FUNCTION p_reloadcubic(z, z1, z2, p1, p2)
       IMPLICIT NONE

       DOUBLE PRECISION, INTENT(IN) :: z
```

```
        DOUBLE PRECISION, INTENT(IN) :: z1, z2, p1, p2
        DOUBLE PRECISION :: z0, zm, p_reloadcubic

        z0 = (z1+z2)/2.0d0
    zm = (z1-z2)/2.0d0
    p_reloadcubic = (p1+p2)/2.0d0 +(p1-p2)/4.0d0*(3.0d0*(z-z0)/zm - ((z-z0)/zm)**3)

END FUNCTION p_reloadcubic

FUNCTION kz_reloadcubic(z, z1, z2, p1, p2)
        IMPLICIT NONE

        DOUBLE PRECISION, INTENT(IN) :: z
        DOUBLE PRECISION, INTENT(IN) :: z1, z2, p1, p2
        DOUBLE PRECISION :: z0, zm, kz_reloadcubic

        z0 = (z1+z2)/2.0d0
    zm = (z1-z2)/2.0d0
    kz_reloadcubic = (p1-p2)/4.0d0*(3.0d0/zm - 3.0d0*(z-z0)**2.0d0/zm**3)

END FUNCTION kz_reloadcubic

!-----------------------------------------------------------------------------------------------------
FUNCTION iterationCubic(z_1controlDeg, z_lastRev, p_1controlDeg, p_lastRev, p_1bound)
        IMPLICIT NONE

        DOUBLE PRECISION, INTENT(IN) :: z_1controlDeg, z_lastRev, p_1controlDeg, p_lastRev, p_1bound
        DOUBLE PRECISION :: iterationCubic, error, p, p_reloadcubic, z

        error = -1
        z = z_lastRev
        DO while (error <= 0)
                z = z + 0.000001
                p = p_reloadcubic(z, z_1controlDeg, z_lastRev, p_1controlDeg, p_lastRev)
                error = p - p_1bound
        END DO
        iterationCubic = z

END FUNCTION iterationCubic

!-----------------------------------------------------------------------------------------------------
FUNCTION iterationHyperbolic(z_1controlDeg, z_lastRev, p_1controlDeg, p_lastRev, p_1bound, k0, w_soil)
        IMPLICIT NONE

        DOUBLE PRECISION, INTENT(IN) :: z_1controlDeg, z_lastRev, p_1controlDeg, p_lastRev, p_1bound, k0
```

```
            , w_soil
        DOUBLE PRECISION :: iterationHyperbolic, error, p, p_reloadHyperbolic, z

        error = -1.0d0
        z = z_lastRev
        write(*,*) 'hei2 p_1bound', p_1bound
        write(*,*) 'z_lastrev z_1controlDeg, p_lastRev, p_1controlDeg', z_lastrev, z_1controlDeg,
            p_lastRev, p_1controlDeg
        DO while (error <= 0.0d0)
               z = z + 0.01
               p = p_reloadHyperbolic(z, 1, z_lastRev, z_1controlDeg, p_lastRev, p_1controlDeg, k0,
                    w_soil)
               error = p - p_1bound

        END DO
         iterationHyperbolic = z

END FUNCTION iterationHyperbolic
```

A.4 Vertical Soil Degradation Model - MATLAB

```
%-------------------------------------------------------------------------%
% VERTICAL RISER-SOIL MODEL (AUBENY-d)
%-------------------------------------------------------------------------%
%Penetration, z, positive downwards

function [work_array, res] = aubeny(z, lsnum, LPU, IOP, input_array, work_array, res)
    %Input parameters
    d = input_array(1);     %Riser diameter
        phi_soil = input_array(2);   %Unload tension limit
        strength_mudline = input_array(3); %Shear strength at mudline
        strength_grad = input_array(4);  %Shear strength gradient
        ks = input_array(5);    %Elastic stiffness
        k0 = input_array(6);     %k0=660*strength_mudline
        w_soil = input_array(7);   %Unload large deflections
        psi_soil = input_array(8);   %Riser-soil separation parameter
        a_back = input_array(9);   %Backbone curve coefficient
        b_back = input_array(10);   %backbone curve exponent
        alpha_deg = input_array(11);  %Degradation parameter for calculation of new z_1bound
        beta_deg = input_array(12);   %Degradation parameter for calculation of new z_1bound

    %Intermediate variables
        path = work_array(1); %Path identifier
        i = work_array(2); %Local load step counter is activated for the nonlinear model
```

```
    lstart = work_array(3); %Load step nr. when nonlinear model is a activated
    path_dir = work_array(4); % -1 for unloading and 1 for loading
    z_prev = work_array(5); %Previous deflection
    %z_1bound = work_array(6); %Point on backbone curve
    %z_2bound = work_array(7); %Deflection at maximum suction
    %z_3bound = work_array(8); %Deflection at full separation
    %z_lastRev = work_array(9); %Last arbitrary reversal
    %z_cubicRev = work_array(10); %Deflection reversal on partial soil-separation curve
    z_1deg = work_array(11); %Deflection at initial penetration due to selfweight
    %z_1controlDeg = work_array(12); %Degradation control parameter
    %z_pmax = work_array(13); %Control parameter at maximum soil resistance
    %z_2boundc = work_array(14);  %Control parameter z_2bound by use of z_pmax
    %z_3boundc = work_array(15);  %Control parameter z_3bound by use of z_pmax
    p_prev = work_array(16);   %Soil resistance at previous load step
    %p_1bound = work_array(17);   %Maximum soil resistance
    %p_2bound = work_array(18);   %Maximum soil suction
    %p_lastRev = work_array(19);  %Soil resistance at last arbitrary reversal
    %p_cubicRev = work_array(20);   %Soil resistance at corresponding z_cubicRev
    %p_1controlDeg = work_array(21); %Degradation control parameter
    %p_2boundc = work_array(22);  %Control parameter p_2bound by use of z_pmax
    %dp_backbone = work_array(23); %Load correction of backbone curve due to degradation
    lambda = work_array(24);   %Accumulated displacement

dz = 0;
switch IOP
    case 1 %Initial linear springs
    p = ks*z;
    kz = ks;
    path = 100;
    %No suction is considered when loss of contact
    if z<0
           path = 101;
    end

    case 2 %Nonlinear Soil Model
    if i<=0
                %Initial calculation, there is no static approximation
                p_prev = a_back*(z_prev/d)^b_back*(strength_mudline+strength_grad*z_prev)*d;
                lstart = lsnum;
                path = 0;
    end

           %Check transition from linear to non-linear
    if i == 0
        if z<0
```

```
            disp('There␣is␣no␣soil␣contact,␣try␣reducing␣the␣starting␣time')
            fprintf(LPU,'There␣is␣no␣soil␣contact,␣try␣reducing␣the␣starting␣time');
            return
        end
    end

            i = lsnum - (lstart-1);
            %Define unloading or re-loading
            lastpath_dir = path_dir;
            if z>z_prev
        path_dir = 1;
            elseif lastpath_dir == 1 && z==z_prev
        path_dir = 1;
            else
                path_dir = -1;
    end

            %Define reversals
    if path_dir ~= lastpath_dir
                work_array(9) = z_prev;
                work_array(19) = p_prev;
    end
%--------------------------------- Define Degradation Control Point -------------------------------%

    %Reset degradation rule when z_1controlDeg is exceeded
            if z_prev>work_array(12) && z<z_prev
                z_1deg= z_prev;
                lambda = 0;
            end

            if z>=work_array(8) && path_dir == -1
                dz = abs(z-z_prev);
            elseif z<work_array(8) && work_array(8)<z_prev
                dz = abs(work_array(8)-z_prev);
            end
            lambda = lambda + dz;
            work_array(12)= z_1deg + alpha_deg*(lambda)^beta_deg;
            work_array(21) = a_back*(work_array(12)/d)^b_back*(strength_mudline+strength_grad*
                 work_array(12))*d - work_array(23);

%----------------------------- Calculation of Soil Resistance and Stiffness ------------------------
    %Backbone curve
            %Define characteristic along bounding loop
            if path == 0
                [p, kz, path, work_array] = path01(z, d, a_back, b_back, strength_mudline,
```

```
                    strength_grad, work_array);
                if z<z_prev && i>=1
            work_array(6) = z_prev;
                    work_array(17) = p_prev;
            %Define characteristic point on bounding loop
            [work_array(7), work_array(18), work_array(8)] = revboundingloop(work_array(6),work_array
                 (17), phi_soil, k0, w_soil, psi_soil);
                    if z<work_array(7) && z>work_array(8)
                        [p, kz, path, work_array] = path23(z, work_array, d, phi_soil,
                            strength_mudline,strength_grad, k0, w_soil, psi_soil, a_back,
                            b_back);
                    elseif z<work_array(8)
                [p, kz, path, work_array] = path30(z, work_array, d, phi_soil, strength_mudline,
                     strength_grad, k0, w_soil, psi_soil, a_back,b_back);
                    else
                [p, kz, path, work_array] = path12(z, work_array, d, phi_soil, strength_mudline,
                     strength_grad, k0, w_soil, psi_soil, a_back,b_back);
                    end
                end
        end

%---------------------------------Continiue on the same path-------------------------------------%
if path == 12
    [p, kz, path, work_array] = path12(z, work_array, d, phi_soil, strength_mudline,strength_grad, k0,
         w_soil, psi_soil, a_back,b_back);
 end

if path == 121
   [p, kz, path, work_array] = path121(z, work_array, d, phi_soil, strength_mudline,strength_grad, k0,
        w_soil, psi_soil, a_back,b_back);
end

if path == 12
    [p, kz, path, work_array] = path122(z, work_array, d, phi_soil, strength_mudline,strength_grad, k0,
         w_soil, psi_soil, a_back,b_back);
end

if path == 23
    [p, kz, path, work_array] = path23(z, work_array, d, phi_soil, strength_mudline,strength_grad, k0,
         w_soil, psi_soil, a_back,b_back);
end

if path == 321
    [p, kz, path, work_array] = path321(z, work_array, d, phi_soil, strength_mudline,strength_grad, k0,
         w_soil, psi_soil, a_back,b_back);
```

```
end

if path == 30
    [p, kz, path, work_array] = path30(z, work_array, d, phi_soil, strength_mudline,strength_grad, k0,
         w_soil, psi_soil, a_back,b_back);
end

%---------------------------------Updating some parameters-----------------------------------------

        work_array(1) = path;
                work_array(2) = i;
                work_array(3) = lstart;
                work_array(4) = path_dir;
                work_array(5) = z; %z_prev
                work_array(11) = z_1deg;
                work_array(16) = p; %p_prev
                work_array(24) = lambda;

%------------------------------- Updating result array -------------------------------------------
        res(lsnum,1) = kz;
        res(lsnum,2) = p;
    end
end

%Path 0-1
%Backbone curve
function [p, kz, path, work_array] = path01(z, d, a_back, b_back, strength_mudline, strength_grad,
     work_array)
    dp_backbone = work_array(23);
    fprintf('dp_back3 %f ', work_array(23))
    p = a_back*(z/d)^b_back*(strength_mudline + strength_grad*z)*d;
    p = p-dp_backbone;
    kz = a_back*b_back *(strength_mudline + strength_grad*z)*(z/d)^(b_back-1) + d*a_back*strength_grad*(
         z/d)^b_back;
    path = 0;
end

%Path 1-2
%Elastic Rebound
function [p, kz, path, work_array] = path12(z, work_array, d, phi_soil, strength_mudline,strength_grad,
     k0, w_soil, psi_soil, a_back,b_back)
    z_1bound = work_array(6);
    p_1bound = work_array(17);
    z_2bound = work_array(7);
    z_prev = work_array(5);
    p = p_1bound + (z-z_1bound)/(1/k0 -1*(z-z_1bound)/((1+w_soil)*p_1bound));
```

```
    A = 1/k0 -1*(z-z_1bound)/((1+w_soil)*p_1bound);
    kz = 1/A-1*(z_1bound-z)/((1+w_soil)*p_1bound*A^2);
    path =12;
    if z <= z_2bound
       [p, kz, path, work_array] = path23(z, work_array, d, phi_soil, strength_mudline,strength_grad, k0
            , w_soil, psi_soil, a_back,b_back);
    end
    if z > z_prev
        [p, kz, path, work_array] = path121(z, work_array, d, phi_soil, strength_mudline,strength_grad,
             k0, w_soil, psi_soil, a_back,b_back);
    end
end

%Path 2-3
%Partial riser-soil separation
function [p, kz, path, work_array] = path23(z, work_array, d, phi_soil, strength_mudline,strength_grad,
     k0, w_soil, psi_soil, a_back,b_back)
    z_prev = work_array(5);
    z_2bound = work_array(7);
    z_3bound = work_array(8);
        p_2bound = work_array(18);
    p_prev = work_array(16);

    z0 = (z_2bound + z_3bound)/2;
    zm = (z_2bound-z_3bound)/2;
    p = p_2bound/2 +p_2bound/4*(3*(z-z0)/zm - ((z-z0)/zm)^3);
    kz = p_2bound/4*(3/zm - 3*(z-z0)^2/zm^3);
    path = 23;
   if z > z_prev
               work_array(10) = z_prev;
               work_array(20) = p_prev;
            [p, kz, path, work_array] = path321(z, work_array, d, phi_soil, strength_mudline,
                 strength_grad, k0, w_soil, psi_soil, a_back,b_back);
        end
    if z <= z_3bound
       [p, kz, path, work_array] = path30(z, work_array, d, phi_soil, strength_mudline,strength_grad, k0
            , w_soil, psi_soil, a_back,b_back);
        end
end

%Path 3-2-1;
%Re-loading after full separation and reversal from partial soil separation curve
function [p, kz, path, work_array] = path321(z, work_array, d, phi_soil, strength_mudline,strength_grad,
      k0, w_soil, psi_soil, a_back,b_back)
    z_prev = work_array(5);
```

```
    z_cubicRev = work_array(10);
    z_1controlDeg = work_array(12);
    p_1bound = work_array(17);
    p_lastRev = work_array(19);
    p_cubicRev = work_array(20);
    p_1controlDeg = work_array(21);
    dp_backbone = work_array(23);

    z0 = (z_1controlDeg+z_cubicRev)/2;
    zm = (z_1controlDeg-z_cubicRev)/2;
    p = (p_1controlDeg+p_cubicRev)/2 +(p_1controlDeg-p_cubicRev)/4*(3*(z-z0)/zm -((z-z0)/zm)^3);
    kz = (p_1controlDeg+p_cubicRev)/4*(3/zm - 3*(z-z0)^2/zm^3);
    path = 321;
        if z >= z_1controlDeg
               [p, kz, path] = path01(z, d, a_back, b_back, strength_mudline, strength_grad, work_array)
                    ;
         work_array(23) = dp_backbone + (p_1controlDeg-p_1bound);
        end
        if p>p_1bound
        p = p_1bound;
               kz = 0;
        end
        if z<z_prev
        if p_lastRev>=p_1bound
                      work_array(6) = z_lastRev;
                      work_array(17) = p_lastRev;
            [work_array(7), work_array(18), work_array(8)] = revboundingloop(z_lastRev, p_1bound,
                 phi_soil, k0, w_soil, psi_soil);
            path = 12;
            [p, kz, path] = path12(z, work_array, d, phi_soil, strength_mudline,strength_grad, k0, w_soil
                 , psi_soil, a_back,b_back);
        end
        work_array(13) = iterationCubic(work_array);
        [work_array(14), work_array(22), work_array(15)] = revboundingloop(work_array(13), p_1bound,
             phi_soil, k0, w_soil, psi_soil);
         path = 122;
               [p, kz, path] = path122(z, work_array, d, phi_soil, strength_mudline,strength_grad, k0,
                    w_soil, psi_soil, a_back,b_back);
        end
end

%Path 1-2-2;
%Unloading from path 3-1 or from an arbitrary reversal within bounding loop
function [p, kz, path, work_array] = path122(z, work_array, d, phi_soil, strength_mudline,strength_grad,
      k0, w_soil, psi_soil, a_back, b_back)
    z_prev = work_array(5);
```

```
z_1bound = work_array(6);
z_2bound = work_array(7);
z_3bound = work_array(8);
z_lastRev = work_array(9);
z_pmax = work_array(13);
z_2boundc = work_array(14);
z_3boundc = work_array(15);
p_1bound = work_array(17);
p_2bound = work_array(18);
p_lastRev = work_array(19);
p_2boundc = work_array(22);

p = p_lastRev + (z-z_lastRev)/(1/k0 -1*(z-z_lastRev)/((1+w_soil)*p_1bound));
A = 1/k0 -1*(z-z_lastRev)/((1+w_soil)*p_1bound);
kz = 1/A-1*(z_lastRev-z)/((1+w_soil)*p_1bound*A^2);
path = 122;
    if z>z_prev
           path = 121;
           [p, kz, path, work_array] = path121(z, work_array, d, phi_soil, strength_mudline,
                strength_grad, k0, w_soil, psi_soil, a_back, b_back);
    else
           p_path12c = p_1bound + (z_lastRev-z_1bound)/(1/k0 - 1*(z_lastRev-z_1bound)/((1+w_soil)*
                p_1bound));
           if z_2bound<z && z_lastRev<=z_1bound && p_lastRev>=p_path12c
        p_path12 = p_1bound + (z-z_1bound)/(1/k0 -1*(z-z_1bound)/((1+w_soil)*p_1bound));
           if p<=p_path12
                        path = 12;
                        [p, kz, path, work_array] = path12(z, work_array, d, phi_soil,
                             strength_mudline,strength_grad, k0, w_soil, psi_soil, a_back,b_back);
                end
           elseif z_3bound<z && z<=z_2bound && z_lastRev<z_1bound && p_lastRev>=p_path12c
        z0 = (z_2bound + z_3bound)/2;
        zm = (z_2bound-z_3bound)/2;
        p_path23= p_2bound/2 +p_2bound/4*(3*(z-z0)/zm - ((z-z0)/zm)^3);
           if p<=p_path23
                        path = 23;
                        [p, kz, path, work_array] = path23(z, work_array, d, phi_soil,
                             strength_mudline,strength_grad, k0, w_soil, psi_soil, a_back,b_back);
                end
           elseif z_pmax>=z && z>z_2boundc
                  p_path12 = p_1bound + (z-z_pmax)/(1/k0 -1*(z-z_pmax)/((1+w_soil)*p_1bound));
        if p<=p_path12
           p = p_path12;
        end
           elseif z_2boundc>z && z>z_3boundc
```

```
            z0 = (z_2boundc + z_3boundc)/2;
            zm = (z_2boundc-z_3boundc)/2;
            p_path23 = p_2boundc/2 + p_2boundc/4*(3*(z-z0)/zm - ((z-z0)/zm)^3);
            if p<=p_path23
                 p = p_path23;
                [work_array(7), work_array(18), work_array(8)] = revboundingloop(z_pmax, p_1bound,
                     phi_soil, k0, w_soil, psi_soil);
                   end
        elseif z<=z_3bound
             [p, kz, path, work_array] = path30(z, work_array, d, phi_soil, strength_mudline,
                 strength_grad, k0, w_soil, psi_soil, a_back,b_back);
         elseif z<=z_3boundc
            p = 0;
            kz = 0;
                end
    end
end

%Path 1-2-1;
%Reloading from path 2-3, 1-2 or from an arbitrary reversal within bounding loop
function [p, kz, path, work_array] = path121(z, work_array, d, phi_soil, strength_mudline,strength_grad,
      k0, w_soil, psi_soil, a_back,b_back)
    z_prev = work_array(5);
    z_lastRev = work_array(9);
    z_cubicRev = work_array(10);
    z_1controlDeg = work_array(12);
    z_pmax = work_array(13);
    p_prev = work_array(16);
    p_1bound = work_array(17);
    p_lastRev = work_array(19);
    p_cubicRev = work_array(20);
    p_1controlDeg = work_array(21);
    dp_backbone = work_array(23);
    path =121;
    if z>=z_prev
        if z >= z_1controlDeg
                      work_array(23) = dp_backbone + (p_1controlDeg-p_1bound);
                     [p, kz, path, work_array] = path01(z, d, a_back, b_back, strength_mudline,
                          strength_grad, work_array);
        end
        b = (z_1controlDeg - z_lastRev)/(p_1controlDeg - p_lastRev)- 1/k0;
        xi_controlP = (z_1controlDeg - z_lastRev)/(p_1controlDeg*(1+w_soil)*b)
               p = p_lastRev + (z - z_lastRev) / (1/k0 + 1*(z-z_lastRev)/((1+w_soil)*p_1controlDeg*
                    xi_controlP));
               a = 1/k0 + 1*(z-z_lastRev)/((1+w_soil)*p_1controlDeg*xi_controlP);
        kz = 1/a + 1*(z_lastRev -z)/((1+w_soil) *p_1controlDeg*xi_controlP*a^2);
```

```
        z0 = (z_1controlDeg+z_cubicRev)/2;
        zm = (z_1controlDeg-z_cubicRev)/2;
        p_bound = (p_1controlDeg+p_cubicRev)/2 +(p_1controlDeg-p_cubicRev)/4*(3*(z-z0)/zm -((z-z0)/zm)
             ^3);
        if p>=p_bound && path ~= 0
                      [p, kz, path, work_array] = path321(z, work_array, d, phi_soil, strength_mudline,
                           strength_grad, k0, w_soil, psi_soil, a_back,b_back);
               end
               if p_lastRev == p_prev
                      work_array(13) = iterationHyperbolic(k0, w_soil,work_array);
               end
               if p>p_1bound
           p=p_1bound;
                      kz = 0;
        end
    else
        if p_prev>=p_1bound
           work_array(6)= z_lastRev;
           work_array(17) = p_lastRev;
           [work_array(7), work_array(18), work_array(8)] = revboundingloop(z_lastRev, p_lastRev,
                phi_soil, k0, w_soil, psi_soil);
           [p, kz, path, work_array] = path12(z, work_array, d, a_back,b_back,strength_mudline,
                strength_grad, k0, w_soil);
        end
        [work_array(14), work_array(22), work_array(15)] = revboundingloop(z_pmax, p_lastRev, phi_soil,
             k0, w_soil, psi_soil);
        [p, kz, path, work_array] = path122(z, work_array, d, phi_soil, strength_mudline,strength_grad,
             k0, w_soil, psi_soil, a_back,b_back);
    end
end

function [z_2bound, p_2bound, z_3bound] = revboundingloop(z_1bound, p_1bound, phi_soil, k0, w_soil,
     psi_soil)
       z_2bound = z_1bound - ((1+w_soil)*p_1bound)/k0 * (1+phi_soil)/(w_soil-phi_soil);
       p_2bound = -phi_soil*p_1bound;
       z_3bound = z_2bound - psi_soil*(z_1bound-z_2bound);
end

function z_pmax = iterationCubic(work_array)
       z_lastRev = work_array(9)
    z_1controlDeg = work_array(12)
    p_1bound = work_array(17)
    p_lastRev = work_array(19)
    p_1controlDeg = work_array(21)

    error = -1;
```

```
    z0 = (z_1controlDeg+z_lastRev)/2;
    zm = (z_1controlDeg-z_lastRev)/2;
        z = z_lastRev;
    while error <= 0
              z = z + 0.000001;
        p = (p_1controlDeg+p_lastRev)/2 +(p_1controlDeg-p_lastRev)/4*(3*(z-z0)/zm - ((z-z0)/zm)^3);
        error = p - p_1bound;
    end
    z_pmax = z;

end

function z_pmax = iterationHyperbolic(k0, w_soil,work_array)
    z_lastRev = work_array(9);
        z_1controlDeg = work_array(12);
    p_1bound = work_array(17);
    p_lastRev = work_array(19);
    p_1controlDeg = work_array(21);

    error = -1;
        z = z_lastRev;
    b = (z_1controlDeg - z_lastRev)/(p_1controlDeg - p_lastRev)- 1/k0;
        xi_controlP = (z_1controlDeg - z_lastRev)/(p_1controlDeg*(1+w_soil)*b);
        while (error <= 0.0d0)
              z = z + 0.01;
              p = p_lastRev + (z - z_lastRev) / (1/k0 + 1*(z-z_lastRev)/((1+w_soil)*p_1controlDeg*
                   xi_controlP));
              error = p - p_1bound;
        end
         z_pmax = z;
end
```

A.5 Mean Stress Range of Riser Elements and Corresponding Number of Cycles

Table A.1: Mean Stress Range and Corresponding Number of Cycles for Element 117

ΔS:	235	205	180	160	140	120	100	80	60	40	20
N (no trench):	1	9	3.5	5	3.5	5	8	3	4.5	10	2.5
N (trench):	1.5	1	0	2	4	1.5	7.5	13.5	10	32.5	34.5

Table A.2: Mean Stress Range and Corresponding Number of Cycles for Element 118

ΔS:	235	205	180	160	140	120	100	80	60	40	20
N (no trench):	1.5	9	3	4.5	1	5	9	3.5	6	10	3.5
N (trench):	1	1.5	0	2	3	2.5	7.5	13.5	15.5	17.5	45

Table A.3: Mean Stress Range and Corresponding Number of Cycles for Element 119

ΔS:	235	205	180	160	140	120	100	80	60	40	20
N (no trench):	1	9.5	1.5	3	3	2.5	5	10	4.5	11	6.5
N (trench):	1.5	0.5	1	2	3.5	2	9.5	12.5	13	39.5	28.5

Table A.4: Mean Stress Range and Corresponding Number of Cycles for Element 120

ΔS:	235	205	180	160	140	120	100	80	60	40	20
N (no trench):	2.5	8	1	1.5	4.5	0.5	3.5	10	10.5	9	6.5
N (trench):	1	0.5	1	3	2.5	2	12.5	9.5	13	35.5	31.5

Table A.5: Mean Stress Range and Corresponding Number of Cycles for Element 121

ΔS:	237.5	205	180	160	140	120	100	80	60	40	20
N (no trench):	2.5	5.5	3.5	0.5	3	2.5	2	6	17	7	8
N (trench):	2	1.5	0	4	1.5	3.5	11	11.5	14	33.5	31.5

Table A.6: Mean Stress Range and Corresponding Number of Cycles for Element 122

ΔS:	245	205	180	160	140	120	100	80	60	40	20
N (no trench):	1.5	4.5	5	1	0.5	3	4	3.5	16	11	9.5
N (trench):	2.5	1.5	0	4	0.5	8	10.5	8.5	20	25.5	37.5

Table A.7: Mean Stress Range and Corresponding Number of Cycles for Element 123

ΔS:	245	205	180	160	140	120	100	80	60	40	20
N (no trench):	1.5	3.5	3.5	2.5	1	1	4.5	4	15.5	12	13.5
N (trench):	2.5	1.5	1.5	2.5	0.5	10	8.5	12	15.5	25.5	36.5

Table A.8: Mean Stress Range and Corresponding Number of Cycles for Element 124

ΔS:	245	205	180	160	140	120	100	80	60	40	20
N (no trench):	1	2.5	1.5	3.5	3.5	0	4	9	9	11.5	19
N (trench):	2	2	2	2	2.5	9	8.5	9	19.5	18.5	44.5

Table A.9: Mean Stress Range and Corresponding Number of Cycles for Element 125

ΔS:	245	205	180	160	140	120	100	80	60	40	20
N (no trench):	1	0.5	2	1.5	4	4	3.5	7.5	7	10	23.5
N (trench):	2	2.5	1.5	2	3	11.5	6.5	12	11.5	18.5	39.5

Table A.10: Mean Stress Range and Corresponding Number of Cycles for Element 126

ΔS:	245	205	180	160	140	120	100	80	60	40	20
N (no trench):	0	1	0.5	2	1.5	4.5	6.5	8.5	6.5	10	23.5
N (trench):	2	2.5	1.5	3	4	12.5	5.5	11	11.5	15.5	34.5

Table A.11: Mean Stress Range and Corresponding Number of Cycles for Element 127

ΔS:	250	205	180	160	140	120	100	80	60	40	20
N (no trench):	0	0.5	0.5	2	1.5	7.5	3.5	8.5	6.5	11	20
N (trench):	2.5	2.5	1	4.5	3.5	13.5	6.5	10	11.5	14.5	33.5

Table A.12: Mean Stress Range and Corresponding Number of Cycles for Element 128

ΔS:	250	205	180	160	140	120	100	80	60	40	20
N (no trench):	0	0	1	2.5	4	6.5	0.5	5.5	10.5	10	22
N (trench):	3	2	5	4	6.5	7.5	7.5	10	10.5	17	29

Table A.13: Mean Stress Range and Corresponding Number of Cycles for Element 129

ΔS:	250	205	180	160	140	120	100	80	60	40	20
N (no trench):	0	0.5	1.5	3.5	6	2	0	5.5	10	10	22.5
N (trench):	3	4.5	3	7	4.5	6.5	8	10	10	15.5	26.5

Table A.14: Mean Stress Range and Corresponding Number of Cycles for Element 130

ΔS:	250	205	180	160	140	120	100	80	60	40	20
N (no trench):	0	1	2	6.5	3.5	0.5	1.5	4.5	8.5	12	21.5
N (trench):	3.5	4	7	3.5	4.5	6	8	10.5	8.5	19.5	28.5

Table A.15: Mean Stress Range and Corresponding Number of Cycles for Element 131

ΔS:	250	205	180	160	140	120	100	80	60	40	20
N (no trench):	0	2.5	4.5	4.5	4.5	2	4.5	2.5	6.5	12	21.5
N (trench):	5.5	4	7	1.5	4.5	7	7	9.5	7.5	18.5	31.5

Table A.16: Mean Stress Range and Corresponding Number of Cycles for Element 132

ΔS:	250	205	180	160	140	120	100	80	60	40	20
N (no trench):	1	8	2.5	1.5	0.5	2.5	4.5	2.5	7.5	10.5	11
N (trench):	4	3.5	5.5	3.5	8	5	9	7.5	6.5	15	35

Table A.17: Mean Stress Range and Corresponding Number of Cycles for Element 133

ΔS:	250	205	180	160	140	120	100	80	60	40	20
N (no trench):	1	3.5	2.5	1.5	0.5	2.5	4.5	2.5	7.5	10.5	11
N (trench):	1	6	4	3	10	7	9	5	11.5	9.5	31

Table A.18: Mean Stress Range and Corresponding Number of Cycles for Element 134

ΔS:	250	205	180	160	140	120	100	80	60	40	20
N (no trench):	3.5	7	1	0.5	0	4	2	5.5	7	11.5	19
N (trench):	2	4	3	5	9	7	9	5	11	5.5	11.5

Table A.19: Mean Stress Range and Corresponding Number of Cycles for Element 135

ΔS:	250	205	180	160	140	120	100	80	60	40	20
N (no trench):	8.5	4	0	0.5	3	3	3	6	5	10	9
N (trench):	1.5	6	3	3	6	4	10.5	9.5	8.5	11.5	18.5

Table A.20: Mean Stress Range and Corresponding Number of Cycles for Element 136

ΔS:	250	205	180	160	140	120	100	80	60	40	20
N (no trench):	9.5	2.5	0.5	1	2.5	2.5	4	5.5	6.5	8	9
N (trench):	2	7.5	3	4	3	6	5	6	10.5	11.5	28.5

Table A.21: Mean Stress Range and Corresponding Number of Cycles for Element 137

ΔS:	250	205	180	160	140	120	100	80	60	40	20
N (no trench):	10	1.5	0.5	1	3.5	3	2.5	6.5	6	6.5	9
N (trench):	5.5	3.5	6.5	2	2	7.5	5	4	8	12.5	26

Table A.22: Mean Stress Range and Corresponding Number of Cycles for Element 138

ΔS:	250	205	180	160	140	120	100	80	60	40	20
N (no trench):	10.5	0.5	0	3	2	3	4.5	5.5	5.5	6.5	8
N (trench):	7	3.5	5.5	2	3	7.5	4	2.5	6.5	11.5	21

Table A.23: Mean Stress Range and Corresponding Number of Cycles for Element 139

ΔS:	250	205	180	160	140	120	100	80	60	40	20
N (no trench):	9	0.5	0	3	2	3	5	5	5.5	7.5	7
N (trench):	8.5	5.5	2	2.5	4.5	7	3.5	3.5	4.5	10.5	16

Table A.24: Mean Stress Range and Corresponding Number of Cycles for Element 140

ΔS:	250	205	180	160	140	120	100	80	60	40	20
N (no trench):	7.5	0.5	0	3	2	4	4	5	5.5	7.5	6
N (trench):	7.5	5.5	3	3	5	5	3.5	3.5	5	10	15